ELECTRON MOMENTUM DISTRIBUTIONS AND COMPTON PROFILES OF ATOMS AND MOLECULES

A Thesis Submitted
In Partial Fulfilment of the Requirements
for the Degree of
DOCTOR OF PHILOSOPHY

by

S. R. GADRE

to the

DEPARTMENT OF CHEMISTRY
INDIAN INSTITUTE OF TECHNOLOGY KANPUR

JULY 1977

DEDICATED

TO THE MEMORY OF

BAPU

DEPARTMENT OF CHEMISTRY
INDIAN INSTITUTE OF TECHNOLOGY, KANPUR

CERTIFICATE I

This is to certify that Mr. S.R. Gadre has satisfactorily completed all the course requirements for the Ph.D. programme in Chemistry. The courses include:

Chm 500	Mathematics for Chemists I
Chm 501	Advanced Organic Chemistry I
Chm 521	Chemical Binding
Chm 523	Chemical Thermodynamics
Chm 524	Modern Physical Methods
Chm 541	Advanced Inorganic Chemistry I
M 562	Numerical Analysis
M 607	Applied Numerical Methods
Chm 800	General Seminar
Chm 801	Special Graduate Seminar
Chm 900	Graduate Research

Mr. S.R. Gadre was admitted to the candidacy of the Ph.D. degree in August 1974, after he successfully completed the written and oral qualifying examinations.

(M.V. George)
Head,
Department of Chemistry

(P.K. Ghosh)
Convener,
Departmental Post-Graduate
Committee

CERTIFICATE II

Certified that the work "ELECTRON MOMENTUM DISTRIBUTIONS AND COMPTON PROFILES OF ATOMS AND MOLECULES" has been carried out by Mr. S.R. Gadre under my supervision and the same has not been submitted elsewhere for a degree.

P.T. Narasimhan

P.T. Narasimhan
Thesis Supervisor
Professor of Chemistry

STATEMENT

I hereby declare that the matter embodied in this thesis is the result of investigations carried out by me in the Department of Chemistry, Indian Institute of Technology, Kanpur under the supervision of Prof. P.T. Narasimhan.

In keeping with the general practice of reporting scientific observations, due acknowledgement has been made whenever the work described is based on the findings of other investigators.

S.R. Gadre

ACKNOWLEDGEMENTS

It is a pleasure to place on record my deep sense of gratitude and indebtedness to Professor P.T. Narasimhan. He introduced me to the field of theoretical chemistry and his views on academic as well as non-academic matters have influenced and inspired me greatly.

I am obliged to Professors I.R. Epstein, V.H. Smith, Jr., R. Pauncz, K. Mansikka and T. Paakkari for their valuable correspondence and critical comments on the author's endeavours in the field of electron momentum distributions in atoms and molecules. I am grateful to Professors G.G. Hall and A.A. Frost for their correspondence regarding the FSGO model and Dr. R.A. Rouse for providing me with the double Gaussian FSGO wavefunctions. Thanks are also due to Dr. A. Lahmam-Bennani, Mr. Praveen Chaddah & Dr. V.C. Sahni and Dr. W.A. Reed for communicating their experimental Compton profile data prior to publication.

I am grateful to Dr. N.S. Satya Murthy, Head, Solid State Physics Section of the Nuclear Physics Division, BARC, Bombay for kindly allowing me to work on the γ-ray Compton profile set-up at BARC. I must thank Mr. Praveen Chaddah for making me conversant with the Compton profile set-up at BARC and many helpful discussions and Dr. V.C. Sahni for his kind interest in my work at BARC.

I wish to thank my colleagues Drs. M.S. Gopinathan, D.N. Nanda, K.V. Raman, S. Aravamudhan and K.D. Sen and Messrs

V.H. Subramanian, P.P. Thankachan, N. Chandrakumar, S. Shankar, K.R. Srivatsan, R. Ramaswamy and R. Ramachandran for their valuable assistance in various stages of this work.

Thanks are also due to

Professors M.V. George and A. Chakravorty for their kind interest in my welfare;

Professor R.M. Singru, Dr. D.G. Kanhere and Dr. Anil Seth for many useful discussions;

Dr. K.D. Sen for his timely help regarding the HFS wavefunctions;

Messrs V.H. Subramanian, N. Chandrakumar, S. Shankar and R. Ramachandran for their kind assistance in proof reading;

Mr. R.D. Singh for the efficient typing of the manuscript, Mr. R.K. Bajpai and Mr. Kalyan Das for diagrams and Mr. B.N. Shukla for cyclostyling of the thesis;

Messrs Umesh, Ram Singh, K.K. Bajpai and Anil Kumar for their unfailing help in the Department of Chemistry;

The QCPE, Indiana University, U.S.A. for providing us with a listing of the Subroutine STEPIT;

The Council of Scientific and Industrial Research (CSIR), New Delhi for the financial assistance in the early stages of this work.

S.R. Gadre

CONTENTS

***

CHAPTER I

INTRODUCTION

CHAPTER I

INTRODUCTION

I.1 GENERAL

The studies of electron momentum distributions (EMD) in atoms, molecules and solids have received renewed attention during the last few years (see Epstein[1] for a detailed recent review). Many new techniques such as γ-scattering etc. have been developed extensively and employed to measure EMD's experimentally. A host of these measurements have since then been carried out on atoms, molecules and solids. A number of theoretical calculations and interpretation of EMD's have been reported. The first review on this subject[2] was published in 1933, followed by a spate of review articles[1,3-7] only after 1970. If the number of review articles is taken as a fair indication

of the activity in a given subject, one can say that studies of EMD's in atoms, molecules and solids have been reactivated after overcoming a prolonged period of dormancy.

Since many exhaustive review articles[1,3-7] on this subject are available, we shall deal in this chapter only with some salient features of experimental and theoretical studies of EMD's and the most recent work done in this area.

I.2 ELECTRON MOMENTUM DISTRIBUTIONS AND COMPTON PROFILE

The first experimental observation of the increase in wavelength of electromagnetic radiation on scattering by matter was made by Eve[8] with γ-rays. This was followed by similar studies by Florance[9] and Gray.[10] Compton[11] gave further experimental evidence of this phenomenon with X-rays, in the form of spectral plots and also a theoretical explanation of the scattering process involved.[12] An identical explanation was developed independently by Debye.[13] Compton[14] showed through further experiments that the modified line was too broad to be explained by the non-monochromatic nature of the incident X-ray beam etc. Jauncey[15] attributed this broadening to the fact that the electron is initially not at rest but has a finite momentum. DuMond[16] studied this Doppler broadening process in detail.

When an electromagnetic radiation of wavelength λ is scattered inelastically by a stationary electron one obtains from the laws of conservation of energy and momentum a single modified

wavelength λ' given by[12,13]

$$\lambda' = \lambda + \frac{2h}{mc} \sin^2 \left(\frac{\phi}{2}\right) \qquad (1.1)$$

where ϕ is the scattering angle ($\frac{h}{mc} = 0.0243$ Å). However, when the dynamical nature of atomic or molecular electrons is taken into account, the scattered photon will carry some information about the EMD's of the scatterer through Doppler broadening. In Fig. 1.1 the basic processes in Compton scattering are shown (vide ref. 3), taking into account dynamical nature of the electron and assigning a linear momentum $\underset{\sim}{p}$ to it. Taking the momentum of the incident photon to be $h\underset{\sim}{k}$ and that of the scattered photon to be $h\underset{\sim}{k}'$, from the law of conservation of momentum we have

$$h\underset{\sim}{k}' - h\underset{\sim}{k} = \underset{\sim}{p} - \underset{\sim}{p}' \qquad (1.2)$$

and from the law of conservation of energy

$$hc|\underset{\sim}{k}'| - hc|\underset{\sim}{k}| = \frac{1}{2m}(p^2 - p'^2) \qquad (1.3)$$

Defining the scattering vector $\underset{\sim}{K} = \underset{\sim}{k}' - \underset{\sim}{k}$ and assuming $|\underset{\sim}{K}| > |\underset{\sim}{k}| - |\underset{\sim}{k}'|$, the final momentum $\underset{\sim}{p}'$ can be eliminated from (1.2) and one obtains

$$\Delta\lambda = \lambda' - \lambda = \frac{2h}{mc} \sin^2 \left(\frac{\phi}{2}\right) - \frac{2\lambda \sin \left(\frac{\phi}{2}\right)}{mc} p_z \qquad (1.4)$$

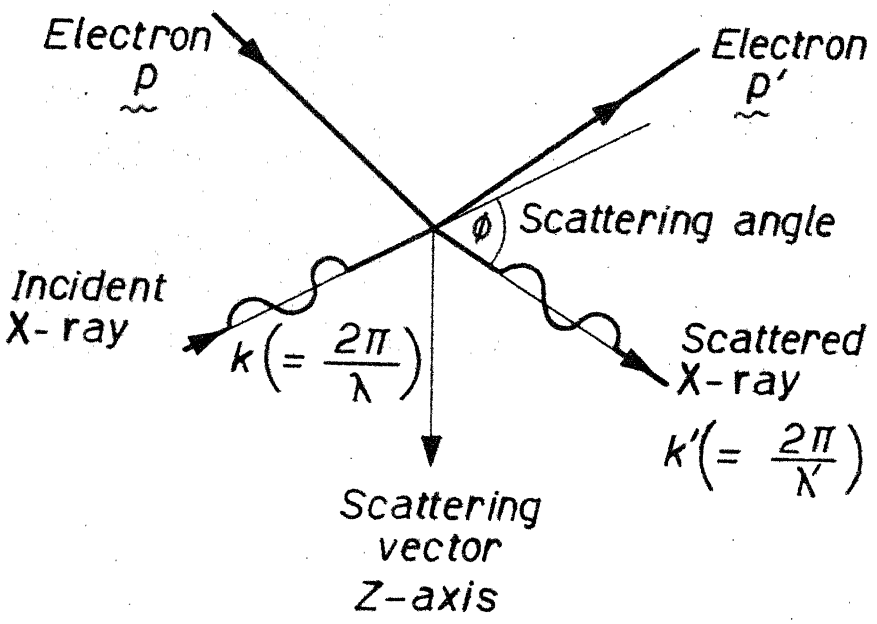

Fig. 1.1 Schematic diagram of the interaction of an X-ray with an electron of momentum $\underset{\sim}{p}$.

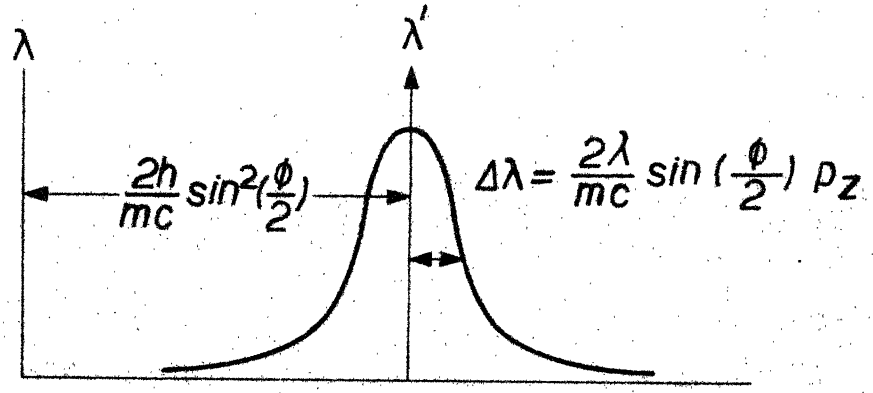

Fig. 1.2 Doppler broadening of the Compton line due to finite initial momentum of the electron.

where p_z is the projection of the electron's initial momentum along the scattering vector. This modified Compton wavelength and Doppler broadening of the Compton line due to finite initial momentum of the electron are shown in Fig. 1.2. The intensity of the line corresponding to the component of momentum p_z will be proportional to the probability of finding that particular component of the momentum:

$$J(p_z) = \int \rho\,(p_x, p_y, p_z)\, dp_x\, dp_y \qquad (1.5)$$

where $\rho\,(\underset{\sim}{p})$ is the momentum density.

In the case of isotropic momentum distributions (1.5) reduces to

$$J(q) = \frac{1}{2} \int_{|q|}^{\infty} \frac{I(p)}{p}\, dp \qquad (1.6)$$

where $$I(p) = \int \rho(\underset{\sim}{p}).p^2.\sin\theta_p\, d\theta_p\, d\phi_p \qquad (1.7)$$

and q is the projection of the electron's initial momentum on the scattering vector. A quantum mechanical derivation of the scattered intensity distribution was given by Kilby.[17] Starting from the Waller-Hartree theory[18] of scattering:

$$\left(\frac{d\sigma}{d\omega\, d\Omega}\right) = \left(\frac{d\sigma}{d\Omega}\right)_{Th} \cdot \left(\frac{\omega'}{\omega}\right) \cdot S(\underset{\sim}{K}, \omega) \qquad (1.8)$$

where $(\frac{d\sigma}{d\Omega})_{Th}$ refers to the Thomson classical scattering cross section[19] and is given by:

$$(\frac{d\sigma}{d\Omega})_{Th} = (\underset{\sim}{\varepsilon}.\underset{\sim}{\varepsilon}')^2 \left(\frac{e^2}{mc^2}\right)^2 \qquad (1.9)$$

Here, $\underset{\sim}{\varepsilon}$ and $\underset{\sim}{\varepsilon}'$ refer to the polarization of incident and scattered photon respectively. ω and ω' denote the angular frequencies of the initial and scattered photon, $S(\underset{\sim}{K}, \omega)$ is now expressed in terms of the quantum mechanical matrix elements, viz.,

$$S(\underset{\sim}{K},\omega) = \sum_j |\langle j | e^{i\underset{\sim}{K}\cdot\underset{\sim}{r}} | 0\rangle|^2 \delta(E_f - E_0 - h\omega) \qquad (1.10)$$

Here $\underset{\sim}{K}$ is the scattering vector and $|j\rangle$ and $|0\rangle$ are the initial and final states of the system. The δ-function ensures conservation of energy during the scattering process under consideration. If one makes the following assumptions:

(i) scattering is by single electrons;

(ii) the final state of the electron is a plane wave;

(iii) the energy transfer in the scattering process is considerably larger than E_B, the binding energy of electrons in the scatterer;

$S(\underset{\sim}{K},\omega)$ reduces to $J(p_z)$ given above (vide Eq. (1.5)). These approximations form the basis of the so-called "impulse approximation".

I.3 IMPULSE APPROXIMATION (IA)

The impulse approximation has been studied in detail.[20] Eisenberger & Platzman[20(d)] calculated $S(\underset{\sim}{K},\omega)$ (in Eq. (1.8)) with exact continuum final state wavefunctions which involve confluent hypergeometric function for 1s electron in hydrogenic atoms. They obtained an analytic expression for $S(\underset{\sim}{K},\omega)$ and showed that it reduces to that obtained with IA if

$$\exp\{ - \frac{1}{2}[\frac{p^2}{2m} , V] t^2\} = 1 \qquad (1.11)$$

By dropping of the commutator in (1.11) one obtains an expression for $S(\underset{\sim}{K},\omega)$ which is independent of V. According to Eisenberger and Platzman, the physics of the situation tells us that V has cancelled out from initial and final-state energies. Thus, for short time of interaction the potential that the electron is moving in is constant. They also showed that this approximation holds well for the atoms belonging to the first row of the periodic table. The correction to IA was shown by them to be $\frac{8}{3}(E_B/E_R)^3$ where E_B is the binding energy of the electron and E_R, its recoil energy. Currat et al.[21] and Bloch and Mendelsohn[22] have also studied the non-IA CP's in more detail. However, as pointed out by Epstein,[1] IA retains its usefulness in the analysis of γ-ray CP data. The corrections to IA can be made, but they spoil the beautifully simple relationship (Eqns (1.5) and (1.6)) to obtain CP from EMD's.

In the next section we discuss briefly the experimental methods which have so far been employed to study EMD's and CP's for atoms, molecules and solids.

I.4. EXPERIMENTAL DETERMINATION OF ELECTRON MOMENTUM DISTRIBUTION

There are six methods which have so far been employed in the experimental measurements of EMD's of atoms, molecules and solids:

a. X-ray Compton scattering.

b. γ-ray Compton scattering.

c. High-Energy electron scattering.

d. Positron annihilation angular correlation.

e. (e, 2e) technique.

f. Synchrotron radiation scattering.

Since a recent exhaustive review[1] dealing with most of the above methods is available we shall discuss here briefly only the basic features of the above methods. Some of the recent experimental results are also included for the sake of completeness.

I.4.A X-ray Compton Scattering

A typical experimental set-up is shown in Fig. 1.3. Sources of radiation commonly used are MoKα (17.4 KeV) and AgKα (22.2 KeV) lines. A collimated X-ray beam is scattered by the sample and

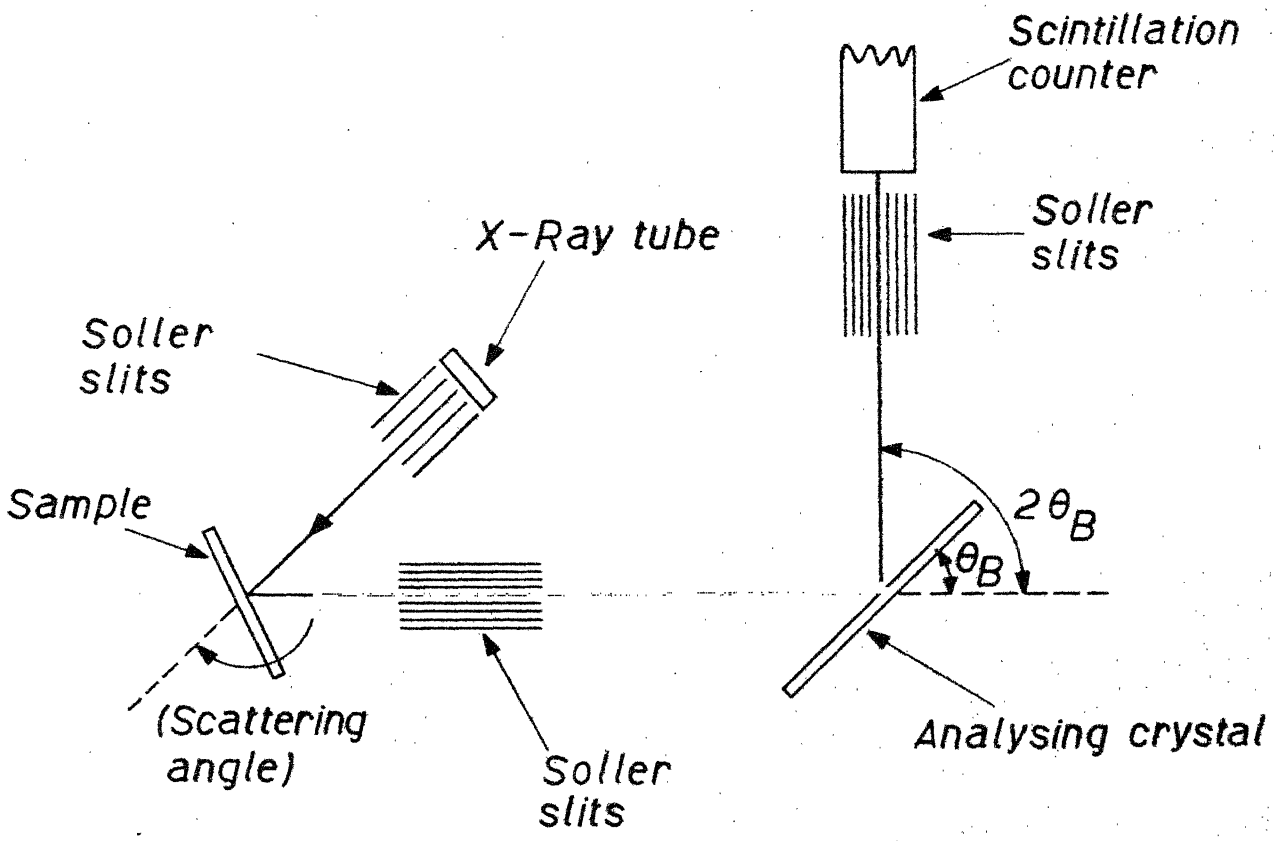

Fig.1.3 Experimental arrangement for X-ray Compton scattering

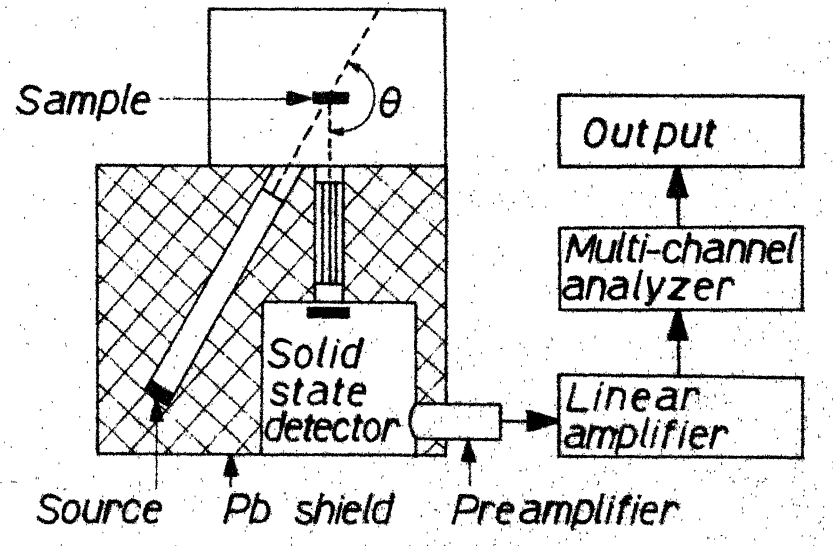

Fig.1.4 Schematic drawing of the experimental arrangement for Y-ray Compton scattering

then diffracted by an analyzing crystal to measure the wavelength (and hence energy) of the scattered radiation via Bragg's law of diffraction. The most severe restriction of X-ray Compton scattering is relatively low intensity of inelastically scattered radiation due to high photoelectric absorption cross-section. As a consequence, high statistical accuracy and good signal to noise ratios are not easily obtained. The incident radiation is non-monochromatic due to the doublet nature of X-rays from the sources discussed above and one cannot afford to lose the scattered intensity further by monochromatizing the incident beam. The CP has to be obtained point by point due to the use of crystal set for only one energy at a time. The background problem is quite complex in the case of X-rays and the resolution is variable. X-rays cannot be effectively employed for elements beyond the first row due to high photoelectric absorption. For higher elements the binding effects are also significant. A factor which favours X-rays over γ-rays is high intensity of the incident radiation, typically $\sim 10^4$ times that of γ-ray sources. X-rays were exclusively employed before the advent of γ-ray techniques for CP measurements (see Epstein[1] and Cooper[3] for reviews). In recent years reports on the use of X-ray technique to measure CP's have virtually disappeared from the literature.

I.4.B γ-ray Scattering

Development of solid-state detectors such as Ge(Li) and Si(Li) has accelerated the growth of this technique. A typical

γ-ray CP set-up is shown in Fig. 1.4. In γ-ray scattering experiment, one can measure all the points of CP simultaneously with a multichannel analyzer. The other chief advantage of γ-ray experiment is that the Compton to photoelectric cross-section ratio, which is proportional to $(E/Z)^3$ is quite high and CP measurements for heavier elements can be carried out. Purity of the incident beam is also ensured automatically. The background problem is much easier to handle in the case of γ-rays than that for X-rays. A critical comparison of X-ray and γ-ray Compton scattering is presented by Eisenberger and Reed.[23] They have also given formulae for all corrections (involved in γ-ray CP measurements) including the relativisitc ones which become significant for highly energetic γ-rays. Fukamachi and Hosoya[24] have studied the optimum conditions in CP measurements by using a solid-state detector. They found that as the energy of the incident photon becomes higher, the optimum scattering angle decreases from its value of 180°. However, the counting efficiency of the detector decreases. They also estimated the effect of both of these factors. More recently, Chaddah and Sahni[25] have reported a careful study of several features governing the choice of γ-ray source, scattering angle, collimation etc. They have pointed out that optimum choice of scattering angle and collimation can offset the poorer penetration of low-energy γ-rays. They also showed that between ^{241}Am (59.54 KeV) and ^{123m}Te (160 KeV) the former can be a worthwhile choice in

contrast to the earlier reports in the literature.

A review of the earlier CP measurements employing γ-ray scattering is available.[1] The γ-ray CP measurements carried out after publication of this review article include comparison of CP's of isomer-pairs: methyl formate and acetic acid[26] as well as cyclopropane and propylene.[27] An annular source of γ-rays was employed in the measurement of CP of solid KF.[28] CP's of a host of ionic solids have been measured (see Paakkari et al.[29] for a review). Sivaramu et al[30] measured differential Compton scattering cross sections for different angles (from 30° to 130°) by interposing cylinders of scatterers of different radii. Swamy et al.[31,32] have obtained Compton spectrum due to L-shell electrons by employing a coincidence technique. Paakkari and Merisalo[33] have measured the CP of gaseous N_2. γ-ray CP's of LiF with scattering vector along <100>, <110> and <111> crystallographic axes have been reported.[34] Manninen et al.[35] have measured CP's of formamide and p-benzoquinone and compared them with theoretical CP's. Reed et al.[36] have obtained CP's of graphite and diamond with γ-ray scattering techniques and compared their results with theory. More recently CP of neopentane has been measured.[37]

The γ-sources commonly used for CP measurements are 59.54 keV ^{241}Am and 160 keV ^{123m}Te. With the latter source, Eisenberger and Reed[23] were able to measure CP of Krypton in three days. A novel method[38] of using a relatively short-lived

isotope of extremely high intensity has also been studied. 412 keV ^{198}Au (half-life 2.7 days) of intensity 70 Ci was used for the measurements of CP's of solid Al and Ge.

I.4.C High-Energy Electron Scattering

Bonham and coworkers[39-42] have developed this technique extensively. The energy-loss spectra of H_2, He, Ne and Ar were measured at low resolution with 45 keV electrons.[39] Wellenstein and Bonham[40] replaced the solid-state detector with an electrostatic differential velocity analyzer. The corrections to be applied for the CP measurements using this method are difficult to estimate and involve exchange as well as correlations between pairs of electronic momenta. However, this method has significant potential due to better resolution and high scattered intensities. Epstein[1] has pointed out that it should be possible to obtain a statistical accuracy of better than 0.1% by this method for light elements. Details of experimental set-up are given by Wellenstein et al.[41,42] CP's of methane and ethylene have been measured by Lahmam-Bennani et al.[43] using high energy electron impact spectroscopy with 35 keV-electrons. Klapthor and Lee have also measured CP of methane by this method.[44] The CP's of ammonia and carbon dioxide have also been recently measured.[45]

I.4.D Positron Annihilation Angular Correlation

De Benedetti et al.[46] pointed out that EMD of positron-electron pairs can be estimated by measuring the angle between

two photons produced in a 2γ-annihilation of a positron and an electron. This method yields more detailed (three dimensional) information about the EMD's than that obtainable with CP measurements. Metal-ammonia solution[47] and organic liquids[48] were the systems of chemical interest studied earlier by this method. Hogg et al.[49] have reviewed the earlier work done with this technique. A recent review[50] which summarizes the positron annihilation work done during 1972-74 is also available.

I.4.E (e,2e) technique

In this method, direction and kinetic energy of scattered as well as ejected electrons are measured in coincidence. By this method one obtains information about the binding energy as well as EMD of the scattering electron. Weigold et al.[51] have attempted to develop this technique by using lower energy electrons and symmetric non-planar geometry. Epstein[1] has pointed out that this method of obtaining EMD's is yet to be developed but is attractive in that the EMD's of electrons in different orbitals may be measured separately by employing this technique.

I.4.F Synchrotron-Radiation Scattering

Recently Cooper et al.[52] have carried out exploratory Compton scattering studies on lithium fluoride, aluminium and copper employing monochromatized radiation from a synchrotron. They employed Ge(Li) detector to obtain energy spectrum of the scattered radiation. Typical time taken to accumulate $\sim$ 10,000

counts at the Compton peak was ~15 minutes in the case of lithium fluoride. However, resolution obtained in this method is rather limited. At shorter wavelengths it is comparable to that obtained in the case of γ-ray CP measurements. Thus, this technique is suitable for carrying out CP measurements at high count rates and good signal to background ratio at modest resolution.

We feel that electron as well as synchrotron radiation scattering and (e,2e) technique are poised for extensive development. However, γ-ray measurements would continue to be popular due to the simplicity of the set-up and a better understanding of the various corrections that are to be applied to the experimental data. In the next section, we shall review various corrections involved in γ-ray and X-ray Compton scattering.

I.5 CORRECTIONS TO X-RAY AND γ-RAY COMPTON SCATTERING DATA

A detailed account of various corrections to X-ray Compton scattering is given by Cooper.[3] Eisenberger and Reed[23] have discussed various corrections applicable to γ-ray CP measurements. The corrections common to both methods are deconvolution and multiple scattering. The other corrections to be applied to X-ray CP data include those for:

(i) wavelength dependence of absorption of X-rays in sample and analyzing crystal.

(ii) Wavelength dependence of polarization factor.

(iii) Removal of white background.

(iv) Doublet nature of the incident beam.

(v) Divergence of the incident beam.

(vi) Application of Breit-Dirac factor.

Corrections applicable to γ-ray CP measurements are:

(i) Background subtraction.

(ii) Absorption of γ-rays in the sample.

(iii) Relativistic corrections.

(iv) Energy dependence of the Compton cross section and other energy dependent factors.

Deconvolution, multiple scattering and relativistic corrections have been studied extensively during the last few years. We shall give here a brief account of these three corrections.

I.5.A Deconvolution

Any spectral measurement can be regarded mathematically as a convolution process

$$h(x) = \int g(x-z).f(z)\,dz \qquad (1.12)$$

where $h(x)$ is the measured spectrum, $f(z)$ is the true spectrum and $g(x-z)$ is the instrumental resolution function. Applying fourier transform (FT) techniques, one obtains

$$F(\zeta) = H(\zeta)/G(\zeta) \qquad (1.13)$$

where F, H and G are FT's of f, h and g respectively, x and z refer to frequency domain and ζ to the time domain. Paatero et al.[53] have discussed three deconvolution schemes in terms of harmonic analysis.

(a) Stokes' method:

$F(\zeta)$ is computed as follows:

$$F(\zeta) = H(\zeta)/G(\zeta) \qquad \text{for } \zeta \leq \zeta_o \tag{1.14}$$

$$F(\zeta) = 0 \qquad \text{for } \zeta > \zeta_o$$

$f(x)$ is synthesized back from $F(\zeta)$.

(b) Generalized least-squares method:

The problem here is to find $f(t)$ such that

$$\int \left(h(x) - \int g(x-t)\, f(t)\, dt \right)^2 dx + \lambda \int \left[\frac{d^k}{dt^k} f(t) \right]^2 dt \tag{1.15}$$

has minimum value. The latter term ensures a smooth solution.

(c) Successive approximations:

The matrix equation corresponding to (1.12) is

$$\underset{\sim}{H} = \underline{\underline{G}}\,\underset{\sim}{F} \tag{1.16}$$

where $\underset{\sim}{H}$ and $\underset{\sim}{F}$ are the vectors containing measured result and the true spectrum, $\underline{\underline{G}}$ is a band matrix containing the instrumental resolution function.

The exact solution of (1.16) is

$$\underset{\sim}{F} = \underline{\underline{G}}^{-1}\,\underset{\sim}{H} \tag{1.17}$$

which can be found iteratively by employing the scheme

$$\underset{\sim}{F}_i = \underset{\sim}{F}_{i-1} + (\underset{\sim}{H} - \underline{\underline{G}}\underset{\sim}{F}_{i-1}), \quad \underset{\sim}{F}_o = \underset{\sim}{H} \tag{1.18}$$

Paatero et al.[53] have given a detailed discussion of practical solution of the least-squares problem and stripping of tails in order that $\underline{\underline{G}}$ in (1.15) does not become unwieldy to handle computationally.

The residual instrumentational function(RIF) is the instrumental function of the whole process, viz. measurement and deconvolution. Paatero et al. have discussed RIF for the above three methods of deconvolution. These RIF's show oscillatory character. However, it would be desirable to have an oscillation-free RIF. Another way to avoid these problems is to convolute the theoretical data with the resolution function and compare directly with experiment after other corrections have been carried out. This approach has been followed in recent measurements.[26]

I.5.B Multiple Scattering

Of late multiple scattering (MS) corrections to the CP measurements have been discussed extensively. Neglecting the contribution due to MS introduces errors typically ~10% in the peak height of the CP. The first attempt to evaluate the effect of MS on CP was done by DuMond,[54] who assumed the electron to be stationary in his treatment. Williams, Pattison and Cooper[55] extended DuMond's work to the case of moving electrons. McIntire[56]

calculated the MS contribution to beryllium CP for back-scattering geometry. Felsteiner et al.[57] and Pattison et al.[58] applied Monte Carlo technique to estimate effects of MS in water and aluminium Compton scattering. Williams and Halonen[59] have investigated qualitatively as well as quantitatively the ratio of double to single scattering. They also carried out Monte Carlo calculations to study this ratio quantitatively and found that the effective sample thickness is a useful parameter for determining the contribution by double-scattering. Halonen et al.[60] applied a Monte Carlo method to calculate spectral distribution of double scattering for aluminium with different sample thicknesses.

More recently Tanner and Epstein have studied MS effects in Compton scattering in a series of papers.[61-63] They calculated[61] the probabilities of single and multiple Compton scattering and angular distribution of scattered radiation analytically assuming Thomson scattering and specific sample geometry. They also gave[62] an analytic as well as numerical treatment of energy profiles for twice scattered photons from stationary electrons from a cylindrical sample. Total probabilities, angular distribution and energy profiles of multiply scattered radiation were evaluated by them[63] by employing Monte Carlo techniques.

As pointed out by Williams et al.[59] MS is the only major outstanding problem in CP measurements and considerable attention is being paid to study it extensively.

I.5.C Relativisitc Corrections

Relativistic corrections become significant in the Compton scattering of high-energy γ-rays. Jauch and Rohrlich[64] have given the expression for total Compton cross section within the relativistic framework. Eisenberger and Reed[65] gave a relativistic treatment of the Compton cross section for the case of free electrons. They also pointed out that a variety of relativistic formulae for the total Compton cross section have previously been employed and this would yield significantly different CP's from a given experimental measurement. Ribberforts[66] has presented a relativistic treatment of differential cross section for Compton scattering against bound electron states for all scattering angles. He also studied[67] this for anisotropic momentum distributions and polarized photons. More recently[68] he has obtained an expression for relativistic differential cross section for the case of a relativistic Maxwell-Boltzmann distribution of electrons.

Having surveyed major experimental methods to measure EMD's and some current developments in the studies of various corrections to the scattering data, we discuss theoretical calculations and interpretation of EMD's and CP's of atoms, molecules and crystals in the following sections.

I.6 SOLUTION OF SCHRÖDINGER's EQUATION IN MOMENTUM SPACE

Starting from the Schrödinger's equation

$$\mathcal{H}\,\psi(\underset{\sim}{r}) = E\psi(\underset{\sim}{r}) \tag{1.19}$$

where $$\mathcal{H} = \frac{p^2}{2} + V(\underset{\sim}{r}) \tag{1.20}$$

and multiplying both sides of (1.19) by $\exp(-i\underset{\sim}{p}.\underset{\sim}{r})$ followed by integration over $\underset{\sim}{r}$, one obtains

$$\frac{p^2}{2}\chi(\underset{\sim}{p}) + \int e^{-i\underset{\sim}{p}\cdot\underset{\sim}{r}} V(\underset{\sim}{r})\,\psi(\underset{\sim}{r})\,d\underset{\sim}{r} = E\chi(\underset{\sim}{p}) \tag{1.21}$$

where $\chi(\underset{\sim}{p})$ is the Fourier transform of $\psi(\underset{\sim}{r})$. This can be formally written as

$$\frac{p^2}{2}\chi(\underset{\sim}{p}) + \int \bar{V}(\underset{\sim}{p'}-\underset{\sim}{p})\,\chi(\underset{\sim}{p'})\,d\underset{\sim}{p'} = E\chi(\underset{\sim}{p}) \tag{1.22}$$

where $$\bar{V}(\underset{\sim}{p'}-\underset{\sim}{p}) = \int V(\underset{\sim}{r}).\exp\left[i(\underset{\sim}{p'}-\underset{\sim}{p}).\underset{\sim}{r}\right] d\underset{\sim}{r} \tag{1.23}$$

(1.21) is an integral equation in momentum space. However for many-electron systems, the solution of (1.22) is a formidable task and such calculations have so far been done only for helium,[69] H_2^+ and H_2.[70]

A simpler approach for obtaining EMD's theoretically is to Fourier transform (FT) the co-ordinate space wave-functions. This approach has been used extensively (see Epstein[1] for formulae for FT's of Gaussian and Slater type orbitals & further references).

I.7 CHEMICAL INTERPRETATION OF ELECTRON MOMENTUM DISTRIBUTIONS

Coulson[71] did the pioneering work in the interpretation of molecular EMD's and CP's from the chemist's point of view. The EMD's for diatomic molecules obtained from Heitler-London as well as MO wavefunctions were analyzed by him. He obtained the result that for both types of wavefunctions the electron is more likely to move perpendicular to the bond rather than along it. Coulson attributed this phenomenon to a "diffraction factor" which arises from the form of the wavefunction employed. Recently a better physical picture has been given[5] in terms of charge accumulation in the internuclear region during bond formation. Coulson[72] also studied the EMD's obtained from hybridized orbitals for hydrocarbons and found that increased p-orbital contribution in a sp^n hybrid orbital makes the momentum distribution broader. Epstein and Lipscomb[73] and Epstein[74] found that the directional characteristics of EMD's are less pronounced in polyatomic molecules than in the diatomic cases due to significant overlap. Epstein[74] has examined the sigma-pi separability in momentum space in the case of benzene. Henneker and Cade[75] have attributed the nearly spherical momentum density in the case of LiF to the high ionic character of the bond in this diatomic molecule. Such a feature is absent in the case of covalent molecules. Tawil and Langhoff[76] analyzed the momentum densities in N_2, O_2 and H_2CO and found that the density shifts from very low momentum values to intermediate momentum. However, the densities for higher values

of the momentum retain essentially atomic nature. More recently Kaijser and Lindner[77] have analyzed the momentum densities for N_2, CO and BF in terms of their sigma and pi symmetries for various states of neutral and singly ionized states. Kaijser and Smith[78] have calculated directional CP's for N_2. They have examined the possibility of obtaining molecular bond lengths from directional Compton profile by studying the oscillatory nature of the Compton profile along the bond. Ahlberg and Lindner[79] have examined the correlation between electrons with parallel spins (Fermi correlation) by introducing a correlation coefficient. They found that the same rules govern the Fermi correlation between electrons in position and momentum space.

Pattison et al.[80] have described a new method of interpreting CP data using the autocorrelation function $B(\underset{\sim}{r})$ of the one-electron wavefunction $\psi(\underset{\sim}{r})$

$$B(\underset{\sim}{r}) = \int \psi(\underset{\sim}{R}) . \psi(\underset{\sim}{r} + \underset{\sim}{R})\, d\underset{\sim}{R} \qquad (1.24)$$

and showed that $B(\underset{\sim}{r})$ can be obtained in any particular direction by taking one-dimensional FT of the corresponding directional CP. They applied this model to LiF and showed that ionic radii can be determined by this approach. More recently Schülke[81] has studied the possibility of mapping the Fermi surface from one-dimensional FT of CP's. He has also given theorems on one dimensional FT of CP's and their applications.[82]

I.8 MOMENTUM EXPECTATION VALUES

Coulson,[83] Benesch and Smith[4] and Epstein[84] have independently derived the relationship between various $< p^n >$ expectation values and CP. $< p^n >$ is given by

$$< p^n > = 2(n+1)\int_0^\infty q^n J(q)\, dq \qquad (1.25)$$

Epstein[84] speculated that it may be possible to correlate $< p >$ with some molecular property such as shielding in nuclear magnetic resonance. $< p^2 >$ is the kinetic energy and relativistic corrections are proportional to $< p^4 >$. Epstein also studied the possibility of calculating these momentum expectation values from CP data. Coulson[83] showed that the energy of a molecular system can be written by employing virial theorem, as

$$E_{mol} = -3\int_0^\infty q^2 J(q)\, dq \qquad (1.26)$$

He pointed out that if individual-component CP's are additive and their sum yields the total molecular CP(as in Localised Molecular Orbital (LMO) approach) E_{mol} is also additive. Thus the additivity of bond energies used extensively in classical thermochemistry is justified in the LMO approach.

I.9 LOCALISED-MOLECULAR ORBITAL STUDIES OF COMPTON PROFILES

Hicks[85] was the first to visualize the use of LMO's in CP calculations. He stated that it may be possible to predict

CP's of a large number of molecles from CP's for relatively smaller number of molecules. Epstein[74] obtained LMO contributions for a large number of bonds and lone pairs from Edmiston-Ruedenberg-localized MO's.[86] However he used an average LMO approach while dealing with multiple bonds. He also showed that the CP's obtained by adding up the individual LMO contributions agree well with those obtained from a full calculation. Eisenberger and Marra[87] utilized this concept of LMO's and derived the LMO profiles for C-H, C-C and C=C bonds from experimental X-ray CP data for a large number of hydrocarbons. More recently Smith and Whangbo[88,89] have also carried out theoretical calculations of LMO contributions to CP's but assuming different contributions for single and multiply bonded cases such as C-C and C=C. This approach can be carried one step further by considering the state of hybridization of each atom in a bond.

I.10 OTHER RECENT CALCULATIONS OF COMPTON PROFILES OF ATOMS, MOLECULES AND CRYSTALS

A thorough review of theoretical calculations of CP's is given by Epstein.[1] This review covers generally the work done upto 1973. Therefore we shall give here an account of only the more recent work done in this area.

Sabin and Trickey[90] have calculated CP's from HFS atomic wavefunctions for various values of the Slater exchange parameter, α. Biggs, Mendelsohn and Mann[91] have prepared extensive tables

of Hartree-Fock CP's for elements upto atomic number 102 for numerical wavefunctions. They have calculated non-relativistic CP's for atomic numbers $Z \leq 36$ and relativistic CP's for higher elements. More recently Benesch[92] has computed CP's for neutral atoms As ($Z = 33$) through Yb ($Z = 70$). These tables[91,92] will serve as reference work for atomic CP's.

Smith and Brown[93,94] and Benesch and Smith[95-97] have investigated the role of correlation in EMD's and CP's using a density matrix approach for Li, Li^+, Be, H_2 and Ne. Smith and Brown[94] found that correlation plays a relatively minor role in EMD's of closed-shell systems such as helium and neon. Correlation, in general, increases J(0) and has little effect on the tail of the CP. Benesch[98] has computed EMD's and CP's from two-electron atomic wavefunctions containing exponential correlation terms. He applied Fourier integral techniques to generate non-diagonal first order density matrices. He also pointed out that the techniques used in his analysis are general and can be applied to larger systems. However, lengthy algebra limits their usefulness.

A review of experimental and theoretical work done in CP's of ionic crystals has been given by Paakkari et al.[29] More recently, Aikala[99,100] has presented a detailed account of theoretical calculations of directional and spherically averaged CP's using a linear combination of atomic orbitals (LCAO) based on Löwdin's orthonormalization procedure.[101] Seth et al.[102] have

calculated LCAO band structure and CP of TiC. Seth and Ellis[103] have computed EMD's and CP's for diamond, silicon and silicon carbide with approximate HFS crystal wavefunctions.

Thulstrump et al.[104] have given formulae for calculation of anisotropic CP's from LCAO-type molecular orbitals. Ramirez et al.[105] have theoretically calculated CP anisotropies in molecules and solids. Snyder and Weber[106] have computed CP of water from a SCF-MO wavefunction in a double-zeta Gaussian basis-set. Whangbo et al.[107] have estimated the effect of hydrogen bonding on CP of water. Smith et al.[108] have investigated the role of correlation on the CP of water. They found that the contribution of electron correlation to CP is not insignificant, but minor in comparison to the effects of basis-set extension. Ahlenius and Lindner[109] have calculated CP's and $\langle p^n \rangle$ values for water, ammonia and methane using large-scale DZ wavefunctions. Ahlenius and Lindner[110] have calculated valence CP's from semi-empirical wavefunctions such as CNDO/2, INDO, EHT etc. and discussed the bond profile transferability. Hirst and Liebmann[111-113] have calculated CP's for 18-, 24- and 42-electron series using MO wavefunctions employing Gaussian basis-sets. Ulsh et al.[114] as well as Braun-Keller and Epstein[115] have analyzed vibrational corrections to the EMD's in the case of H_2 using Wang's[116] wavefunction. Ulsh et al. found that applying the vibrational correction increases the discrepancy between the experiment and theory. Braun-Keller and Epstein, on the other hand, pointed out that

the sign of the vibrational correction is very sensitive to small amount of variation of the electronic wavefunction used in their study.

I.11 SCOPE OF THE PRESENT WORK

It can be seen from the review of the studies of EMD's in atoms, molecules and solids presented in Sections I.1 through I.10 that a vast amount of work has been carried out in this area. However, very few studies have been carried out on atoms using the Slater exchange potential.[117] It is also possible to simulate the wave functions of ions in crystals using a spherical potential around the ion. In Chapter II, CP's of crystal-ions obtained from Hartree-Fock and Hartree-Fock-Slater wave-functions will be discussed. A spherical potential first proposed by Watson[118] has been employed in this model to simulate the behaviour of ions in crystals.

The present work attempts to examine EMD's and CP's obtained from models typically employed in chemistry for studying molecules. EMD's from two-centre VB wavefunctions including ionic terms will be analyzed in Chapter III. It may be noted that the only other theoretical analysis of VB wavefunction was carried out in 1941.[71] In Chapter IV, EMD's and CP's from floating spherical Gaussian orbital (FSGO) model of molecular structure,[119] which has been extremely popular ab-initio model among chemists, will be

discussed. It may be pointed out here that FSGO's have not so far been used for the calculation of EMD's. In Chapter V, CP's of a few hydrocarbons computed from semi-empirical Complete Neglect of Differential Overlap (CNDO) wavefunctions will be examined with a view to study bond-additivity of CP's. As noted in Section I.9, LMO approach to CP's has been recently shown to be promising. In Chapter VI, CP's of acetone and allyl alcohol obtained by the author by scattering of 59.54 keV ^{241}Am γ-rays will be presented and results compared with LMO-theoretical CP's.[74] A method to evaluate atomic and molecular energies from experimental CP's by fitting the CP data to a linear combination of Gaussians will be presented in Chapter VII. The energies thus obtained from experimental CP's will then be compared with the experimental and HF theoretical ones. The possibility of employing this method to obtain accurate molecular energies will then be discussed. We have recently observed a remarkable empirical correlation between the CP and molecular energy in iso-electronic series. Results of this empirical correlation and their implications will be discussed in Chapter VIII.

I.12 SUMMARY AND CONCLUDING REMARKS

In the present chapter, we have given a brief account of phenomenon of Compton scattering for non-stationary electrons. An account of impulse approximation and various assumptions

underlying it was presented in Section I.3. Various experimental methods of determining EMD's of atoms, molecules and solids were surveyed in Section I.4, followed by recent work done on various corrections involved in the CP measurements. Direct solution of Schrödinger's equation in momentum space was briefly discussed in I.6. An account of chemical interpretation of EMD's and momentum expectation-values was given in the next two sections. In I.9, the LMO approach to molecular CP's was discussed, followed by a review in I.10 of recent computations of EMD's of atoms, molecules and crystals. Scope of the work presented in this thesis was discussed in Section I.11.

Recent theoretical and experimental work in the area of EMD's and CP's clearly point to the importance of these re-emerging topics. Further work may bring us closer to the answer for the classic question posed by Mulliken several years ago: "What are the electrons doing in molecules?"

REFERENCES

1. I.R. Epstein in "MTP International Review of Science", Physical Chem., Series II, Theoretical Chem., Eds. A.D. Buckingham and C.A. Coulson, Butterworths, London (1975).

2. J.W.M. DuMond, Rev. Mod. Phys., 5, 1 (1933).

3. M.J. Cooper, Advan. Phys., 20, 453 (1971).

4. R. Benesch and V.H. Smith, Jr., in "Wave Mechanics - The First Fifty Years", Ed. W.C. Price, S.S. Chissick and T. Ravensdale, Butterworths, London (1973).

5. I.R. Epstein, Acct. Chem. Research, 6, 145 (1973).

6. I.R. Epstein and A.C. Tanner in "The Compton Effect", Ed. B.G. Williams, McGraw Hill (to be published).

7. R.M. Singru, Phys. Stat. Sol.(a) 30, 11 (1975).

8. A.S. Eve, Phil. Mag., 8, 669 (1904).

9. D.C.H. Florance, Phil. Mag., 20, 921 (1910).

10. J.A. Gray, J. Franklin Inst., 190, 633 (1920).

11. A.H. Compton, Bull. Nat. Res. Council, 20, 19 (1922).

12. A.H. Compton, Phys. Rev., 21, 483 (1923).

13. P.P. Debye, Phys. Z., 24, 161 (1923).

14. A.H. Compton, Phys. Rev., 22, 412 (1923).

15. G.E.M. Jauncey, Phys. Rev., 24, 204 (1924).

16. J.W.M. DuMond, Phys. Rev., 33, 643 (1929).

17. G.E. Kilby, Proc. Phys. Soc. (London), 86, 1037 (1965).

18. I. Waller and D.R. Hartree, Proc. Roy. Soc., A124, 119 (1929).

19. J.J. Thomson, "Conduction of Electricity Through Gases", Vol., 2, Cambridge University Press (1933).

20. (a) G. Wentzel, Z. Phys., 43, 1 (1927); 43, 779 (1927); 58, 348 (1929); (b) J.W.M. DuMond (ref.16); (c) G.E. Kilby, (ref. 17); (d) P. Eisenberger and P.M. Platzman, Phys. Rev., A2, 415 (1970).

21. R. Currat, P.D. DeCicco and R.J. Weiss, Phys. Rev., 134, 425 (1971).

22. B.J. Bloch and L.B. Mendelsohn, Phys. Rev., A9, 129 (1974).

23. P. Eisenberger and W.A. Reed, Phys. Rev., A5, 2085 (1972).

24. T. Fukamachi and S. Hosoya, Phys. Stat. Sol. (a) 15, 629 (1973).

25. P. Chaddah and V.C. Sahni, Phys. Stat. Sol. (a) 32, 677 (1975).

26. P. Chaddah and V.C. Sahni, Chem. Phys. Letters, 46, 311 (1977).

27. R. Holt, P. Pattison and M. Cooper, Chem. Phys. Letters, 43, 606 (1976).

28. W. Weyrich, Ber. Buns. Phys. Chem., 79, 1085 (1975).

29. T.Paakkari, E.-L. Kohonen, O. Aikala, K. Mansikka, and S. Mikkola, Phys. Fenn., 9, 207 (1974).

30. S. Sivaramu, S. Gopal and B. Sanjeevaiah, Nud. Instr. Methods, 140, 529 (1977).

31. S.T.P.V.J. Swamy and D.S.R. Murthy, Phys. Lett., 55A, 17 (1975).

32. S.T.P.V.J. Swamy, Spectr. Letters, 9, 833 (1976).

33. T.Paakkari and M. Merisalo, Chem. Phys. Letters, 33, 432 (1975).

34. K.-F. Berggren, F. Martino, P. Eisenberger and W.A. Reed, Phys. Rev., B13, 2292 (1976).

35. S. Manninen, P. Pattison, M. Cooper, T. Ahlenius and P. Lindner, Chem. Phys. Letters, 36, 92 (1976).

36. W.A. Reed, P. Eisenberger, K.C. Pandey and L.C. Synder, Phys. Rev., B10, 1507 (1974).

37. W.A. Reed, L.C. Synder, P. Eisenberger, X.J. Pinder, T. Weber and Z. Wasserman, J. Chem. Phys. (1977) (to be published); Private communication from W.A. Reed (May 1977).

38. M. Cooper, P. Pattison and J.R. Schneider, Phil. Mag., 34, 243 (1976).

39. H. Schmoranzer, R.C. Ulsh, R.A. Bonham and J. Ely, J. Chem. Phys., 59, 152 (1973).

40. H.F. Wellenstein and R.A. Bonham, Phys. Rev., A7, 1568 (1973).

41. H.F. Wellenstein, H. Schmoranzer, R.A. Bonham, T.C. Wong and J.S. Lee, Rev. Sci. Instr., 46, 40 (1975).

42. H.F. Wellenstein, H. Schmoranzer, R.A. Bonham, T.C. Wong and J.S. Lee, Rev. Sci. Instr., 46, 89 (1975).

43. A. Lahmam-Bennani, A. Duguet, B. Nguyen and A.D. Barlas, Chem. Phys. Letters, 41, 470 (1976).

44. R.W. Klapthor and J.S. Lee, Chem. Phys. Letters, 45, 413 (1977).

45. A. Lahmam-Bennani, private communication (1977).

46. S. De Benedittti, C.E. Cowan, W.R. Konneker and H. Primakoff, Phys. Rev., 77, 205 (1950).

47. J.A. Arias-Limonta and P.G. Varlashkin, J. Chem. Phys., 52, 581 (1972) and references therein.

48. D.P. Kerr, S.Y. Chuang and B.G. Hogg, Mol. Phys., 10, 13 (1965).

49. B.G. Hogg, G.M. Laidlaw, V.I. Goldanskii and V.P. Shantarovich, At. Energy. Rev., 6, 149 (1968).

50. R.M. Singru, K.B. Lal and S.J. Tao, At. Data Nucl. Data Tables, 17, 271 (1976).

51. E. Weigold, S.T. Hood and P.J.O. Teubner, Phys. Rev. Letters, 30, 475 (1973).

52. M. Cooper, R. Holt, P. Pattison and K.R. Lee, Commun.Phys., 1, 159 (1976).

53. P. Paatero, S.Manninen and T.Paakkari, Phil. Mag., 30, 1281 (1974).

54. J.W.M. DuMond, Phys. Rev., 36, 1685 (1930).

55. B.G. Williams, P. Pattison and M.J. Cooper, Phil. Mag., 30, 307 (1974).

56. W.R. McIntire, Phys. Stat. Sol. (a) 23, 359 (1974).

57. J. Felsteiner, P. Pattison and M.J. Cooper, Phil. Mag., 30, 537 (1974).

58. P. Pattison, S.Manninen, J. Felsteiner and M.J. Cooper, Phil. Mag., 30, 973 (1974).

59. B.G. Williams and V. Halonen, Phys. Fenn., 10, 5 (1975).

60. V. Holonen, B.G. Williams and T.Paakkari, Phys. Fenn., 10, 107 (1975).

61. A.C. Tanner and I.R. Epstein, Phys. Rev., A13, 335 (1976).

62. A.C. Tanner and I.R. Epstein, Phys. Rev., A14, 313 (1976).

63. A.C. Tanner and I.R. Epstein, Phys. Rev., A14, 328 (1976).

64. J.M. Jauch and F. Rohrlich, "The Theory of Photons and Electrons", Addison Wesley, pp. 163-169, 228-235 (1955).

65. P. Eisenberger and W.A. Reed, Phys. Rev., B9, 3237 (1974).

66. R. Ribberforts, Phys. Rev., B12, 2067 (1975).

67. R. Ribberforts, Phys. Rev., B12, 3136 (1975).

68. R. Ribberforts, J. Quant. Spectr. Rad. Transfer, 16, 689 (1976).

69. R. McWeeny and C.A. Coulson, Proc. Phys. Soc. (London), 62A, 509 (1949).

70. R. McWeeny, Proc. Phys. Soc. (London), 62A, 519 (1949).

71. C.A. Coulson, Proc. Camb. Phil. Soc., 37, 55 (1941).

72. C.A. Coulson, Proc. Camb. Phil. Soc., 37, 79 (1941).

73. I.R. Epstein and W.N. Lipscomb, J. Chem. Phys., 53, 4418 (1970).

74. I.R. Epstein, J. Chem. Phys., 53, 4425 (1970).

75. W.H. Henneker and P.E. Cade, Chem. Phys. Letters, 2, 8 (1968).

76. R.A. Tawil and S.R. Langhoff, J. Chem. Phys., 63, 1572 (1975).

77. P. Kaijser and P. Lindner, Phil. Mag., 31, 871 (1975).

78. P. Kaijser and V.H. Smith, Mol. Phys., 31, 1557 (1976).

79. R. Ahlberg and P. Lindner, J. Phys., B9, 1963 (1977).

80. P. Pattison, W. Weyrich and B. Williams, Sol. St. Commun., 21, 967 (1977).

81. W. Schülke, Phys. Stat. Sol. (b) 80, K67 (1977).

82. W. Schülke, Phys. Stat. Sol. (b) to be published (July 1977).

83. C.A. Coulson, Mol. Phys., 26, 507 (1973).

84. I.R. Epstein, Phys. Rev., A8, 160 (1973).

85. B.L. Hicks, Phys. Rev., 57, 665 (1940).

86. C. Edmiston and K. Ruedenberg, Rev. Mod. Phys., 35, 459 (1963).

87. P. Eisenberger and W.C. Marra, Phys. Rev. Letters, 27, 1413 (1971).

88. V.H. Smith, Jr., and M.H. Whangbo, Chem. Phys., 5, 234 (1974).

89. M.H. Whangbo, V.H. Smith, Jr., and W. Von Niessen, Chem. Phys., 6, 282 (1974).

90. J.R. Sabin and S.B. Trickey, J. Phys. B8, 2593 (1975).

91. F. Biggs, L.B. Mendelsohn and J.B. Mann, At. Data Nucl. Data Tables, 16, 201 (1975).

92. R. Benesch, Can. J. Phys., 54, 2155 (1976).

93. R.E. Brown and V.H. Smith, Jr., Phys. Rev., A5, 140 (1972).

94. V.H. Smith, Jr. and R.E. Brown, Chem. Phys. Letters, 20, 424 (1973).

95. R. Benesch and V.H. Smith, Jr., Chem. Phys. Letters, 5, 601 (1970).

96. R. Benesch and V.H. Smith, Jr., Int. J. Quant. Chem., 4, 131 (1971).

97. R. Benesch and V.H. Smith, Jr., Phys. Rev., A5, 114 (1972).

98. R. Benesch, J. Phys., B9, 2587 (1976).

99. O. Aikala, Phil. Mag., 32, 333 (1975).

100. O. Aikala, Phil. Mag., 31, 935 (1975).

101. P.-O. Löwdin, Adv. Phys., 5, 1 (1956).

102. A. Seth, T. Paakari, S. Mannien and A.N. Christensen, Helsinki, No. 1-77 (Jan. 1977).

103. A. Seth and D.E. Ellis, J. Phys. C10, 181 (1977).

104. P.W. Thulstrump, J. Chem. Phys., 65, 3386 (1976).

105. B.I. Ramirez, W.R. McIntire and R.L. Matcha, J. Chem. Phys., 6 , 373 (1977).

106. L.C. Snyder and T.A. Weber, J. Chem. Phys., 63, 113 (1975).

107. M.H. Whangbo, V.H. Smith, Jr., E. Clementi, G.H. Diercksen and W. Von Niessen, J. Phys., B7, L427 (1974).

108. V.H. Smith, Jr., G.H.F. Diercksen and W.P. Kraemer, Phys. Letters, 54A, 319 (1975).

109. T. Ahlenius and P. Lindner, Chem. Phys. Letters, 34, 723 (1975).

110. T. Ahlenius and P. Lindner, J. Phys., B8, 778 (1975).

111. D.M. Hirst and S.P. Liebmann, Mol. Phys., 30, 597 (1975).

112. D.M. Hirst and S.P. Liebmann, Mol. Phys., 30, 1693 (1975).

113. D.M. Hirst and S.P. Liebmann, Chem. Phys. Letters, 42, 403 (1976).

114. R.C. Ulsh, R.A. Bonham, and L.S. Bartell, Chem. Phys. Letters, 13, 6 (1972).

115. E. Braun-Keller and I.R. Epstein, Chem. Phys. Letters, 40, 215 (1976).

116. S. Wang, Phys. Rev., 31, 579 (1928).

117. J.C. Slater, Phys. Rev., 81, 385 (1951).

118. R.E. Watson, Phys. Rev., 111, 1108 (1958).

119. A.A. Frost, J. Chem. Phys., 47, 3707 (1967).

CHAPTER II

COMPTON PROFILES OF FREE AND CRYSTAL-IONS WITH HARTREE-FOCK AND HARTREE-FOCK-SLATER WAVEFUNCTIONS

CHAPTER II

COMPTON PROFILES OF FREE AND CRYSTAL-IONS WITH HARTREE-FOCK AND HARTREE-FOCK-SLATER WAVEFUNCTIONS

II.1 INTRODUCTION

Recently in atomic structure theory, models in which the potential energy is a local functional only of the density, ρ, have been studied extensively (see Slater[1] for an extensive review). The $\rho^{1/3}$ approximation introduced by Slater[2] is probably the most popular one. Writing the Hamiltonian operator in the case of atomic systems as

$$\mathcal{H} = T + V_C + V_X \qquad (2.1)$$

where T, V_C and V_X represent the kinetic energy, Coulomb energy and exchange energy operators respectively. The exchange operator within the Slater approximation expressed in Rydberg units

is given by

$$V_X = - \frac{3\alpha}{2} \{ \frac{3}{\pi} \rho(r) \}^{1/3} \qquad (2.2)$$

Here α is the Slater exchange parameter. The value of $\alpha=1$ has been proposed by Slater[2] while the value of $\alpha=2/3$ has been proposed by Gaspar[3] as well as Kohn and Sham[4]. From model calculations on atomic systems and by comparison with Hartree-Fock calculations the value $\alpha = 1$ has been shown to overestimate the exchange potential whereas the value of $\alpha=2/3$ underestimates it. Several other recipes for choosing the value of α have been given Lindgren and Schwarz[5] suggest the use of different α's for different shells, whereas Schwarz[6] recommend that value of α for which the energy from the Hartree-Fock Slater (HFS) wavefunction agrees closely with the corresponding Hartree-Fock (HF) energy. Several properties of atoms,molecules and crystals have been studied[1] with these models which employ this local functional of density. However, very few attempts have so far been reported in the literature regarding the calculation of electron momentum distributions (EMD) and Compton profiles (CP) of atomic systems employing $\rho^{1/3}$ Slater exchange potential. Singh and Smith[7] have studied the electronic radial momentum distributions of two-, three- and four-electron ions using HF and HFS wavefunctions. They found that the HFS momentum distributions depend significantly on the value of α used. Euwema and Surrat[8]

compared the HF and HFS CP's for Ne, Ar and Kr. They also found that there is a strong dependence of CP's on the value of α used. These authors also found that for Ar and Kr when the value of α is chosen such that the virial theorem is satisfied ($\alpha = \alpha_{VT}$), fairly good agreement between the corresponding HFS and HF CP's results. However, for Ne, this is not the case. More recently, Sabin and Trickey[9] have compared the atomic CP's of He, Li, Be, B and Ne obtained from four model local density functionals. They found that the CP employing the model for which $\alpha = \alpha_{VT}$ gives smallest standard deviation from the CP obtained from correlated wavefunctions for the five atoms studied. However, to the best of our knowledge no extensive calculations of CP's of free ions using HFS wavefunctions have been reported in the literature so far.

On the experimental side, CP's of several ionic solids have recently been measured (see Aikala[10] for a review). An overlap model[10] employing crystals constructed by means of Lowdin's symmetrical orthonormalization method[11] has been used to calculate CP's of these ionic crystals. This model improves upon the free ion results and gives better agreement between the theoretical and experimental CP's. There is yet another simplified model, which simulates the behaviour of ions in crystals, due to Watson.[12] In this model, a spherically symmetric external potential around the ion is employed to simulate the environment of the ion in a crystal. This additional potential is of the form

$$V = n/r_o \qquad \text{for} \quad r \leq r_o \qquad (2.3a)$$

$$= n/r \qquad \text{for} \quad r > r_o \qquad (2.3b)$$

r_o is the radius of the sphere surrounding the ion and the number n of charges is chosen as $n_{sphere} = n_{ion}$, where n_{ion} is the charge on the ion. This potential is shown schematically in Fig. 2.1. Watson model employing the spherical potential has been used by Paschalis and Weiss[13] to calculate various properties of crystals such as diamagnetic susceptibility, dipole polarizability etc. These authors employed STO basis set within the Hartree-Fock framework in their calculation. More recently Sen and Narasimhan[14] have studied the Sternheimer anti-shielding factors and dipole polarizabilities of ions using crystal-ion HFS wavefunctions. Thus, it was felt that it would be worthwhile studying the CP's obtained with the Watson model using HF and HFS wavefunctions and compare the CP's of ionic crystals thus obtained with other theoretical and/or experimental data. When the present work was in progress, a report on measurement of CP of solid KF was published by Weyrich.[15] He also employed the crystal ion wavefunctions of Paschalis and Weiss[13] for calculating crystal ion CP's of K^+ and F^- and found that the crystal CP thus obtained agreed better with the experimental one than the corresponding free ion CP.

We had independently confirmed this observation of Weyrich in the case of CP's of several other ionic crystals calculated from free and crystal ion wavefunctions of Paschalis and Weiss.

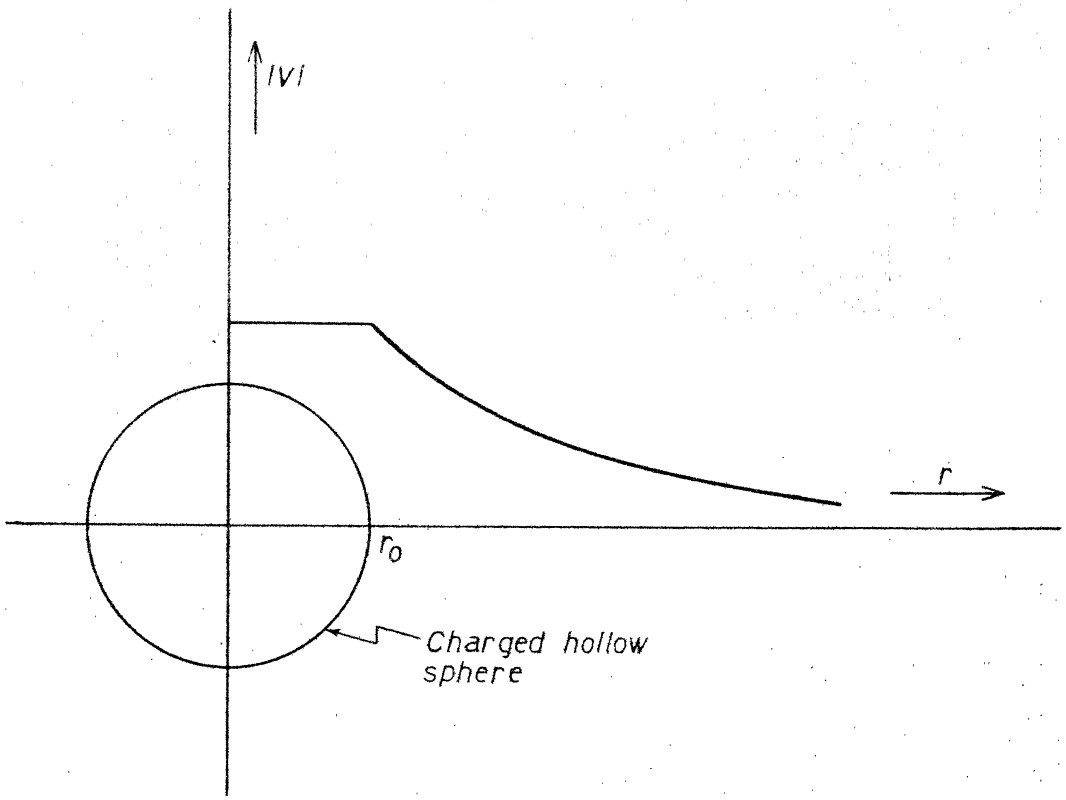

Fig. 2.1 The potential of a charged hollow sphere with a radius r_0 as a function of r.

In the following sections, we present the CP's of Li^+, Be^{2+}, Mg^{2+}, Na^+, K^+ and Cl^- calculated from HF and HFS wavefunctions for both the free and crystal-ion cases. CP's of F^- and O^{2-} using HF free as well as crystal-ion wavefunctions and CP of free Br^- within the HFS framework are also presented. The CP's of ionic crystals thus obtained are then compared with the corresponding experimental CP's. The variation of HFS ionic CP's with the Slater exchange parameter α is also studied.

II.2 METHODS OF CALCULATION

The HF free as well as crystal ion wavefunctions were taken from the tables of Paschalis and Weiss.[13] The sphere radius r_o closest to the Pauling ionic radius[16] was chosen. Radial momentum densities I(p) were computed analytically using the formulae given by Epstein.[17] CP's, J(q), within the impulse approximation,[18] were calculated numerically from these momentum densities by numerical integration using Simpson's rule:

$$J(q) = \frac{1}{2} \int_{|q|}^{\infty} I(p)\, dp / p \qquad (2.4)$$

The HFS free-ion wavefunctions were generated in the present calculations with a modified version of Herman-Skillman[19] atomic structure program. The crystal-ion wavefunctions were generated by using the crystal-potential in equations (2.3a&b). The HFS programs developed in our laboratory by Drs. K.M.S. Saxena[20]

and K.D. Sen[21] were used in these calculations. A 441-point mesh was employed to carry out the integration in the equation

$$I(p) = \sum_{nl} \left| \int r^2 \phi_{nl}(r)\, j_l(pr)\, dr \right|^2 . 4\pi p^2 \qquad (2.5)$$

Here $j_l(pr)$ is the Bessel function and ϕ_{nl} is the HFS orbital. The general subroutine developed by Dr. Saxena was used to carry out this integration numerically. The CP's were calculated from I(p) (which was obtained with equation (2.5)) by employing equation (2.4). The CP's were normalized to the corresponding number of electrons in the range $0 \leq q \leq 15$. Calculation of CP of a shell took a computer time of 5-8 minutes on our IBM 7044/ 1401 system.

II.3 RESULTS AND DISCUSSION

It is well-known[19] that for $\alpha = 1$ and with Latter-Correction to give proper asymptotic behaviour, the HFS wavefunctions agree fairly well with the corresponding HF wavefunctions. When Latter correction is employed along with the value of $\alpha = 2/3$ it is known that poorer HFS wavefunctions result. We may also note here that the free-ion HFS wavefunctions and their α-dependence have already been studied extensively in the literature.[1] However, no study of the variation of α in the HFS framework with the Watson sphere potential for ions has been reported so far in the literature. Hence, in the present program of work we have

included a study of the variation of α and its effect on crystal ion HFS wavefunctions. Weyrich has noted in the case of K^+ and F^- ions that the influence of the radius r_o of the Watson sphere is small compared to the main effect of the charged Watson sphere. Hence, in all the ions studied here, we have fixed the r_o value at the corresponding Pauling ionic-radius[16] and not examined the effect of variation of r_o on the crystal-ion CP's.

Tables 2.1 to 2.5 present our results on cations while Tables 2.6 to 2.9 present our results on anions. Table 2.1 shows the CP's of Li^+ calculated from HF as well as HFS ($\alpha = 1$) free-ion wavefunctions. The HF and HFS (α=1, 0.77, and 2/3) crystal-ion CP's are also shown in this Table. Tables 2.2, 2.3, 2.4, 2.5 and 2.8 show the CP's of Be^{2+}, Na^+, Mg^{2+}, K^+ and Cl^- ions respectively calculated from HF and HFS (α=1) free ion wavefunctions. These tables also show the CP's of the above crystal-ions with HF as well as HFS (with α-variation) wavefunctions. It is known that the convergence in HFS calculations is slow in the case of F^- and O^{2-} ions. Hence these ions were not studied within the HFS framework. In Table 2.9 CP of Br^- calculated from HFS free-ion wavefunction is presented.

We note that the agreement between the free-ion CP's calculated with HF and HFS (α=1) wavefunctions is fairly good in all the cases studied, viz., Li^+, Be^{2+}, Na^+, Mg^{2+}, K^+ and Cl^-. The CP's of crystals LiF, NaF, KF, LiCl, KCl, NaCl, LiBr, NaBr, KBr, BeO and MgO calculated by using these free-ion CP's are

Table 2.1

Compton Profile of Li^+

q	HF free	HFS free	HF r_o=1.13	HFS r_o=1.13 α=1	HFS r_o=1.13 α=0.77	HFS r_o=1.13 α=2/3
0.0	0.656	0.664	0.674	0.716	0.738	0.750
0.1	0.652	0.660	0.672	0.712	0.734	0.746
0.2	0.644	0.650	0.660	0.700	0.722	0.732
0.3	0.628	0.636	0.644	0.680	0.700	0.710
0.4	0.608	0.614	0.620	0.656	0.672	0.680
0.5	0.584	0.580	0.594	0.624	0.640	0.644
0.6	0.556	0.560	0.562	0.590	0.600	0.606
0.7	0.526	0.528	0.528	0.552	0.560	0.562
0.8	0.494	0.496	0.494	0.512	0.518	0.520
0.9	0.460	0.460	0.458	0.472	0.476	0.476
1.0	0.426	0.426	0.422	0.432	0.432	0.432
1.2	0.360	0.359	0.354	0.354	0.352	0.358
1.4	0.298	0.296	0.292	0.286	0.282	0.280
1.6	0.244	0.242	0.238	0.228	0.222	0.220
1.8	0.198	0.196	0.194	0.180	0.174	0.172
2.0	0.160	0.156	0.156	0.142	0.136	0.134
3.0	0.054	0.052	0.052	0.044	0.040	0.038
4.0	0.018	0.020	0.018	0.014	0.014	0.013
5.0	0.008	0.008	0.008	0.006	0.006	0.005

Table 2.2

Compton Profile of Be^{2+}

q	HF free	HFS free	HF r_o=1.11	HFS r_o=1.11 α=1	HFS r_o=1.11 α=0.77
0.0	0.472	0.476	0.520	0.583	0.590
0.1	0.472	0.476	0.518	0.581	0.587
0.2	0.468	0.472	0.514	0.577	0.581
0.3	0.462	0.466	0.504	0.565	0.571
0.4	0.456	0.458	0.492	0.551	0.556
0.5	0.446	0.449	0.478	0.534	0.538
0.6	0.434	0.437	0.462	0.513	0.518
0.7	0.422	0.424	0.444	0.491	0.495
0.8	0.408	0.410	0.424	0.467	0.470
0.9	0.392	0.393	0.402	0.442	0.444
1.0	0.376	0.376	0.380	0.415	0.417
1.2	0.342	0.343	0.338	0.362	0.362
1.4	0.306	0.306	0.296	0.310	0.312
1.6	0.272	0.271	0.258	0.262	0.262
1.8	0.238	0.237	0.222	0.218	0.217
2.0	0.208	0.206	0.192	0.181	0.180
3.0	0.096	0.095	0.088	0.066	0.065
4.0	0.044	0.042	0.040	0.025	0.024
5.0	0.020	0.020	0.020	0.010	0.010

Table 2.3

Compton Profile of Na^+

q	HF free	HFS free	HF r_o=1.80	HFS r_o=1.80 α =1	HFS r_o=1.80 α =0.73
0.0	2.285	2.236	2.294	2.328	2.509
0.1	2.282	2.236	2.288	2.324	2.503
0.2	2.268	2.222	2.274	2.310	2.485
0.3	2.240	2.197	2.246	2.288	2.448
0.4	2.210	2.163	2.216	2.250	2.395
0.5	2.118	2.118	2.124	2.201	2.330
0.6	2.104	2.063	2.110	2.135	2.246
0.7	2.040	1.999	2.040	2.065	2.149
0.8	1.962	1.925	1.961	1.981	2.041
0.9	1.882	1.842	1.882	1.884	1.927
1.0	1.792	1.755	1.792	1.787	1.809
1.2	1.602	1.572	1.602	1.575	1.570
1.4	1.404	1.385	1.404	1.367	1.341
1.6	1.218	1.208	1.212	1.178	1.132
1.8	1.048	1.048	1.042	1.018	0.952
2.0	0.896	0.901	0.890	0.876	0.804
3.0	0.424	0.443	0.422	0.419	0.388
4.0	0.232	0.246	0.232	0.240	0.224
5.0	0.146	0.152	0.146	0.150	0.142

Table 2.4

Compton Profile of Mg^{2+}

q	HF free	HFS free $\alpha=1$	HF $r_o=1.23$	HFS $r_o=1.23$ $\alpha=1$	HFS $r_o=1.23$ $\alpha=0.73$	HFS $r_o=1.23$ $\alpha=2/3$
0.0	1.974	1.941	2.002	2.182	2.289	2.315
0.1	1.970	1.937	2.000	2.178	2.285	2.311
0.2	1.960	1.927	1.990	2.165	2.270	2.295
0.3	1.946	1.912	1.976	2.142	2.245	2.267
0.4	1.924	1.890	1.948	2.108	2.209	2.230
0.5	1.884	1.860	1.918	2.067	2.161	2.182
0.6	1.858	1.822	1.882	2.016	2.102	2.121
0.7	1.816	1.784	1.840	1.955	2.033	2.050
0.8	1.770	1.736	1.788	1.866	1.953	1.968
0.9	1.714	1.680	1.726	1.809	1.865	1.877
1.0	1.650	1.624	1.668	1.725	1.770	1.779
1.2	1.522	1.497	1.534	1.547	1.569	1.572
1.4	1.384	1.364	1.384	1.366	1.367	1.365
1.6	1.242	1.226	1.236	1.191	1.176	1.171
1.8	1.104	1.093	1.092	1.030	1.005	0.997
2.0	0.972	0.968	0.960	0.887	0.858	0.847
3.0	0.278	0.290	0.266	0.253	0.222	0.233
4.0	0.170	0.182	0.170	0.164	0.159	0.155
5.0	0.116	0.122	0.116	0.110	0.107	0.104

Table 2.5

Compton Profile of K^+

q	HF free	HFS free $\alpha=1$	HF $r_o=2.51$	HFS $r_o=2.51$ $\alpha=2/3$	HFS $r_o=2.51$ $\alpha=0.71$	HFS $r_o=2.51$ $\alpha=1$	HFS $r_o=2.51$ $\alpha=1.1$
0.0	4.428	4.477	4.456	4.857	4.805	4.534	4.468
0.1	4.406	4.459	4.438	4.856	4.786	4.508	4.452
0.2	4.358	4.416	4.387	4.769	4.719	4.470	4.400
0.3	4.282	4.339	4.295	4.646	4.601	4.374	4.308
0.4	4.143	4.214	4.168	4.462	4.424	4.225	4.182
0.5	3.978	4.035	3.996	4.216	4.188	4.043	3.993
0.6	3.774	3.802	3.789	3.921	3.903	3.796	3.774
0.7	3.541	3.542	3.546	3.594	3.588	3.537	3.527
0.8	3.288	3.273	3.282	2.254	3.257	3.376	3.253
0.9	3.024	2.984	3.018	2.926	2.937	2.970	2.991
1.0	2.762	2.706	2.748	2.617	2.633	2.701	2.727
1.2	2.275	2.213	2.251	2.093	2.114	2.213	2.146
1.4	1.864	1.820	1.852	1.701	1.721	1.820	1.854
1.6	1.550	1.523	1.540	1.424	1.440	1.523	1.555
1.8	1.316	1.309	1.311	1.242	1.253	1.309	1.331
2.0	1.146	1.141	1.145	1.081	1.087	1.141	1.162
3.0	0.747	0.756	0.746	0.740	0.745	0.756	0.757
4.0	0.541	0.542	0.540	0.537	0.540	0.547	0.548
5.0	0.391	0.386	0.390	0.384	0.385	0.386	0.389

Table 2.6

Compton Profile of F^-

q	HF free	HF r_o=2.57	q	HF free	HF r_o=2.57
0.0	3.440	3.274	1.0	1.844	1.926
0.1	3.426	3.261	1.2	1.473	1.545
0.2	3.380	3.221	1.4	1.170	1.221
0.3	3.292	3.148	1.6	0.931	0.968
0.4	3.154	3.045	1.8	0.754	0.775
0.5	2.971	2.906	2.0	0.616	0.629
0.6	2.756	2.740	3.0	0.276	0.277
0.7	2.525	2.550	4.0	0.160	0.161
0.8	2.288	2.342	5.0	0.106	0.106
0.9	2.060	2.134			

Table 2.7

Compton Profile of O^{2-}

q	HF free	HF r_o=2.646	q	HF free	HF r_o=2.646
0.0	5.426	3.930	1.0	1.546	1.870
0.1	5.358	3.906	1.2	1.186	1.414
0.2	4.892	3.840	1.4	0.916	1.062
0.3	4.140	3.716	1.6	0.710	0.814
0.4	3.478	3.530	1.8	0.566	0.632
0.5	2.986	3.286	2.0	0.464	0.502
0.6	2.596	3.006	3.0	0.222	0.226
0.7	2.280	2.712	4.0	0.134	0.140
0.8	2.004	2.410	5.0	0.088	0.086
0.9	1.776	2.126			

Table 2.8

Compton Profile of Cl^-

q	HF free	HFS free α=1	HF r_o=3.42	HFS r_o=3.42 α=1.1	HFS r_o=3.42 α=1.0	HFS r_o=3.42 α=0.72
0.0	6.018	5.833	5.796	5.482	5.568	5.929
0.1	5.975	5.798	5.760	5.452	5.531	5.891
0.2	5.844	5.664	5.640	5.355	5.425	5.757
0.3	5.586	5.399	5.410	5.177	5.246	5.494
0.4	5.193	5.015	5.080	4.913	4.961	5.110
0.5	4.707	4.557	4.669	4.573	4.600	4.633
0.6	4.176	4.073	4.204	4.176	4.182	4.159
0.7	3.654	3.604	3.736	3.756	3.758	3.668
0.8	3.178	3.173	3.292	3.335	3.321	3.202
0.9	2.748	2.790	2.882	2.944	2.929	2.776
1.0	2.405	2.460	2.523	2.592	2.571	2.108
1.2	1.876	1.946	1.957	2.028	2.014	1.865
1.4	1.530	1.593	1.578	1.637	1.623	1.529
1.6	1.306	1.353	1.331	1.376	1.370	1.307
1.8	1.166	1.188	1.172	1.201	1.202	1.154
2.0	1.051	1.070	1.059	1.073	1.072	1.054
3.0	0.728	0.732	0.727	0.732	0.729	0.730
4.0	0.492	0.504	0.496	0.504	0.502	0.502
5.0	0.325	0.364	0.327	0.365	0.364	0.364

Table 2.9

Compton Profile of Br^-

q	HFS free $\alpha=1$	q	HFS free $\alpha=1$
0.0	7.998	1.0	3.946
0.1	7.961	1.2	3.406
0.2	7.711	1.4	3.054
0.3	7.367	1.6	2.816
0.4	6.959	1.8	2.645
0.5	6.395	2.0	2.506
0.6	5.793	3.0	1.884
0.7	5.229	4.0	1.328
0.8	4.730	5.0	0.944
0.9	4.306		

shown in the Tables 2.10 through 2.20. Also shown in these tables are the results of Aikala[10] using the overlap model. In all the cases examined, we see that the J(0) value is overestimated by both the HF and HFS ($\alpha=1$) free-ion CP's as compared to the corresponding experimental CP's. Thus the model employing free-ion CP's is not a good one to study the CP's of ionic crystals. It may also be noted here that the agreement between HF and HFS ($\alpha=1$) inner-shell CP's of free ions is excellent in all the cases examined. However, the valence-CP's in the HF and HFS ($\alpha=1$) frameworks differ considerably.

We will now examine the HF-crystal-ion CP's presented in Tables 2.1 through 2.9. We see that in the case of all the crystal-anions examined, viz., F^- and O^{2-} and Cl^-, the J(0) value is <u>less</u> than that in the corresponding free HF anions. On the other hand, in the case of crystal-cations, viz., Li^+, Be^{2+}, Na^+, Mg^{2+} and K^+, the HF crystal-ion J(0) value is <u>more</u> than the corresponding free ion J(0) value. The external spherical-potential used to simulate the behaviour of ions in crystals is known[13] to expand the charge distribution in the case of cations and contract it in the case of anions. From this behaviour, it may be expected that in the case of anions, the crystal ion CP's should be broader than the corresponding free-ion ones, leading to a lower J(0) value than that for the free ion. On the other hand, in the case of cations, the crystal-ion CP's are expected to be narrower than the corresponding free ion CP. These expected

Table 2.10

Theoretical and Experimental CP's of LiF

q	HF free	HF crystal	Overlap model	Expt.
0.0	4.096	3.948	3.855	3.849
0.1	4.078	3.933	3.840	3.822
0.2	4.024	3.831	3.794	3.776
0.3	3.920	3.792	3.716	3.704
0.4	3.762	3.665	3.603	3.608
0.5	3.555	3.550	3.461	3.478
0.6	3.312	3.302	3.293	3.318
0.7	3.052	3.078	3.101	3.124
0.8	2.782	2.838	2.886	2.901
0.9	2.520	2.592	2.653	2.666
1.0	2.270	2.348	2.411	2.427
1.2	1.833	1.899	1.932	1.951
1.4	1.468	1.513	1.517	1.519
1.6	1.175	1.206	1.197	1.178
1.8	0.952	0.969	0.962	0.942
2.0	0.776	0.785	0.787	0.769
3.0	0.330	0.329	0.330	0.341
4.0	0.178	0.179	0.181	0.192
5.0	0.116	0.116	0.113	0.112

Table 2.11

Theoretical and Experimental CP's of NaF

q	HF free	HF Crystal	Overlap model	Expt.
0.0	5.725	5.568	5.559	5.662
0.1	5.708	5.549	5.542	5.622
0.2	5.647	5.495	5.488	5.531
0.3	5.532	5.394	5.391	5.395
0.4	5.364	5.261	5.250	5.231
0.5	5.089	5.030	5.068	5.044
0.6	4.860	4.850	4.850	4.828
0.7	4.565	4.590	4.599	4.586
0.8	4.250	4.303	4.322	4.324
0.9	3.942	4.016	4.026	4.045
1.0	3.636	3.718	3.723	3.753
1.2	3.075	3.147	3.130	3.175
1.4	2.574	2.625	2.605	2.623
1.6	2.149	2.180	2.167	2.132
1.8	1.802	1.817	1.808	1.750
2.0	1.512	1.519	1.516	1.473
3.0	0.700	0.699	0.706	0.700
4.0	0.392	0.393	0.396	0.401
5.0	0.254	0.254	0.253	0.241

Table 2.12

Theoretical and Experimental CP's of KF

q	HF free	HF crystal	Expt.
0.0	7.868	7.730	7.654
0.1	7.832	7.699	7.619
0.2	7.738	7.608	7.507
0.3	7.564	7.443	7.321
0.4	7.297	7.213	7.086
0.5	6.949	6.902	6.809
0.6	6.530	6.529	6.489
0.7	6.066	6.096	6.106
0.8	5.576	5.624	5.694
0.9	5.084	5.152	5.265
1.0	4.606	4.674	4.785
1.2	3.748	3.796	3.890
1.4	3.034	3.079	3.127
1.6	2.481	2.508	2.535
1.8	2.070	2.086	2.095
2.0	1.762	1.774	1.780
3.0	1.023	1.023	1.021
4.0	0.701	0.702	0.683
5.0	0.497	0.496	0.487

Table 2.13

Theoretical and Experimental CP's of LiCl

q	HF free	HFS free $\alpha=1$	HF crystal	HFS crystal $\alpha=1$	Overlap model	Expt.
0.0	6.674	6.497	6.470	6.284	6.245	6.360
0.1	6.627	6.458	6.432	6.243	6.209	6.207
0.2	6.488	6.314	6.300	6.125	6.096	6.163
0.3	6.214	6.035	6.054	5.926	5.904	5.932
0.4	5.801	5.629	5.700	5.618	5.642	5.625
0.5	5.291	5.137	5.263	5.224	5.312	5.264
0.6	4.732	4.633	4.766	4.772	4.911	4.861
0.7	4.180	4.132	4.264	4.310	4.443	4.421
0.8	3.672	3.669	3.786	3.833	3.935	3.962
0.9	3.208	3.250	3.340	3.401	3.432	3.506
1.0	2.831	2.886	2.945	3.003	2.973	3.072
1.2	2.236	2.305	2.311	2.268	2.270	2.343
1.4	1.828	1.889	1.870	1.909	1.836	1.854
1.6	1.550	1.595	1.619	1.598	1.562	1.550
1.8	1.364	1.384	1.366	1.382	1.366	1.357
2.0	1.211	1.226	1.215	1.214	1.217	1.221
3.0	0.782	0.784	0.779	0.773	0.780	0.775
4.0	0.510	0.524	0.514	0.516	0.513	0.493
5.0	0.333	0.372	0.335	0.370	0.337	0.334

Table 2.14

Theoretical and Experimental CP's of NaCl

q	HF free	HFS free	HF crystal	HFS crystal $\alpha = 1$	Overlap model	Expt.
0.0	8.303	8.069	8.090	7.896	8.001	8.130
0.1	8.257	8.034	8.048	7.855	7.961	8.040
0.2	8.112	7.886	7.914	7.735	7.834	7.861
0.3	7.826	7.595	7.656	7.534	7.611	7.601
0.4	7.403	7.178	7.296	7.211	7.294	7.263
0.5	6.825	6.693	6.793	6.801	6.893	6.858
0.6	6.280	6.136	6.314	6.317	6.412	6.404
0.7	5.694	5.603	5.776	5.823	5.871	5.919
0.8	5.140	5.098	5.253	5.302	5.307	5.417
0.9	4.630	4.632	4.764	4.813	4.762	4.921
1.0	4.197	4.215	4.315	4.358	4.271	4.455
1.2	3.478	3.518	3.559	3.589	3.494	3.630
1.4	2.934	2.978	2.982	2.990	2.944	2.979
1.6	2.524	2.561	2.543	2.548	2.531	2.493
1.8	2.204	2.236	2.214	2.220	2.206	2.166
2.0	1.957	1.971	1.949	1.948	1.948	1.910
3.0	1.152	1.175	1.149	1.148	1.149	1.160
4.0	0.724	0.750	0.728	0.738	0.726	0.706
5.0	0.471	0.516	0.473	0.514	0.476	0.453

Table 2.16

Theoretical and Experimental CP's of MgO

q	HF free	HF crystal	Overlap model	Expt.
0.0	7.400	5.932	5.597	5.840
0.1	7.328	5.906	5.575	5.821
0.2	6.852	5.830	5.507	5.758
0.3	6.094	5.692	5.39	5.641
0.4	5.402	5.472	5.270	5.465
0.5	4.870	5.204	5.127	5.232
0.6	4.454	4.888	4.946	4.951
0.7	4.096	4.552	4.705	4.632
0.8	3.774	4.198	4.400	4.290
0.9	3.490	3.942	4.048	3.938
1.0	3.196	3.538	3.678	3.595
1.2	2.708	2.948	2.891	2.966
1.4	2.300	2.446	2.432	2.425
1.6	1.952	2.050	2.021	1.988
1.8	1.670	1.724	1.712	1.665
2.0	1.436	1.462	1.467	1.414
3.0	0.500	0.492	0.739	0.710
4.0	0.304	0.310	0.411	0.409
5.0	0.204	0.208	0.259	0.250

Table 2.17

Theoretical and Experimental CP's of BeO

q	HF free	HF crystal	Expt.
0.0	5.898	4.450	3.80
0.1	5.830	4.424	-
0.2	5.360	4.354	3.73
0.3	4.610	4.220	-
0.4	3.934	4.022	3.54
0.5	3.432	3.764	-
0.6	3.030	3.468	3.22
0.7	2.702	3.156	-
0.8	2.410	2.834	2.76
0.9	2.168	2.528	-
1.0	1.922	2.250	2.27
1.2	1.528	1.752	1.81
1.4	1.222	1.358	1.45
1.6	0.982	1.072	1.15
1.8	0.804	0.854	0.93
2.0	0.672	0.694	0.79
3.0	0.318	0.314	0.43
4.0	0.178	0.176	0.25
5.0	0.108	0.106	0.14

Table 2.18

Theoretical and Experimental CP's of LiBr*

q	HFS free $\alpha=1$	Overlap model	Expt.
0.0	8.592	8.320	8.265
0.1	8.551	8.274	8.191
0.2	8.291	8.129	8.000
0.3	7.933	7.886	7.705
0.4	7.502	7.557	7.327
0.5	6.905	7.142	6.890
0.6	6.283	6.630	6.422
0.7	5.687	6.037	5.939
0.8	5.156	5.415	5.449
0.9	4.697	4.830	4.974
1.0	4.398	4.331	4.529
1.2	3.697	3.638	3.789
1.4	3.282	3.239	3.288
1.6	2.990	2.974	2.963
1.8	2.774	2.767	2.726
2.0	2.596	2.592	2.551
3.0	1.870	1.850	1.889
4.0	1.280	1.254	1.266
5.0	0.884	0.854	0.843

*1s Contribution to CP of Br^- subtracted out in order to enable comparison with literature data (ref. 10).

Table 2.19

Theoretical and Experimental CP's of NaBr*

q	HFS free	Overlap model	Expt.
0.0	10.164	10.093	10.053
0.1	10.127	10.043	9.969
0.2	9.863	9.882	9.779
0.3	9.494	9.599	9.483
0.4	9.052	9.205	9.078
0.5	8.443	8.705	8.585
0.6	7.786	8.106	8.027
0.7	7.158	7.442	7.436
0.8	6.585	6.774	6.839
0.9	6.078	6.161	6.270
1.0	5.631	5.640	5.762
1.2	4.978	4.873	4.938
1.4	4.369	4.346	4.334
1.6	3.956	3.941	3.897
1.8	3.628	3.609	3.586
2.0	3.339	3.395	3.298
3.0	2.259	2.218	2.288
4.0	1.506	1.467	1.465
5.0	1.030	0.993	1.005

*Br^- 1s core contribution subtracted out in order to enable comparison with literature data (ref. 10).

Table 2.20

Theoretical and Experimental CP's of KBr*

q	HFS free	Overlap model	Expt.
0.0	12.405	12.238	12.347
0.1	12.350	12.176	12.265
0.2	12.057	12.978	12.030
0.3	11.636	11.630	11.620
0.4	11.103	11.135	11.086
0.5	10.360	10.503	10.461
0.6	9.525	9.752	9.767
0.7	8.701	8.927	9.015
0.8	7.933	8.097	8.244
0.9	6.600	7.322	7.497
1.0	5.962	6.639	6.805
1.2	5.619	5.564	5.683
1.4	4.806	4.806	4.922
1.6	4.271	4.271	4.351
1.8	3.886	3.882	3.893
2.0	3.579	3.578	3.563
3.0	2.572	2.541	2.611
4.0	1.807	1.777	1.748
5.0	1.264	1.233	1.151

*Contribution to CP from 1s shell of Br^- subtracted out in order to enable comparison with literature data (ref. 10).

trends are borne out by the HF free and crystal-ion CP data for Li^+, Be^{2+}, Na^+, Mg^{2+}, K^+, F^-, O^{2-} and Cl^-. We may note here that the CP's of inner shells are nearly identical for each of the HF free and crystal-ions examined. The CP's of ionic crystals LiF, NaF, KF, LiCl, NaCl, KCl, BeO and MgO (shown in Tables 2.10, 2.11, 2.12, 2.13, 2.14, 2.15, 2.19 and 2.20 respectively) were calculated from the HF crystal-ion data. These crystal CP's can be seen to be in better agreement with the experimental ones than the corresponding free-ion CP's, These Tables also show the CP's calculated for these ionic crystals by Aikala et al.[10] with a more elaborate overlap model. The CP's calculated by the overlap model give, in general, better agreement with the experimental ones.

We shall now discuss the main features shown by HFS crystal-ion CP's. Firstly we note that the inner-shell crystal-ion CP's do not differ significantly from the corresponding free-ion ones. Secondly, J(0) value for crystal-cation is <u>more</u> than that for the corresponding free cation, whereas J(0) value for crystal-anion is <u>less</u> than that for the free anion. This is in agreement with the earlier discussion of Paschalis and Weiss in terms of contraction of anions and expansion of cations when placed in an external spherical potential. Thirdly, the HFS crystal-ion CP for a given ion varies significantly with α . This is seen to be the case for all the ions examined (viz., Li^+, Be^{2+}, Na^+, Mg^{2+}, K^+ and Cl^-). We notice that in all the ions under study, the J(0)

value decreases with increasing α. This behaviour can also be expected since a numerically high value of exchange potential is known[19] to lead to a contracted charge distribution. Such a contracted charge distribution implies a broader CP and lower J(O) value. Examining the effect of variation of α on the CP's orbitalwise reveals an interesting phenomenon. The valence orbital CP's are more sensitive to α-variation than the core orbital CP's. To illustrate this we list the different orbital CP's in Mg^{2+} in the HFS framework with the Watson sphere potential as a function of three different α values (see Table 2.21).

Considering α purely as a parameter in the spirit of Lindgren and Schwarz[5,6] we see from the above tables, that there should be a good agreement between the HF and HFS crystal-cation CP's when a value of $\alpha > 1$ is used in the HFS calculations. The J(O) value for K^+ calculated from HFS crystal ion wavefunction with α=1.1 can be seen to be in good agreement with the corresponding HF crystal ion J(O) value. However, in the case of Cl^- ion, as seen from Table 2.8, a value of α lying between 0.72 and 1.0 is expected to give good agreement between the HFS and HF crystal-ion CP's. It is clear from these results that with the addition of the external Watson sphere potential to the ionic HFS hamiltonian the nature of exchange-correlation potential is considerably altered from that of the free ion. This results in the necessity for correcting the exchange correlation potential in a manner which is different for the core and valence orbitals.

Table 2.21

Individual-Orbital Contributions to the CP of Mg^{2+} Crystal Ion (for various α-values) within HFS Framework

	$\alpha = 1$			$\alpha = 0731$			$\alpha = 2/3$		
0.0	0.0747	0.3752	0.2136	0.0753	0.3896	0.2266	0.0756	0.3930	0.2298
0.1	0.0747	0.3730	0.2136	0.0753	0.3872	0.2266	0.0756	0.3905	0.2293
0.2	0.0746	0.3667	0.2136	0.0753	0.3801	0.2265	0.0756	0.3833	0.2297
0.3	0.0745	0.3563	0.2133	0.0752	0.3686	0.2262	0.0755	0.3715	0.2293
0.4	0.0744	0.3424	0.2126	0.0751	0.3533	0.2254	0.0754	0.3558	0.2284
0.5	0.0743	0.3255	0.2113	0.0749	0.3346	0.2237	0.0752	0.3367	0.2267
0.6	0.0742	0.3062	0.2092	0.0747	0.3134	0.2210	0.0743	0.3151	0.2239
0.8	0.0738	0.2630	0.2020	0.0745	0.2664	0.2119	0.0746	0.2671	0.2143
1.0	0.0730	0.2177	0.1906	0.0742	0.2178	0.1978	0.0743	0.2178	0.1995
1.2	0.0722	0.1745	0.1757	0.0728	0.1721	0.1798	0.0730	0.1715	0.1807
1.6	0.0704	0.1034	0.1405	0.0709	0.0988	0.1394	0.0711	0.0978	0.1391
2.0	0.0681	0.0566	0.1063	0.0692	0.0524	0.1024	0.0693	0.0514	0.1014

The CP's of ionic crystals calculated from the HFS ($\alpha=1$) crystal-ion CP's are shown in Tables 2.12, 2.13 and 2.14 for LiCl, NaCl and KCl respectively. These CP's are, in general, in better agreement with the corresponding experimental CP's than the respective free-ion HFS ($\alpha=1$) CP's. However, HFS crystal ion results with $\alpha=1$ do not appear to be as good as HF crystal ion results. Better agreement might result in HFS calculations when α is treated as a parameter.

Commenting on the work of Paschalis and Weiss,[13] Weyrich[15] has pointed out that the virial theorem is violated in their model employing external crystalline potential due to two reasons:

(i) The constant potential inside the sphere does not obey $\frac{1}{r^2}$ force-law.

(ii) The STO's used in their HF calculation were not optimized in the case of crystal-ion wavefunction.

We may note here that the Watson model using HFS wavefunctions does not suffer from the defect (ii) above due to the numerical procedure employed in obtaining the wavefunctions. This fact, coupled with the approach of using α as a parameter makes the HFS-crystal ion model attractive.

II.4 SUMMARY AND CONCLUSIONS

CP's were calculated from HF and HFS ($\alpha=1$) free ion wavefunctions as well as HF and HFS (with α-variation) crystal-ion wavefunctions employing an external spherical potential proposed

by Watson. Use of these crystal-ion CP's gives better agreement with experiment than the use of corresponding free ion CP's. This result holds good both in the HF as well as HFS frameworks. The HFS crystal-ion CP's for valence orbitals show a marked dependence on the value of the α used. Treating α purely as a parameter, it has been shown that a value of α greater than unity gives better agreement between HF and HFS crystal-ion CP's for all the cations examined (viz., Li^+, Be^{2+}, Na^+, Mg^{2+} and K^+) while, for Cl^-, such an agreement may be expected for a value of α less than unity. The introduction of an external potential in the free ion HFS hamiltonian alters the delicate representation of the exchange-correlation term.

One of the reasons for the violation of virial theorem in the case of HF crystal-ion wavefunctions is that the STO exponents used in these wavefunctions have not been optimized. Due to their numerical nature HFS crystal ion wavefunctions do not suffer from this defect. HFS crystal ion wavefunctions obtained with parametrized α seem to offer promise in the calculation of crystal CP's.

REFERENCES

1. J.C. Slater, "The Self Consistent Field for Molecules and Solids", Vol. 4 of 'Quantum Theory of Molecules and Solids", McGraw Hill (1974).

2. J.C. Slater, Phys. Rev., 81, 385 (1951).

3. R. Gaspar, Acta Phys. Acad. Sci. Hung., 3, 263 (1954).

4. W. Kohn and L.J. Sham, Phys. Rev., 140, A 1133 (1966).

5. I. Lindgren and K. Schwarz, Phys. Rev., A5, 542 (1972).

6. K. Schwarz, Phys. Rev., B5 , 2466 (1971).

7. S.R. Singh and V.H. Smith, Jr., Z. Phys., 225, 83 (1972).

8. R.N. Euwema and G.T. Surratt, J. Phys. C 7, 3655 (1974).

9. J.R. Sabin and S.B. Trickey, J. Phys. B8, 2593 (1975).

10. O. Aikala, K. Mansikka and T. Paakkari in "The Compton Effect", Ed. B.G. Williams, McGraw Hill (to be published).

11. P.-O. Löwdin, "A Theoretical Investigation into some Properties of Ionic Crystals", Ph.D. Thesis, Almquist and Wicksell, Uppsala (1948).

12. R.E. Watson, Phys. Rev., 111, 1108 (1958).

13. E. Paschalis and A. Weiss, Theoret. Chim. Acta (Berl.), 13, 381 (1969).

14. K.D. Sen and P.T. Narasimhan, Phys. Rev., B15, 95 (1977).

15. W. Weyrich, Ber. Buns. Phys. Chemie, 79, 1085 (1975).

16. L. Pauling, "Nature of Chemical Bond", Cornell, New York (1960), p. 514.

17. I.R. Epstein, Chem. Phys. Letters, 9, 9 (1970).

18. P. Eisenberger and P.M. Platzman,

19. F. Herman and S. Skillman, "Atomic Structure Calculations", Prentice Hall, New Jersey (1963).

20. K.M.S. Saxena, "Hartree-Fock-Slater Wave Functions and Magnetic Properties of Atoms and Ions and Saturation in Multilevel-Multiresonance Zeeman Systems, "Ph.D. Thesis, I.I.T., Kanpur (1967).

21. K.D. Sen,"Hartree-Fock-Slater Wave Functions and Sternhermer Shielding- Antishielding Factors in Atoms and Ions", Ph.D. Thesis, I.I.T., Kanpur (1975).

CHAPTER III

ELECTRON MOMENTUM DISTRIBUTIONS FROM VALENCE-BOND WAVEFUNCTIONS

CHAPTER III

ELECTRON MOMENTUM DISTRIBUTIONS FROM VALENCE-BOND WAVEFUNCTIONS*

III.1 INTRODUCTION

In 1941 Coulson[1] presented the first paper on the chemical interpretation of electron momentum distributions (EMD) in molecules. He analyzed the EMD's obtained from the Heitler-London (HL) as well as molecular orbital (MO) wavefunctions for diatomic molecules. The momentum-space ($\underset{\sim}{p}$-space) wavefunctions were obtained by him by Dirac transformation[2] of the corresponding co-ordinate-space ($\underset{\sim}{r}$-space) wavefunctions:

$$\chi(\underset{\sim}{p}_1, \underset{\sim}{p}_2, \ldots \underset{\sim}{p}_N) = (2\pi)^{\frac{-3N}{2}} \int e^{-i\{\underset{\sim}{p}_1 \cdot \underset{\sim}{r}_1 + \underset{\sim}{p}_2 \cdot \underset{\sim}{r}_2 + \ldots + \underset{\sim}{p}_N \cdot \underset{\sim}{r}_N\}} \cdot \psi(\underset{\sim}{r}_1, \underset{\sim}{r}_2 \ldots \underset{\sim}{r}_N)\, d\underset{\sim}{r}_1 \ldots d\underset{\sim}{r}_N \quad \ldots(3.1)$$

*The material presented in this chapter has been accepted for publication in the form of a paper: S.R. Gadre and P.T. Narasimhan, Int. J. Quant. Chem. (to be published).

where the electrons are numbered 1,2...N. Coulson also pointed out that the form of the wavefunction is retained in the Dirac transformation (3.1). Thus if one is working within the orbital approximation and with the wavefunction

$$\psi(\underset{\sim}{r}_1, \underset{\sim}{r}_2, \ldots \underset{\sim}{r}_N) = \psi_1(\underset{\sim}{r}_1) \cdot \psi_2(\underset{\sim}{r}_2) \ldots\ldots \psi_N(\underset{\sim}{r}_N) \qquad (3.2)$$

then it is easy to see on substituting in (3.1) that

$$\chi(\underset{\sim}{p}_1, \underset{\sim}{p}_2 \ldots \underset{\sim}{p}_N) = \chi_1(\underset{\sim}{p}_1)\ \chi_2(\underset{\sim}{p}_2) \ldots\ \chi_N(\underset{\sim}{p}_N) \qquad (3.3)$$

Similarly for the electron-pair method, where

$$\psi(\underset{\sim}{r}_1, \underset{\sim}{r}_2 \ldots \underset{\sim}{r}_{2N}) = \psi_{1,2}(\underset{\sim}{r}_1, \underset{\sim}{r}_2) \cdot \psi_{3,4}(\underset{\sim}{r}_3, \underset{\sim}{r}_4) \ldots\ \psi_{2N-1,2N}(\underset{\sim}{r}_{2N-1}, \underset{\sim}{r}_{2N}) \qquad (3.4)$$

one obtains, on substitution in (3.1),

$$\chi(\underset{\sim}{p}_1, \underset{\sim}{p}_2 \ldots \underset{\sim}{p}_{2N}) = \chi_{1,2}(\underset{\sim}{p}_1, \underset{\sim}{p}_2) \cdot \chi_{3,4}(\underset{\sim}{p}_3, \underset{\sim}{p}_4) \ldots\ \chi_{2N-1,2N}(\underset{\sim}{p}_{2N-1}, \underset{\sim}{p}_{2N}) \qquad (3.5)$$

The momentum densities for the HL and MO wavefunctions were obtained by Coulson by squaring the $\underset{\sim}{p}$-space wavefunction. Thus, for a bond A-B, the Heitler-London wavefunction can be written as

$$\psi(\underset{\sim}{r}_1, \underset{\sim}{r}_2) = \{\phi_a(1)\ \phi_b(2) + \phi_a(2)\ \phi_b(1)\}/(2 + 2S^2)^{1/2} \qquad (3.6)$$

where ϕ_a and ϕ_b are the atomic orbitals (AO) centred at the nuclear positions $\underset{\sim}{r}_a$ and $\underset{\sim}{r}_b$ respectively and S is the overlap integral:

$$S = \int \phi_a(\underset{\sim}{r}) . \phi_b(\underset{\sim}{r}) \, d\underset{\sim}{r} \tag{3.7}$$

The following expression was obtained for a homonuclear diatomic molecule starting from the corresponding HL wavefunction (Eq. 3.6) on Fourier transformation and subsequent squaring:

$$|\chi(\underset{\sim}{p}_1, \underset{\sim}{p}_2)|^2 = \frac{1 + \cos\{(\underset{\sim}{p}_1 - \underset{\sim}{p}_2).(\underset{\sim}{r}_a - \underset{\sim}{r}_b)\}}{1 + S^2} \, |A(\underset{\sim}{p}_1)|^2 . |A(\underset{\sim}{p}_2)|^2 \tag{3.8}$$

where $\underset{\sim}{p}_1$ and $\underset{\sim}{p}_2$ are the momenta of electrons 1 and 2 respectively and $A(\underset{\sim}{p})$ is the Fourier transform of the AO $\phi(\underset{\sim}{r})$, viz.,

$$A(\underset{\sim}{p}) = (2\pi)^{-3/2} \int \phi(\underset{\sim}{r}) \, e^{-i\underset{\sim}{p}.\underset{\sim}{r}} \, d\underset{\sim}{r} \tag{3.9}$$

Coulson pointed out that the momentum density corresponding to electron 1 can be obtained from (3.8) by integration over $\underset{\sim}{p}_2$. It can also be obtained more easily by employing a mixed wavefunction of $\underset{\sim}{p}_1$ and $\underset{\sim}{r}_2$ followed by integration over the co-ordinate $\underset{\sim}{r}_2$. The momentum densities obtained from valence-bond (VB) wavefunctions by these two procedures can be shown to lead to identical results. This technique of using a mixed wavefunction to obtain momentum density corresponding to electron 1 was

introduced by Coulson[1] who obtained the following expression for this quantity:

$$|\chi(\underset{\sim}{p}_1)|^2 = \frac{1+S\cos\{\underset{\sim}{p}_1\cdot(\underset{\sim}{r}_a-\underset{\sim}{r}_b)\}}{1+S^2}\,|A(\underset{\sim}{p}_1)|^2 \qquad (3.10)$$

The corresponding result for a MO wavefunction for a homonuclear diatomic molecule

$$\psi(\underset{\sim}{r}) = (\phi_a+\phi_b)/(2+2S^2)^{1/2} \qquad (3.11)$$

is

$$|\chi(\underset{\sim}{p})|^2 = \frac{1+\cos\{\underset{\sim}{p}\cdot(\underset{\sim}{r}_a-\underset{\sim}{r}_b)\}}{1+S}\,|A(\underset{\sim}{p})|^2 \qquad (3.12)$$

It was pointed out by Coulson that the momentum densities in (3.10) and (3.12) show maxima when the electron moves perpendicular to the bond direction. Expression (3.8) shows additional maxima for $\underset{\sim}{p}_1=\underset{\sim}{p}_2$. This means, according to Coulson, that if atoms A and B are considered in terms of oscillators, there is binding when the oscillators are "in phase". Considering the repulsive-state wavefunction

$$\psi_{rep}(\underset{\sim}{r}_1,\underset{\sim}{r}_2) = \{\phi_a(1)\phi_b(2)-\phi_b(1)\phi_a(2)\}/(2-2S^2)^{1/2} \qquad (3.13)$$

he obtained

$$|\chi(\underset{\sim}{p}_1,\underset{\sim}{p}_2)|^2 = \frac{1-\cos\{(\underset{\sim}{p}_1-\underset{\sim}{p}_2)\cdot(\underset{\sim}{r}_a-\underset{\sim}{r}_b)\}}{1+S^2}\,|A(\underset{\sim}{p}_1)|^2\cdot|A(\underset{\sim}{p}_2)|^2 \qquad (3.14)$$

and by employing mixed wavefunction involving $\underset{\sim}{p}_1$ and $\underset{\sim}{r}_2$ followed by integration over $\underset{\sim}{r}_2$, the momentum density corresponding to electron 1 is obtained as

$$| \chi_{rep}(\underset{\sim}{p}_1) |^2 = \frac{1-S\cos\{\underset{\sim}{p}_1.(\underset{\sim}{r}_a-\underset{\sim}{r}_b)\}}{1-S^2} |A(\underset{\sim}{p}_1)|^2 \qquad (3.15)$$

According to (3.14), the momentum density vanishes for $\underset{\sim}{p}_1=\underset{\sim}{p}_2$ for all values of the internuclear distance $R=|\underset{\sim}{r}_a-\underset{\sim}{r}_b|$. Expression (3.15) shows a minimum when the electron moves perpendicular to the bond.

In this chapter, we present an analysis carried out by us on lines similar to those of Coulson but explicitly including ionic terms as well. To the best of our knowledge, no such analysis has been done previously. Earlier, Hicks[3] calculated the shape of the Compton line for H_2 using VB wavefunction of Weinbaum[4] which includes ionic terms as well as polarization (2p orbital). However, Hicks did not analyse the detailed characteristics of VB momentum densities and their dependence on ionic terms. Here we will discuss specifically the effect of adding ionic terms on the momentum densities (Section III.2). In Section III.3 we discuss the Compton profile (CP) of H_2 with a view to assess the importance of ionic terms as well as polarization. We also present the CP calculated from an MO wavefunction of Shull and Ebbing[5] which employs floating functions. Comparison with other available theoretical data as well as experimental CP

is also made. In Section III.4, the VB wavefunction constructed from the orthogonalized atomic orbitals (OAO) is examined in the $\underset{\sim}{p}$-space. The results are then compared with an analysis of Slater[6] who showed that an HL wavefunction constructed from OAO's shows no minimum diagonal energy for the H_2 molecule.

III.2 WAVEFUNCTION WITH IONIC-TERMS

The $\underset{\sim}{r}$-space wavefunction for a homonuclear diatomic molecule A-B including the ionic terms A^+B^- and A^-B^+ is

$$\psi(\underset{\sim}{r}_1,\underset{\sim}{r}_2) = \frac{\phi_a(1)\phi_b(2)+\phi_b(1)\phi_a(2)+\lambda\{\phi_a(1)\phi_a(2)+\phi_b(1)\phi_b(2)\}}{\{(1+\lambda^2)(2+2S^2)+8\lambda S\}^{1/2}} \tag{3.16}$$

This yields the following expression for the momentum density

$$|\chi(\underset{\sim}{p}_1,\underset{\sim}{p}_2)|^2 = \frac{|A(\underset{\sim}{p}_1)|^2\cdot|A(\underset{\sim}{p}_2)|^2}{(1+\lambda^2)(1+S^2)+4\lambda S}\{1+\cos[(\underset{\sim}{p}_1-\underset{\sim}{p}_2)\cdot(\underset{\sim}{r}_a-\underset{\sim}{r}_b)]+\lambda^2 + \lambda^2\cos[(\underset{\sim}{p}_1+\underset{\sim}{p}_2)\cdot(\underset{\sim}{r}_a-\underset{\sim}{r}_b)] + \lambda(\cos[\underset{\sim}{p}_1\cdot(\underset{\sim}{r}_a-\underset{\sim}{r}_b)]+\cos[\underset{\sim}{p}_2(r_a-r_b)])\} \tag{3.17}$$

On comparing this result with Eq. (3.8) for the purely covalent HL wavefunction (3.6), we find additional terms such as $\cos\{(\underset{\sim}{p}_1+\underset{\sim}{p}_2)\cdot(\underset{\sim}{r}_a-\underset{\sim}{r}_b)\}$, $\cos\{\underset{\sim}{p}_1\cdot(\underset{\sim}{r}_a-\underset{\sim}{r}_b)\}$ etc. in the "diffraction factor". Hence no definite phase relationship which leads to

maxima in $|\chi(\underset{\sim}{p}_1,\underset{\sim}{p}_2)|^2$ can be obtained in terms of the oscillator picture. Thus the "in-phase" oscillator picture seems to be valid only for the purely covalent HL wavefunction. We also note here that the purely ionic terms A^+B^- and A^-B^+ individually give rise to the term $\cos\{(\underset{\sim}{p}_1+\underset{\sim}{p}_2).(\underset{\sim}{r}_a-\underset{\sim}{r}_b)\}$ which implies that the momentum density is maximum for $\underset{\sim}{p}_1=-\underset{\sim}{p}_2$. Thus the momentum density for a purely ionic term shows a maximum when the oscillators are "out-of-phase". The momentum density corresponding to electron 1 obtained from the VB wavefunction (3.16) following the use of a mixed wavefunction involving $\underset{\sim}{p}_1$ and $\underset{\sim}{r}_2$ is:

$$|\chi(\underset{\sim}{p}_1)|^2 = \frac{1+\lambda^2+2\lambda S+\{S+S\lambda^2+2\lambda\}\cos\{\underset{\sim}{p}_1.(\underset{\sim}{r}_a-\underset{\sim}{r}_b)\}}{\{(1+\lambda^2)(1+S^2)+4\lambda S\}}\,|A(\underset{\sim}{p}_1)|^2 \qquad (3.18)$$

Analogous to (3.5) and (3.8), this expression also shows maxima for $\underset{\sim}{p}_1.(\underset{\sim}{r}_a-\underset{\sim}{r}_b)=0$. Thus the present results obtained for VB wavefunction (3.11) agree with the earlier analysis by Coulson, of HL and MO wavefunctions, in terms of greater probability of an electron moving perpendicular to the bond rather than along it. However, the phase relationship, in the oscillator picture, existing for the HL wavefunction is seen to be absent for the VB wavefunction which includes "covalent" as well as "ionic" terms. It must, however, be borne in mind that this phase relationship is an artefact of the purely covalent VB wavefunction and should not be considered to have any physical significance.

We will now present a similar analysis for the wavefunction of a heteronuclear diatomic molecule. If, according to chemical intuition based upon the electronegativities, only one ionic term, say A^-B^+, is included then the expression for the momentum density apart from the normalisation constant is, with an obvious notation,

$$
\begin{aligned}
|\chi(\underset{\sim}{p}_1, \underset{\sim}{p}_2)|^2 = {} & |A(\underset{\sim}{p}_1)|^2 |B(\underset{\sim}{p}_2)|^2 + |A(\underset{\sim}{p}_2)|^2 . |B(\underset{\sim}{p}_1)|^2 + \\
& \lambda^2 |A(\underset{\sim}{p}_1)|^2 . |A(\underset{\sim}{p}_2)|^2 + 2|A(\underset{\sim}{p}_1)| . |B(\underset{\sim}{p}_1)| . |A(\underset{\sim}{p}_2)| . |B(\underset{\sim}{p}_2)| . \\
& \times \cos\{(\underset{\sim}{p}_1 - \underset{\sim}{p}_2)(\underset{\sim}{r}_a - \underset{\sim}{r}_b) + \arg \frac{B(\underset{\sim}{p}_1)}{A(\underset{\sim}{p}_1)} - \arg \frac{B(\underset{\sim}{p}_2)}{A(\underset{\sim}{p}_2)} \} \\
& + 2\lambda . |A(\underset{\sim}{p}_1)|^2 . |B(\underset{\sim}{p}_2)| . |A(\underset{\sim}{p}_2)| . \cos\{\underset{\sim}{p}_2(\underset{\sim}{r}_a - \underset{\sim}{r}_b) + \arg \frac{B(\underset{\sim}{p}_2)}{A(\underset{\sim}{p}_2)} \} \\
& + 2\lambda |A(\underset{\sim}{p}_1)|^2 . |A(\underset{\sim}{p}_2)| . |B(\underset{\sim}{p}_1)| . \cos\{\underset{\sim}{p}_1(\underset{\sim}{r}_a - \underset{\sim}{r}_b) + \arg \frac{B(\underset{\sim}{p}_1)}{A(\underset{\sim}{p}_1)} \}
\end{aligned}
\tag{3.19}
$$

If we take into account the fact, as previously pointed out by Coulson[1] that in most cases where bonds are formed, conditions of symmetry imply $\arg A(\underset{\sim}{p}) = \arg B(\underset{\sim}{p})$, the above expression is considerably simplified. The result thus obtained from (3.19) by imposing this symmetry criterion is similar to (3.17), but the term $\cos\{(\underset{\sim}{p}_1 + \underset{\sim}{p}_2).(\underset{\sim}{r}_a - \underset{\sim}{r}_b)\}$ is absent, corresponding to the inclusion of only one ionic term A^-B^+. Such a term reappears on inclusion of both the ionic terms A^-B^+ and A^+B^-. The general conclusion that can be drawn from (3.19) is similar to that obtained

from (3.17), viz., the "phase relationship" in the oscillator picture becomes complex with the introduction of one or more ionic terms even in the heteronuclear cases.

III.3 EFFECT OF INCLUSION OF IONIC TERMS AND POLARIZATION ON THE COMPTON PROFILE OF H_2

As mentioned earlier in Section III.1, Hicks[3] calculated the shape of the Compton line of H_2 using Weinbaum's[4] wavefunction constructed from AO's of the form $1s(\underset{\sim}{r}) + \sigma 2p(\underset{\sim}{r})$ and including ionic terms as well (wavefunction of ionic-polarization type). More recently Eisenberger[7] has reported the CP of H_2 measured with 17.37 keV Mo X-rays, alongwith the theoretical HF-SCF and MC-SCF CP's. We may note here that the agreement between theoretical and experimental CP's is not good even with high quality MC-SCF wavefunction. Brown and Smith[8] have calculated CP of H_2 using Liu's configuration-interaction (CI) wavefunction which includes 39 configurations. This gives satisfactory agreement with experiment. We may note here that the comparison between theory and experiment must be done cautiously due to several experimental factors. The experimental results have to be corrected for multiple scattering.[9] However, multiple scattering is not expected to be appreciable in the case of H_2. The deconvolution procedure employed to remove the effects of instrumental broadening is known to lead to oscillatory behaviour[10] and yet the results have to be corrected for

the residual instrumental function.[10]

Since the ionic terms in VB theory play a role similar to that of CI in MO theory, it is desirable to analyze the effect of adding ionic terms to the HL wavefunction on the CP of H_2. We have examined here the simple VB wavefunctions of Wang,[11] Weinbaum[4] and MO wavefunction of Shull and Ebbing[5] employing floating functions. The details of these wavefunctions are given in Table 3.1. Hicks[3] calculated the shape of the Compton line using Weinbaum's[4] wavefunction of ionic-polarization type but assuming experimental internuclear distance of 1.40 a.u. He carried out the integrations involved in the calculation graphically to within 1% accuracy. We have repeated the calculations of Hicks for the internuclear distances of 1.40 a.u. and 1.43 a.u. The momentum densities & CP's given by these two sets of values agree with each other to within 0.2%. The CP's, within the impulse approximation,[12] are obtained from one-electron momentum densities via (3.20) and (3.21).

$$I(p) = \int p^2 \rho(\underset{\sim}{p}) \sin\theta_p . d\theta_p d\phi_p \qquad (3.20)$$

$$J(q) = \int_{|q|}^{\infty} \frac{I(p)}{2p} dp \qquad (3.21)$$

For the wavefunctions employing only s-type AO's, the integration in (3.20) is simple. Though more complex, it can be done analytically for a wavefunction involving polarization. The

Table 3.1

Details of the H_2 Wavefunctions Employed in the Present Compton Profile Calculations

No.	Author & reference	-Energy (a.u.)	Inter-nuclear distance (a.u.)	Form of the wavefunction	Orbital exponent	Other parameters
1.	Wang[11]	1.139	1.406	$1s_a 1s_b + 1s_b 1s_a$	1.166	-
2.	Weinbaum[4] ionic-type	1.148	1.42	$1s_a 1s_b + 1s_b 1s_a + \lambda(1s_a 1s_a + 1s_b 1s_b)$	1.193	$\lambda = 0.256$
3.	Weinbaum[4] ionic-polarization type	1.152	1.43	$\phi_a \phi_b + \phi_b \phi_a + \lambda(\phi_a \phi_a + \phi_b \phi_b)$ $\phi = 1s(\underset{\sim}{r}) + \sigma\, 2p(\underset{\sim}{r})$	1.19	$\lambda = 0.171$ $\sigma = 0.07$
4.	Shull & Ebbing[5]	1.144	1.42	$1s_c 1s_d + 1s_d 1s_c + (1s_c 1s_c + 1s_d 1s_d)$	1.19	c and d are inside the molecule, 0.036 a.u. from the corresponding nuclei.

integration in (3.21) was carried out numerically by using Simpson's rule. The CP's obtained were normalized to two electrons by

$$\int_0^\infty J(q)\, dq = 1 \qquad (3.22)$$

Overlap integrals were evaluated by the standard formulae of Mulliken et al.[13] Theoretical CP, J(q), normalized to two electrons for the above mentioned wavefunctions alongwith the experimental and CI-theoretical profiles are presented in Table 3.2. The CP's calculated from Weinbaum's wavefunctions can be seen to be quite close to the CI-theoretical profiles. The J(0) value for the polarized wavefunction is higher than that for the unpolarized one since the 2p orbital leads to a narrower CP. On the other hand, the CP computed from Wang's wavefunction does not agree so well with either the experimental or CI-theoretical profile in the smaller q-region. The observation that the CP calculated from VB wavefunction including ionic terms agrees well with the CI-theoretical profile in the case under study does not imply that the CP's obtained from the VB wavefunctions will always give a very good agreement with the corresponding CI-theoretical profiles. However, the addition of ionic terms seems to improve the EMD's markedly. In the light of this experience with H_2 molecule one may say that the inclusion of ionic terms would be quite necessary for the calculation of CP's of heteronuclear molecules from VB wavefunctions.

Table 3.2

Comparison of Theoretical and Experimental Compton Profiles of H_2
(all values in a.u.)

q	Heitler-London[a]	Heitler-London +ionic terms[b]	VB wavefunction including polarization[c]	Floating-orbital MO wavefunction[d]	Configuration interaction[e]	Expt.[f]
1	2	3	4	5	6	7
0.0	1.545	1.530	1.537	1.536	1.529	1.513
0.1	1.509	1.495	1.501	1.501	1.493	1.475
0.2	1.407	1.396	1.401	1.401	1.393	1.378
0.3	1.255	1.250	1.253	1.253	1.245	1.240
0.4	1.076	1.076	1.076	1.078	1.069	1.065
0.5	0.892	0.895	0.894	0.896	0.888	0.887
0.6	0.718	0.723	0.722	0.724	0.717	0.712
0.7	0.565	0.571	0.569	0.570	0.566	0.561
0.8	0.436	0.442	0.440	0.442	0.440	0.435
0.9	0.333	0.338	0.336	0.337	0.337	0.334
1.0	0.251	0.256	0.254	0.254	0.253	0.255
1.2	0.141	0.144	0.142	0.142	0.147	0.150
1.4	0.079	0.080	0.080	0.079	0.084	0.089

Table III.2 (contd.)

1	2	3	4	5	6	7
1.6	0.045	0.045	0.045	0.044	0.049	0.051
1.8	0.026	0.026	0.026	0.025	0.029	0.030
2.0	0.016	0.016	0.015	0.015	0.017	0.015

[a] Calculated from Wang's[11] wavefunction.

[b] Calculated from Weinbaum's[4] wavefunction without polarization.

[c] Calculated from Weinbaum's[4] wavefunction of ionic-polarization type constructed from AO's of the form $1s(\underset{\sim}{r}) + \sigma\, 2p(\underset{\sim}{r})$.

[d] Calculated from MO wavefunction of Shull and Ebbing[5] constructed from floating orbitals.

[e] Calculated by Brown and Smith[8] using CI wavefunction of Liu.

[f] Experimental data from ref 7. Following error estimates were reported: $\pm$0.7% at q=0.0; $\pm$1% at q=0.6; $\pm$3% at q=1.2 and $\pm$10% at q=1.8.

III.4 ANALYSIS OF OAO RESULTS OF SLATER IN TERMS OF MOMENTUM DENSITIES

Slater[6] has shown, with the example of H_2 molecule that if a VB calculation is done using only the covalent wavefunction constructed from OAO's instead of overlapping AO's, the resultant diagonal energy of the lowest singlet shows no minimum. We present here our momentum density results from a wavefunction constructed from OAO's $\bar{\phi}_a$ and $\bar{\phi}_b$ which are, in turn, linear combinations of the overlapping AO's ϕ_a and ϕ_b

$$\begin{aligned} \bar{\phi}_a &= C_1 \phi_a + C_2 \phi_b \\ \bar{\phi}_b &= C_2 \phi_a + C_1 \phi_b \end{aligned} \tag{3.23}$$

where C_1 and C_2 are determined by the normalization condition

$$C_1^2 + 2C_1C_2S + C_2^2 = 1 \tag{3.24}$$

S is the overlap between ϕ_a and ϕ_b and the orthogonality between $\bar{\phi}_a$ and $\bar{\phi}_b$ is given by

$$\int \bar{\phi}_a \bar{\phi}_b \, d\underset{\sim}{r} = 0 \tag{3.25}$$

which leads to

$$2C_1C_2 + (C_1^2 + C_2^2)S = 0 \tag{3.26}$$

Following Slater,[6] the HL wavefunction constructed from the OAO's is

$$\bar{\psi}_{cov} = \bar{\phi}_a(1)\bar{\phi}_b(2) + \bar{\phi}_a(2)\bar{\phi}_b(1)$$

$$= \frac{1}{\sqrt{2(1-S^2)}}\left[\phi_a(1)\phi_b(2) + \phi_b(1)\phi_a(2) - S\{\phi_a(1)\phi_a(2) + \phi_b(1)\phi_b(2)\}\right] \tag{3.27}$$

With this wavefunction, the momentum density corresponding to electron 1 is

$$|\chi(\underset{\sim}{p}_1)|^2 = \frac{1-S\cos\{\underset{\sim}{p}_1.(\underset{\sim}{r}_a-\underset{\sim}{r}_b)\}}{1-S^2}\,|A(\underset{\sim}{p}_1)|^2 \tag{3.28}$$

It will be seen that this equation is exactly identical with Eq. (3.15) obtained for the repulsive-state wavefunction (3.13). Thus, since the momentum densities corresponding to electron 1 are identical, for all the values of $\underset{\sim}{p}_1$, in the case of wavefunctions (3.27) and (3.13) and as (3.13) is a repulsive state, (3.27) also may not be expected to show binding. This conclusion is in accordance with the earlier discussion of Slater.

We can reach the same conclusion on comparing the "diffraction factors" for (3.6) and (3.27). The diffraction factor for the former is maximum whereas that for the latter is minimum when the electron moves perpendicular to the bond. The latter reaches maximum for $\underset{\sim}{p}_1.(\underset{\sim}{r}_a-\underset{\sim}{r}_b) = \pi$ where $|A(\underset{\sim}{p}_1)|^2$ is already quite small.

Thus, for the wavefunction (3.27), the probability of the electron moving perpendicular to the bond is less than that for the motion along the bond direction and hence it should not show binding.

The ionic wavefunction constructed from OAO's is

$$\bar{\psi}_{\text{ionic}} = \bar{\phi}_a(1)\bar{\phi}_a(2) + \bar{\phi}_b(1)\bar{\phi}_b(2) \qquad (3.29)$$

$$= \frac{1}{\sqrt{2(1-S^2)}}\left[\phi_a(1)\phi_a(2) + \phi_b(1)\phi_b(2) - S\{\phi_a(1)\phi_b(2) + \phi_a(2)\phi_b(1)\}\right]$$

This wavefunction leads to an expression for the momentum density which is identical to (3.28). Thus, purely covalent and ionic wavefunctions constructed from OAO's yield momentum densities identical to that for the repulsive-state wavefunction. Wavefunctions (3.13), (3.27) and (3.29) can be shown to lead to identical $\underset{\sim}{r}$-space density matrices of first order,[14]

$\gamma(\underset{\sim}{r}_1' | \underset{\sim}{r}_1)$ where

$$\gamma(\underset{\sim}{r}_1' | \underset{\sim}{r}_1) = N \int \psi^*(\underset{\sim}{r}_1', \underset{\sim}{r}_2) \cdot \psi(\underset{\sim}{r}_1, \underset{\sim}{r}_2)\, d\underset{\sim}{r}_2 \qquad (3.30)$$

The corresponding density matrix in the momentum space[15] is given by

$$\gamma(\underset{\sim}{p}' | \underset{\sim}{p}) = (2\pi)^{-3} \int \gamma(\underset{\sim}{r}' | \underset{\sim}{r}) \cdot e^{-i(\underset{\sim}{p}\cdot\underset{\sim}{r} - \underset{\sim}{p}'\cdot\underset{\sim}{r}')}\, d\underset{\sim}{r}\, d\underset{\sim}{r}' \qquad (3.31)$$

Since $\gamma(\underset{\sim}{r}'|\underset{\sim}{r})$ is identical for these wavefunctions, $\gamma(\underset{\sim}{p}'|\underset{\sim}{p})$ is also identical. As discussed above, for a given value of the momentum, the momentum density perpendicular to the bond direction is less than that along the bond direction and hence these wavefunctions are not expected to show binding. But a linear combination of $\bar{\psi}_{cov}$ and $\bar{\psi}_{ionic}$, viz.,

$$\bar{\psi} = \bar{\phi}_a(1)\bar{\phi}_b(2) + \bar{\phi}_a(2)\bar{\phi}_b(1) + \mu\{\bar{\phi}_a(1)\bar{\phi}_a(2) + \bar{\phi}_b(1)\bar{\phi}_b(2)\}$$

$$= \frac{(1-\mu S)\,\phi_a(1)\phi_b(2) + \phi_a(2)\phi_b(1) + (\mu - S)\{\phi_a(1)\phi_a(2) + \phi_b(1)\phi_b(2)\}}{\{(1-\mu S)(2+2S^2) + (\mu - S)(2+2S^2) + 8(\mu - S)\mu S(1-\mu S)\}^{1/2}} \tag{3.32}$$

should show binding effects for higher values of μ, since this restores the property of exhibiting higher momentum densities perpendicular to the bond-direction than along the bond-direction. For $\mu = S$, the wavefunction (3.32) is the same as the HL wavefunction (3.6) and then the momentum density is the same as given by (3.10). For $\mu > S$, (3.32) behaves similar to (3.16) and the momentum density is similar to (3.18). In fact for $\lambda = \frac{(\mu - S)}{(1-\mu S)}$ (3.32) and (3.16) are exactly identical. Thus the wavefunction (3.32) is expected to show binding for $\mu \geq S$.[16] Since only non-negative values of μ are permitted, an additional condition $(1-\mu S) \geq 0$ can also be imposed. This leads to the result $\mu \leq (1/S)$.

It is a well-established result that the overlap integral between the two wavefunctions $\psi_1(\underset{\sim}{r})$ and $\psi_2(\underset{\sim}{r})$ is the same as

that between their Fourier transforms $\chi_1(\underset{\sim}{p})$ and $\chi_2(\underset{\sim}{p})$. The wavefunctions in the $\underset{\sim}{r}$-space were depicted by Slater[6] as vectors and an interpretation given for the overlap integral as the cosine of the angle between the corresponding vectors. It is equally possible to represent the $\underset{\sim}{p}$-sapce wavefunctions as vectors and the relationships in terms of angles between them follow those given by Slater[6] for the $\underset{\sim}{r}$-space wavefunctions.

III.5 SUMMARY AND CONCLUSION

Momentum densities obtained from the HL and corresponding VB wavefunction including ionic terms are compared for diatomic molecules. In both the cases, one-electron momentum density shows a maximum along the direction perpendicular to the bond. The phase relationship for the HL wavefunction given by the oscillator-picture of Coulson[1] is not exhibited by the wavefunction which includes the ionic terms. However, no physical significance should be attached to this phase-relationship. Since the ionic terms in the VB theory play the same role as CI in MO theory, the effect of adding ionic terms on the CP of H_2 was examined. The effect of polarization on the CP of H_2 was also studied. The wavefunction which includes ionic terms is found to give better agreement with the CI-theoretical and experimental profiles, especially for the lower q-values. The effect of including polarization is not so dramatic, but seems to improve the

agreement with the CI-theoretical profile for the intermediate q-values. CP calculated from an MO wavefunction constructed from floating AO's is also presented for comparison with the VB profiles. It agrees well with the results for the VB wavefunction which incorporates ionic terms. These calculations point towards the importance of including the ionic terms in the calculation of molecular CP's from VB wavefunctions. In Section III.4, the covalent and ionic wavefunctions constructed from OAO's were examined in the momentum space. Both the wavefunctions lead to an electron density identical to that given by the repulsive state wavefunction and, for a given value of the momentum, show minimum momentum density perpendicular to the bond direction. Hence these wavefunctions are not expected to show binding individually. This is in agreement with the earlier discussion of Slater[6] that the HL wavefunction constructed from OAO's does not show minimum diagonal energy. However, a linear combination (3.32) of the covalent and ionic wavefunctions constructed from OAO's, which leads to binding, restores the maxima of the momentum density perpendicular to the bond direction. Thus the criterion of maximum in the momentum density in a direction perpendicular to a bond is seen to be a sound one for assessing the bonding nature of a two-centre VB wavefunction.

REFERENCES

1. C.A. Coulson, Proc. Camb. Phil. Soc. Math. Phys. Sci., 37, 55 (1941).
2. P.A.M. Dirac, "Quantum Mechanics," Oxford, (1935), p. 103.
3. B. Hicks, Phys. Rev., 52, 436 (1937).
4. S. Weinbaum, J. Phys. Chem., 1, 593 (1933).
5. H. Shull and D. Ebbing, J. Chem. Phys., 28, 866 (1958).
6. J.C. Slater, J. Chem. Phys., 19, 220 (1951).
7. P. Eisenberger, Phys. Rev., A2, 1678 (1970).
8. R.E. Brown and V.H. Smith, Jr., Phys. Rev., A5, 140 (1972).
9. J. Felsteiner, P. Pattison and M. Cooper, Phil. Mag., 30, 537 (1974).
10. P. Paatero, S. Manninen and T. Paakkari, Phil. Mag., 30, 1281 (1974).
11. S. Wang, Phys. Rev., 31, 579 (1928).
12. P. Eisenberger and P.M. Platzman, Phys. Rev., A2, 415 (1970).
13. R.S. Mulliken, C.A. Rieke, D. Orloff and H. Orloff, J. Chem. Phys., 17, 1248 (1949).
14. P.-O. Löwdin, Phys. Rev., 97, 1474 (1955).
15. R. Benesch, S.R. Singh and V.H. Smith, Jr., Chem. Phys. Letters, 10, 151 (1971).
16. F.L. Pilar, "Elementary Quantum Chemistry," McGraw Hill (1968), p. 567.

CHAPTER IV

ELECTRON MOMENTUM DISTRIBUTIONS AND COMPTON PROFILES WITH FSGO MODEL

CHAPTER IV

ELECTRON MOMENTUM DISTRIBUTIONS AND COMPTON PROFILES WITH FSGO MODEL*

IV.1 INTRODUCTION

There has been a spurt in the experimental as well as theoretical studies of electron momentum distributions (EMD) and Compton profiles (CP) of molecules during the last five years (see Epstein and Tanner[1] for a review). In the present chapter we shall confine our attention to the theoretical calculations of EMD's and CP's of some small and medium-sized molecular systems.

The first calculation of the shape of the Compton line for a molecule was reported by Hicks[2] using a valence-bond wave-function[3] of ionic-polarization type for H_2 molecule. Duncanson

---

*The material presented in this chapter has been/to be published:

(i) S.R. Gadre, R. Ramaswamy and P.T. Narasimhan, Pramana, 8, 99 (1977);

(ii) S.R. Gadre and P.T. Narasimhan, Chem. Phys. Letters (to be published).

and Coulson[4] calculated CP's of methane, ethane, ethylene and acetylene using Heitler-London wavefunctions for the corresponding bonds. However, the wavefunctions employed by them were of limited accuracy. Epstein and Lipscomb[5] were the first to obtain a general algorithm for evaluating EMD's from HF-SCF wavefunctions of polyatomic molecules. This algorithm was used to evaluate CP's of boron hydrides[5] and hydrocarbons.[6] In the latter case a localized molecular orbital (LMO) approach was used. Some more studies using LMO approach have recently been reported[7] for a host of molecules including hydrocarbons. The CP of water has been calculated using a variety of wavefunctions and compared with recent experimental results.[8] The effect of hydrogen bonding on the theoretical CP of water has also been examined in detail.[9] CP's of molecules belonging to 18, 24 and 42-electron isoelectronic series have been calculated from ab-initio HF wavefunctions and the results compared with the LMO CP's.[10-12] Thus with growing interest on theoretical side and the use of LMO's, the suggestion[13] that CP's of large molecules may be predicted from an analysis of smaller molecules seems to be coming true.

There has been a revival of interest on the experimental side as well. X-ray CP measurements have been carried out on H_2 molecule.[14] The CP of lithium hydride has been measured with X-rays as well as γ-rays.[15-17] CP's of a host of hydrocarbons have been measured with X-rays.[18] The CP of methane has been measured recently with high-energy electron impact spectroscopy.[19]

where a_i is the orbital exponent and (A_i, B_i, C_i) are the Cartesian co-ordinates of the orbital centre, is used to represent an electron-pair. a_i, the orbital exponent is related to ρ_i, the orbital radius by

$$a_i = \frac{1}{\rho_i^2} \qquad (4.2)$$

The energy is minimized by optimization of nuclear co-ordinates, orbital exponents and some or all of the orbital centres. The use of only one Gaussian per orbital is a gross oversimplification and limits the accuracy of such calculations severely. The energies obtained with this single-Gaussian version of the FSGO model are typically 85% of the corresponding Hartree-Fock (HF) energies. However, such a restricted, sub-minimal basis makes this model extremely simple. Due to floating of the orbital centres, the FSGO wavefunctions satisfy the virial theorem very closely. The wavefunctions also correspond to the chemist's picture in terms of bond pairs, inner shells and lone pairs.

Single FSGO wavefunctions do not represent the inner shell properly. Since the inner shells govern the long-range behaviour of the CP's, the CP's computed from single Gaussian version of the FSGO model are not expected to give good agreement with the experimental as well as the HF-SCF theoretical ones. Use of a double Gaussian for each electron pair instead of a single one improves the energies markedly, leading typically to 96% of the corresponding HF-SCF energies.[26] Models incorporating a larger

number of Gaussians have also been studied.[24,27] A model which employs two Gaussians for the inner shell has also been studied.[28] Hence it was felt that it would be worthwhile to calculate CP's from single as well as double Gaussian versions of the FSGO model and compare the results with those obtained from more accurate HF-SCF wavefunctions and experiment.

Following Epstein and Lipscomb[5] we find that the momentum density $|\chi(\underset{\sim}{p})|^2$ is given by

$$\sum_{jk} \rho_{jk} f_j(p) f_k(p) Y_{l_j m_j}(\theta_p, \phi_p) Y_{l_k m_k}(\theta_p, \phi_p) . e^{-i\underset{\sim}{p}.\underset{\sim}{r}_{jk}} \qquad (4.3)$$

where $\underset{\sim}{\rho}$ is the density matrix and $f_j(p)$ is the Fourier transform of the radial part of the j^{th} orbital. As shown in the above work,[5] $e^{-i\underset{\sim}{p}.\underset{\sim}{r}_{jk}}$ can be expanded in terms of spherical Bessel functions

$$e^{-i\underset{\sim}{p}.\underset{\sim}{r}_{jk}} = 4\pi \sum_{l,m} (-i)^l . j_l(pr_{jk}) Y_{lm}(\theta_p, \phi_p) . Y_{lm}(\theta_{jk}, \phi_{jk}) \qquad (4.4)$$

Since only s-type Gaussians are involved in the present model, the radial momentum density can be written, for the single FSGO case, as

$$I(p) = \int |\chi(\underset{\sim}{p})|^2 p^2 . \sin\theta_p \, d\theta_p \, d\phi_p \qquad (4.5)$$

$$= \sum_{j,k} \rho_{jk} f_j(p) f_k(p) . j_o(pr_{jk}) . p^2 \qquad (4.6)$$

apart from some numerical constants. Here $j_o(pr_{jk})$ is the Bessel function given by

$$j_o(pr_{jk}) = \sin(pr_{jk})/(pr_{jk}) \tag{4.7}$$

ρ_{jk} is equal to $2T_{jk}$ where T_{jk} is the (j,k)th element of the inverse overlap matrix. The Fourier transforms $f_j(p)$ and $f_k(p)$ are also Gaussians,

$$f_j(p) = \left(\frac{1}{2\pi a_j}\right)^{3/4} \exp(-p^2/4\,a_j) \tag{4.8}$$

The spherically averaged CP, J(q), within the impulse approximation,[29] can be written as

$$J(q) = \int_{|q|}^{\infty} \frac{I(p)}{2p}\, dp \tag{4.9}$$

where q is the projection of the initial momentum of the electron on the scattering vector.

Directional CP, $J(p_z)$, is given by

$$J(p_z) = \int \rho(p_x, p_y, p_z)\, dp_x\, dp_y \tag{4.10}$$

which, on substituting for $\rho(p)$, yields the following expression for $J(p_z)$:

$$J(p_z) = \sum 2T_{ij}\left(\frac{1}{a_i a_j}\right)^{3/4} \exp(-\alpha_{ij} p_z^2) \cdot$$

$$\exp\left(-\frac{\{A_{ij}^2 + B_{ij}^2\}}{4\alpha_{ij}}\right) \cdot 2\cos(C_{ij} p_z) \qquad (4.11)$$

where $A_{ij} = |A_i - A_j|$ etc and $\alpha_{ij} = \frac{(a_i + a_j)}{(a_i a_j)}$. Thus, due to the use of only s-type Gaussians, $J(q)$ as well as $J(p_z)$ can be obtained quite easily from single-Gaussian version of the FSGO model.

CP's can be obtained similarly from wavefunctions employing concentric double Gaussian, viz.,

$$\psi_i(\underset{\sim}{r}) = C_{i1} \exp\{-a_{i1}|\underset{\sim}{r} - \underset{\sim}{R}_i|^2\} + C_{i2} \exp\{-a_{i2}|\underset{\sim}{r} - \underset{\sim}{R}_i|^2\} \qquad (4.12)$$

by using Eq. (4.6) and (4.9).

All the computations for the results reported in this chapter were carried out on an IBM 7044/1401 system at I.I.T., Kanpur. The integration in Eq. (4.9) was done numerically using Simpson's rule. The total computer time for all the calculations presented here was approximately 25 minutes on our IBM 7044/1401 system. In the next section we present the results of our calculations of CP's of some molecules. Comparison with other HF-SCF data as well as experimental results, wherever available, is also made.

IV.3 RESULTS AND DISCUSSION

IV.3.A Hydrogen

The CP of H_2 was calculated from FSGO wavefunction employing just one Gaussian centred at the mid-point of the bond.[30] This wavefunction leads to an energy value approximately 85 per cent of the HF-SCF energy for H_2. The FSGO-theoretical profile along with the experimental one[14] and SCF-theoretical profile[31] obtained from Liu's wavefunction is shown in Fig. 4.1. The FSGO-theoretical profile has J(0) value less than the experimental one by about 6 per cent. It also dies out faster than the experimental CP for higher values of q.

IV.3.B Lithium hydride

The radial momentum density, I(p), calculated for single-Gaussian FSGO wavefunction[23] is shown in Fig. 4.2. This shows an interesting feature in that the I(p) for the molecule is very nearly equal to the sum of the individual-orbital contributions neglecting the non-diagonal contribution to the momentum density. In other words, the curve is nearly identical with the solid line in Fig. 4.2 which is the sum of the bond-pair and inner-shell contributions. There are two maxima appearing in this curve corresponding to the maxima of the individual contributions from the inner-shell and bond pair. The reason for this additivity in the case of LiH is obviously that the off-diagonal terms of the inverse overlap matrix, T, are small. The CP calculated

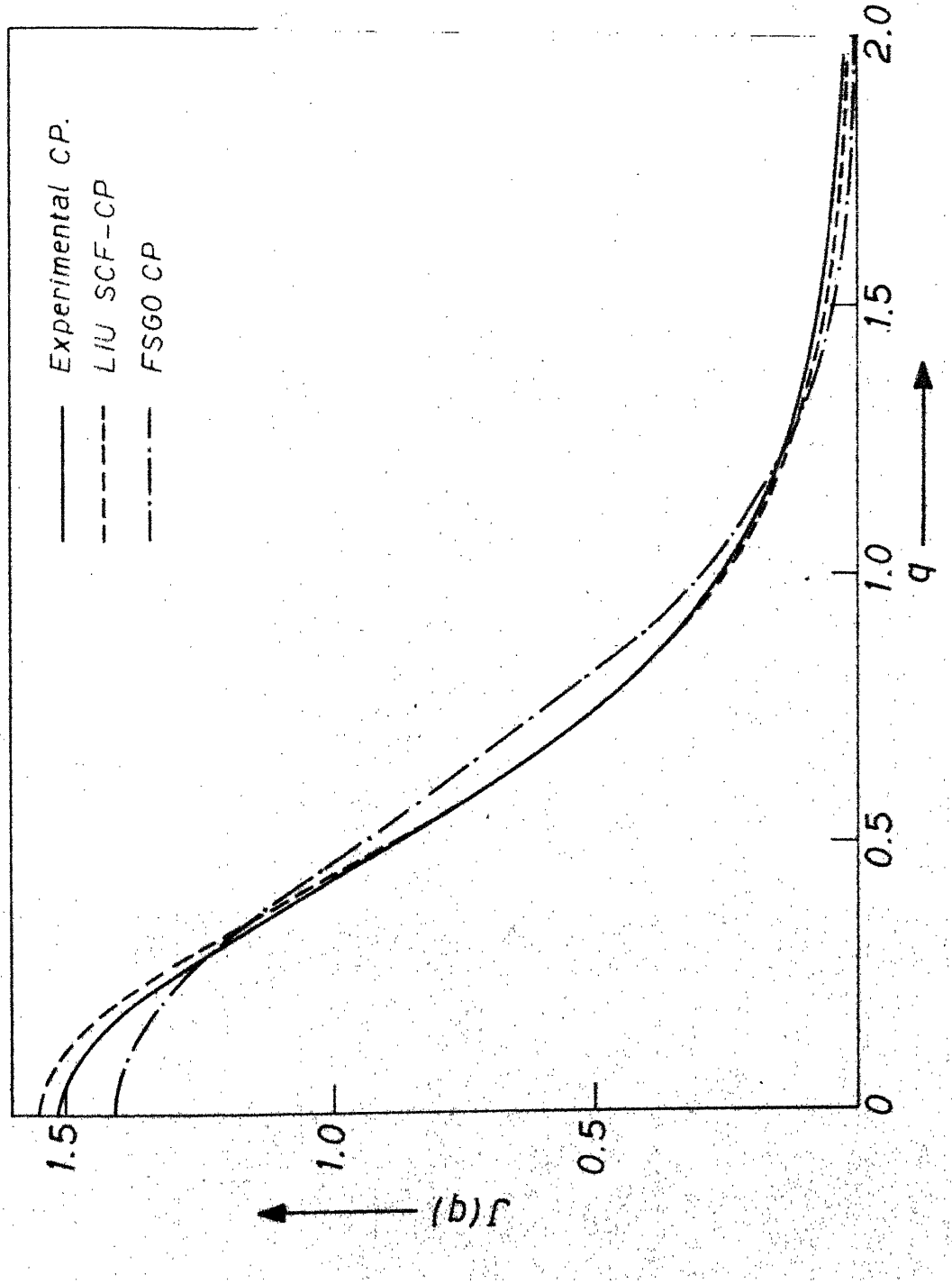

Fig. 4.1 Compton profile of H_2

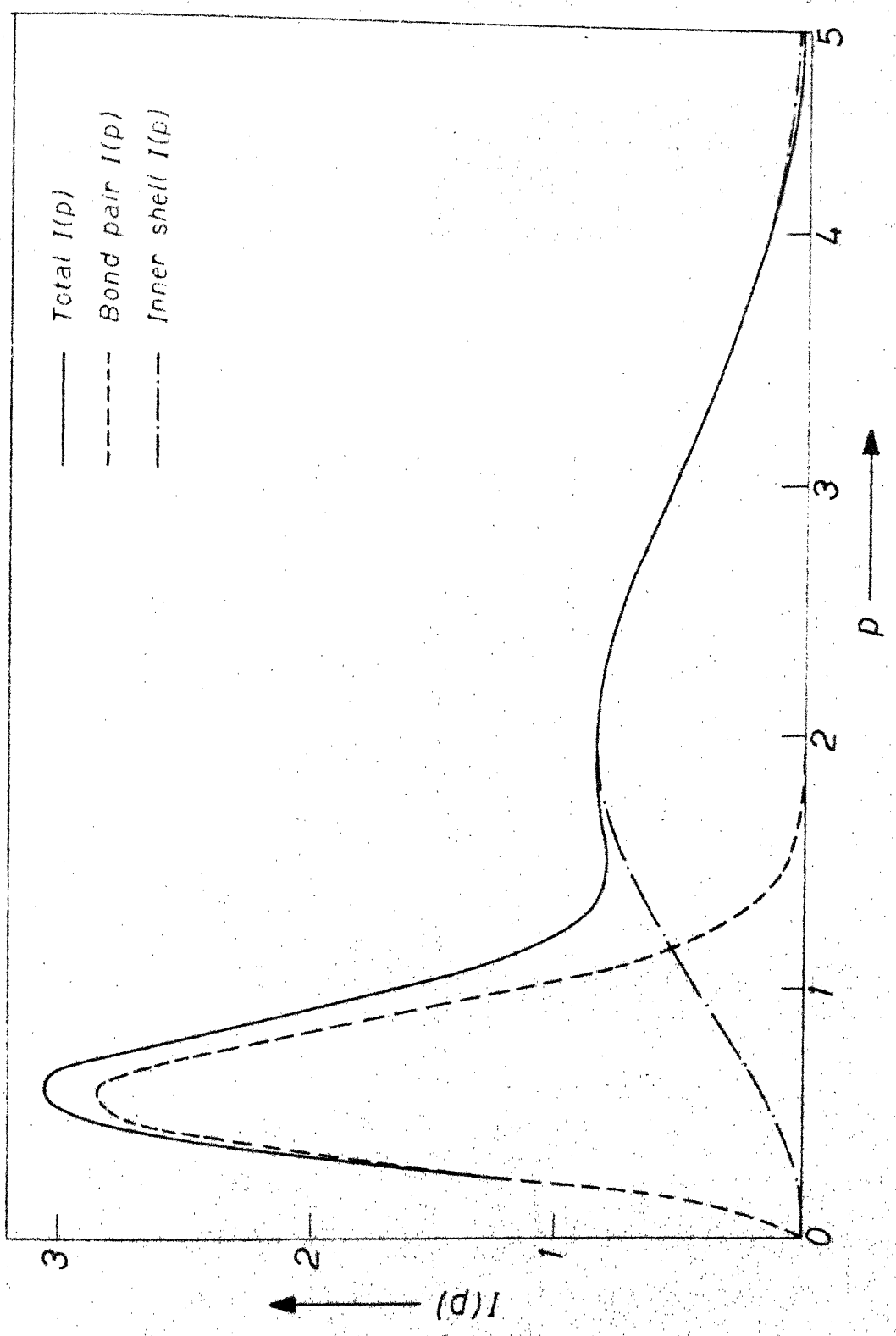

Fig. 4.2 I(p) for LiH

from this wavefunction along with the experimental one[16] is shown in Fig. 4.3. Our FSGO-theoretical J(0) value is higher than the experimental one by about 10% and the width $q_{0.5}$ of the profile, that is the value of q at which $J(q) = \frac{1}{2}J(0)$, is lower than that for the experimental CP. This is a consequence of using a wavefunction of relatively poor energy in which the inner shell is not well-represented.

IV.3.C Water

The FSGO theoretical profile calculated from the single-Gaussian wavefunction[32] reported in the literature along with the directional CP, $J(p_z)$, along the C_2-symmetry axis of the molecule is shown in Table 4.1. The CP calculated from a double-Gaussian FSGO wavefunction[33] and the experimental CP are also presented. The single-FSGO CP dies out faster than the experimental one for the higher q-values. In this regard, the present results bear a similarity to those obtained earlier for the CP of water using minimal basis-set.[8] The corresponding directional CP differs from the spherically averaged single-Gaussian CP by about 0.3% at the peak of the CP. The CP calculated from the double-Gaussian version of the FSGO model agrees better with the experimental one. This is, of course, expected because the double-Gaussian FSGO's lead to energy which is typically 96% of the corresponding HF energy. The inner shell is better represented in the double Gaussian version, leading to broader "tail" of CP.

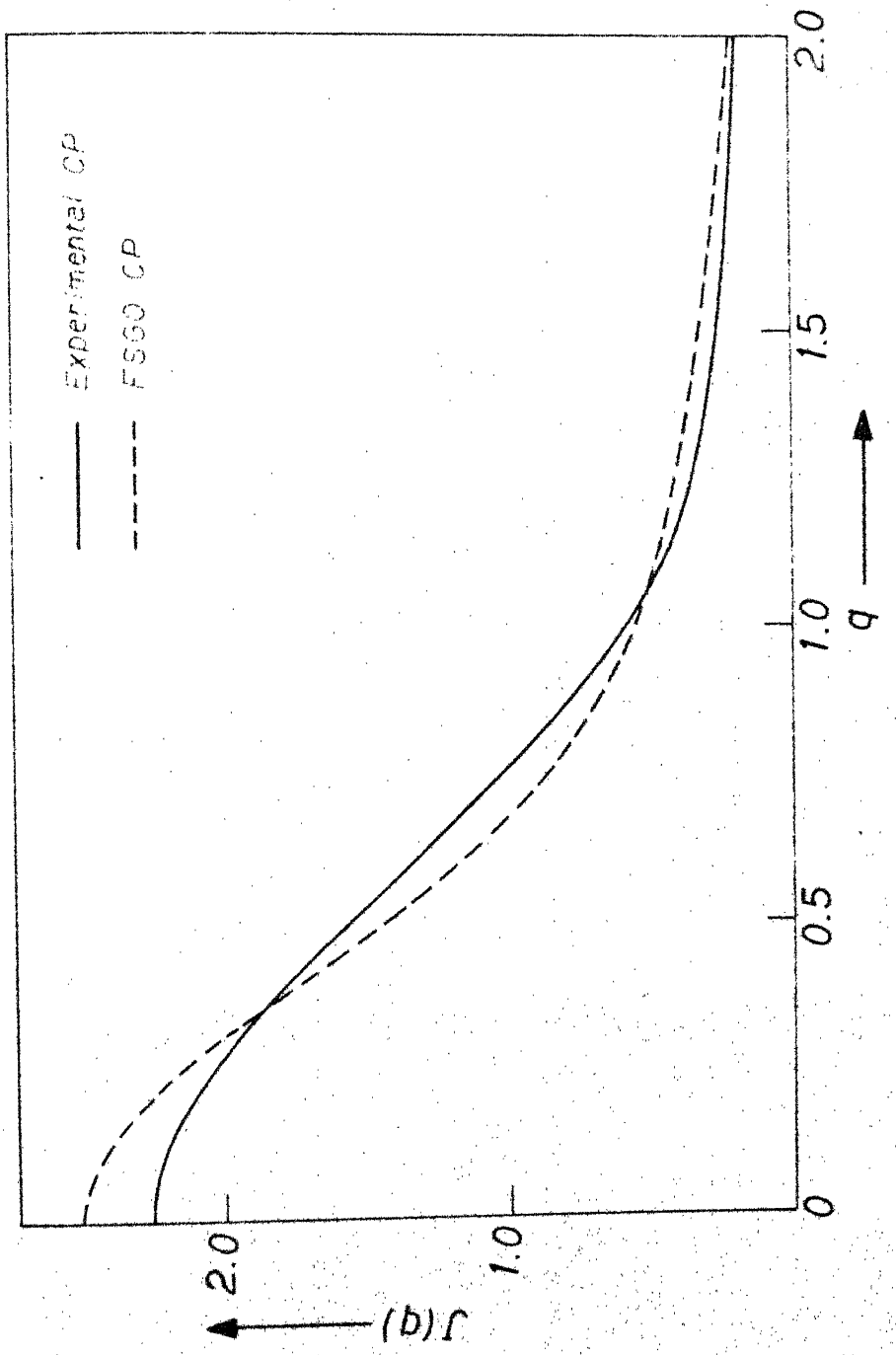

Fig. 4.3 Compton profile of LiH

Table 4.1

Compton Profile of Water

q/p_z	$J(p_z)$ along the C_2-axis. Single-Gaussian FSGO	$J(q)$ spherical average. Single-Gaussian FSGO	$J(q)$ spherical average. Double-Gaussian FSGO	$J(q)$ expt.+
0.0	3.387	3.378	3.545	3.73
0.1	3.777	3.368	3.531	3.71
0.2	3.345	3.338	3.488	3.66
0.3	3.292	3.286	3.416	3.58
0.4	3.216	3.211	3.314	3.43
0.5	3.114	3.111	3.180	3.27
0.6	2.982	2.986	3.016	3.04
0.7	2.835	2.835	2.824	2.77
0.8	2.660	2.661	2.609	2.50
0.9	2.464	2.467	2.379	2.21
1.0	2.253	2.256	2.140	1.94
1.2	1.081	1.810	1.670	1.47
1.4	1.371	1.375	1.254	1.01
1.6	0.991	0.994	0.992	0.83
1.8	0.691	0.692	0.678	0.64
2.0	0.475	0.476	0.508	0.52

+Experimental γ-ray CP quoted by Tanner and Epstein.[8] The experimental CP data is given here only upto two decimals.

IV.3.D Methane

The single-Gaussian profile computed from a wavefunction reported in the literature,[34] the various directional profiles along with the double Gaussian CP and the experimental CP[19] are presented in Table 4.2. As noted in the case of water, the double-Gaussian CP is in better agreement with the experimental one. The directional profiles differ from the spherically averaged CP by about 0.5% at the peak of the CP.

IV.3.E Ethane

The single-Gaussian wavefunctions for staggered and eclipsed ethane available in the literature[34] were employed to obtain EMD's and CP's. In Fig. 4.4, the calculated I(p) *vs* p for staggered ethane is shown along with the sum of the individual-orbital contributions. These two curves do not agree with each other. The reason for this discrepancy appears to be that the non-diagonal entries in the inverse overlap matrix T, are numerically large in this case and hence, the contribution to I(p) from the non-diagonal terms ($j \neq k$) in expression (4.6) is quite large.

We present the various CP's for staggered and eclipsed ethane in Tables 4.3 and 4.4 respectively. Here the directional CP of staggered ethane, $J(p_z)$, along the direction perpendicular to and symmetrical w.r.t. the C-C bond differs at the peak of the CP by about 1.3% from the corresponding spherically averaged CP.

Table 4.2

Compton Profile of Methane

q/p_z	$J(p_z)$ along C-H bond. Single-Gaussian FSGO	$J(p_z)$ along H-H direction. Single-Gaussian FSGO	J(q) spherical average. Single-Gaussian FSGO	J(q) spherical average. Double-Gaussian FSGO	J(q) Expt.[+]
1	2	3	4	5	6
0.0	4.723	4.725	4.741	4.989	5.02
0.1	4.692	4.695	4.709	4.948	4.94
0.2	4.598	4.601	4.612	4.822	4.85
0.3	4.439	4.443	4.447	4.610	4.51
0.4	4.213	4.217	4.216	4.314	4.18
0.5	3.923	3.926	3.920	3.943	3.71
0.6	3.575	3.577	3.568	3.514	3.25
0.7	3.183	3.183	3.173	3.052	2.82
0.8	2.766	2.763	2.754	2.587	2.39
1.0	1.939	1.932	1.927	2.146	2.00
1.2	1.239	1.235	1.235	1.129	1.13
1.4	0.750	0.748	0.750	0.735	0.78
1.6	0.461	0.461	0.463	0.505	0.55

Table 4.4 (contd.)

1	2	3	4	5	6
1.8	0.314	0.315	0.316	0.376	0.41
2.0	0.247	0.248	0.248	0.300	0.33

+Experimental CP from high energy electron-impact spectroscopy.[19]

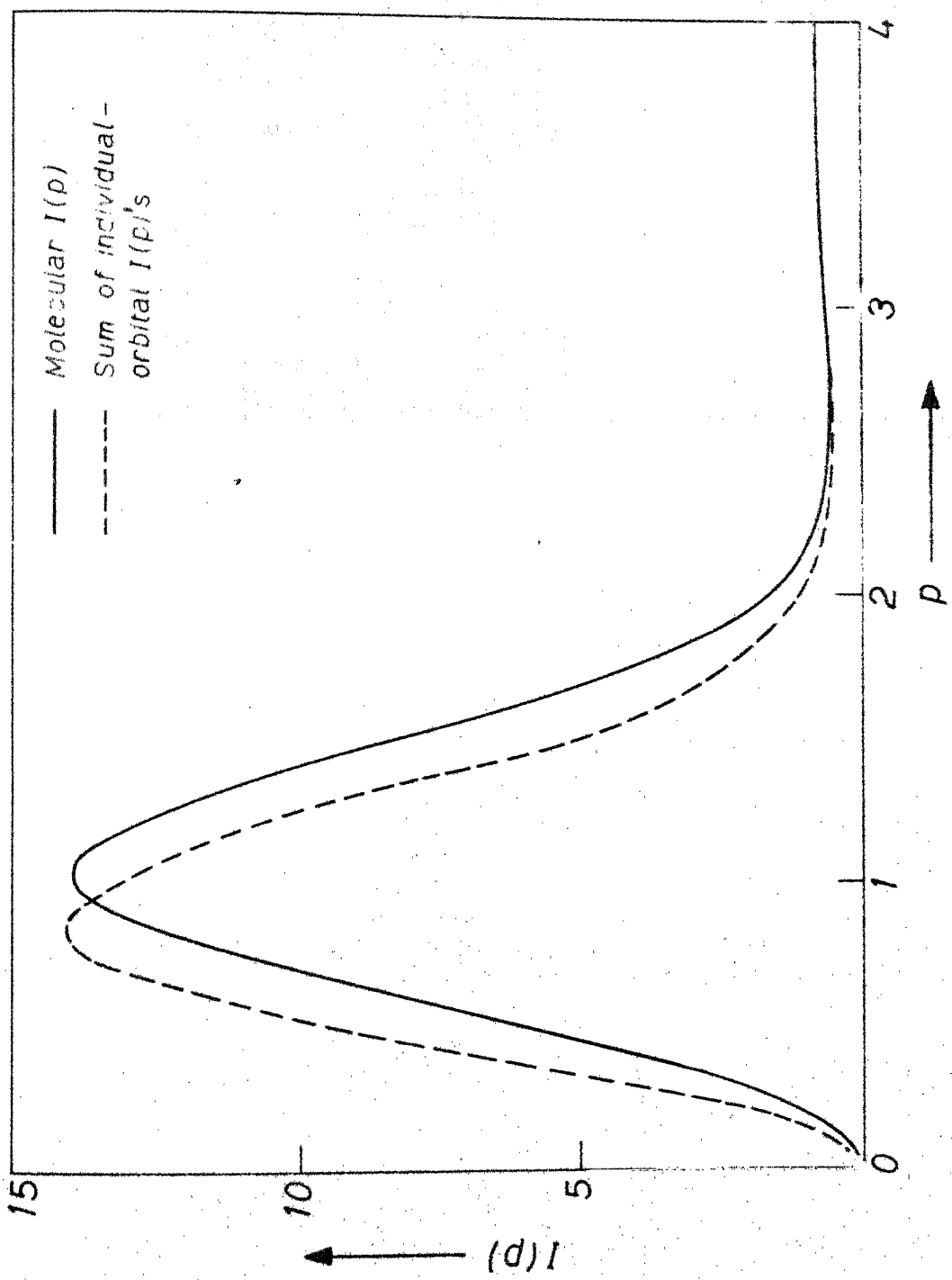

Fig. 4.4 I(p) for staggered Ethane

Table 4.3

Compton Profile of Staggered Ethane

q/p_z	$J(p_z)$ along C-C bond. Single-Gaussian FSGO	$J(p_z)$ perpendicular to C-C. Single-Gaussian FSGO	$J(q)$ spherical average. Single-Gaussian FSGO	$J(q)$ spherical average. Double-Gaussian FSGO	$E-M^+$
1	2	3	4	5	6
0.0	8.225	8.093	8.204	8.568	8.46
0.1	8.158	8.051	8.147	8.496	8.37
0.2	7.964	7.920	7.976	8.281	8.13
0.3	7.652	7.690	7.695	7.930	7.61
0.4	7.240	7.352	7.307	7.453	7.21
0.5	6.743	6.901	6.822	6.866	6.58
0.6	6.178	6.342	6.250	6.194	5.90
0.7	5.561	5.694	5.611	5.464	5.19
0.8	4.909	4.987	4.928	4.715	4.48
0.9	4.241	4.258	4.229	3.982	3.80
1.0	3.583	3.546	3.545	3.300	3.18
1.2	2.391	2.305	2.334	2.181	2.17

Table 4.3 (contd.)

1	2	3	4	5	6
1.4	1.492	1.421	1.449	1.427	1.50
1.6	0.928	0.891	0.908	0.976	1.11
1.8	0.631	0.618	0.625	0.721	0.89
2.0	0.494	0.492	0.494	0.575	0.73

+Constructed from the corresponding C-C and C-H bond and inner shell contributions to experimental CP data of Eisenberger and Marra.[18]

Table 4.4

Compton Profile of Eclipsed Ethane

q/p_z	$J(p_z)$ perpendicular to C-C bond. Single-Gaussian FSGO	$J(q)$ spherical average. Single-Gaussian FSGO
0.0	8.099	8.202
0.1	8.055	8.145
0.2	7.922	7.975
0.3	7.690	7.695
0.5	7.350	7.308
0.6	6.897	6.824
0.7	6.338	6.253
0.8	5.690	5.615
0.9	4.984	4.931
1.0	3.547	3.546
1.2	2.309	2.330
1.4	1.422	1.448
1.6	0.892	0.916
1.8	0.618	0.624
2.0	0.491	0.493

The spherically averaged CP's of these two rotational isomers of ethane can be seen to be quite close to each other in both the single and double Gaussian frameworks. Thus, within the FSGO-model, it is not possible to distinguish between the CP's of these two rotamers.

IV.3.F Ethylene and acetylene

The CP's calculated from single[34] and double Gaussian wavefunctions[33] are presented in Table 4.5. As in the previous cases, the agreement between the theory and experiment is improved considerably by the use of double Gaussian FSGO wavefunctions.

IV.3.G Cyclopropane and cyclobutane

The single-FSGO CP's calculated from wavefunctions reported in the literature[34] alongwith the experimental CP's are presented in Table 4.6. The agreement between these spherically averaged single-Gaussian theoretical CP's and those obtained from the data of Eisenberger and Marra[18] is not good for higher q-values.

IV.3.H Ammonia and hydrogen fluoride

The CP's calculated from double-Gaussian FSGO wavefunctions are presented in Table 4.7 alongwith the experimental or HF-SCF theoretical profiles. The agreement of FSGO-theoretical values is fairly good, especially in the higher q-region.

All the CP's presented in Tables 4.1 to 4.7 are normalized to the corresponding number of electrons for $0 \leq q \leq 15$ a.u. or $0 \leq p_z \leq 15$.

Table 4.5

Compton Profiles of Ethylene and Acetylene

q	ETHYLENE			ACETYLENE	
	J(q) spherical average.Single-Gaussian FSGO	J(q) spherical average.Single-Gaussian FSGO	E-M[+]	J(q) spherical average.Single-Gaussian FSGO	J(q) HF-SCF Theory[*]
1	2	3	4	5	6
0.0	7.065	7.425	7.36	5.933	5.953
0.1	7.013	7.362	7.28	5.896	
0.2	6.872	7.175	7.07	5.757	
0.3	6.638	6.870	6.71	5.602	
0.4	6.314	6.454	6.25	5.341	
0.5	5.905	5.942	5.70	5.007	4.853
0.6	5.423	5.356	5.10	4.607	
0.7	4.880	4.724	4.49	4.154	
0.8	4.299	4.078	3.88	3.666	
0.9	3.703	3.453	3.31	3.166	
1.0	3.120	2.874	2.78	2.677	2.526
1.2	2.084	1.933	1.92	1.815	

Table 4.5 (contd.)

1	2	3	4	5	6
1.4	1.324	1.302	1.37	1.188	
1.6	0.855	0.919	1.04	0.796	
1.8	0.609	0.698	0.86	0.586	
2.0	0.489	0.567	0.72	0.485	0.653

+Constructed from the corresponding C=C, C-H and C_{1s} contributions to experimental CP data of Eisenberger and Marra.[18]

*Calculated from C-H, C_{1s} and C≡C LMO CP's.[7]

Table 4.6

Compton Profiles of Cyclopropane and Cyclobutane

q	CYCLOPROPANE		CYCLOBUTANE	
	J(q) spherical average. Single-Gaussian FSGO	E-M+	J(q) spherical average. Single-Gaussian FSGO	E-M+
0.0	10.480	10.414	13.891	13.836
0.1	10.408	10.318	13.796	13.757
0.2	10.193	10.075	13.515	13.435
0.3	9.844	9.662	13.057	12.882
0.4	9.370	9.115	12.432	12.152
0.5	8.782	8.412	11.659	11.270
0.6	8.095	7.693	10.738	10.257
0.7	7.324	6.889	9.752	9.185
0.8	6.494	6.059	8.670	8.079
0.9	5.633	5.247	7.548	6.996
1.0	4.776	4.475	6.427	5.966
1.2	3.218	3.155	4.364	4.207
1.4	2.042	2.198	2.774	2.931
1.6	1.304	1.599	1.761	2.132
1.8	0.913	1.250	1.223	1.668
2.0	0.731	1.038	0.975	1.384

+Constructed from the corresponding C-C, C-H and C_{1s} contributions to experimental CP data of Eisenberger and Marra.[18]

Table 4.7

Compton Profiles of NH_3 and HF

q	NH_3		HF
	J(q) spherical average. Double-Gaussian FSGO	J(q) Expt.+	J(q) spherical average. Double-Gaussian FSGO
0.0	4.215	4.38	2.960
0.1	4.192	4.34	2.952
0.2	4.121	4.27	2.928
0.3	4.000	4.11	2.887
0.4	3.828	3.88	2.827
0.5	3.604	3.58	2.753
0.6	3.334	3.25	2.659
0.7	3.027	2.88	2.548
0.8	2.697	2.50	2.421
0.9	2.359	2.16	2.279
1.0	2.028	1.83	1.126
1.2	1.438	1.30	1.800
1.4	0.988	0.94	1.473
1.6	0.680	0.68	1.172
1.8	0.485	0.50	0.915
2.0	0.365	0.40	0.709

+A. Lahmam-Bennani, private communication.[21]

IV.4 SUMMARY AND CONCLUSIONS

The single-Gaussian FSGO CP's agree fairly well with the experimental profiles, except for the higher q-values. A model employing a double Gaussian per electron-pair[26] represents the inner shell better and improves considerably upon the single-Gaussian EMD's and CP's. The simplicity of the FSGO model is an attractive feature. This is an ab-initio model employing, in its simplest version, a sub-minimal basis of s-type Gaussians with no empirical or semi-empirical parameters. The orbitals used here are "local"[24] and can be interpreted in terms of classical chemical pictures such as inner shell, bond pair and lone-pair. Christoffersen[25] has extended the single-Gaussian FSGO model to "synthesize" larger molecules from the corresponding molecular fragments. Hence the calculation of EMD's and CP's of large molecules of chemical interest such as various amino-acids, acetylcholine etc. can be undertaken.

However, as noted earlier, the single Gaussian version has severe drawbacks in that it does not represent the inner shell properly and leads to poor energies. In this model, the lone-pair and pi-bond orbital-centres have to be constrained rather arbitrarily as they tend to collapse into the nucleus.[32] The double-Gaussian version does not have this drawback and gives better agreement with the experimental CP's of molecules having pi-bonds or lone-pairs. It also represents the inner shell better and leads to "tails" of CP which are in better agreement

with HF-SCF theory and experiment.

Since the present model is within the orbital approximation, electron-electron correlation effects are not represented properly. However, these effects are important in the EMD's and CP's of atoms and molecules.[35] In spite of these drawbacks, the FSGO model offers a very simple way of theoretically calculating CP's for fairly large molecules.

REFERENCES

1. I.R. Epstein and A.C. Tanner in "The Compton Effect", Ed. B.G. Williams, McGraw Hill (to be published).

2. B. Hicks, Phys. Rev., 52, 436 (1937).

3. S. Weinbaum, J. Chem. Phys., 1, 593 (1933).

4. W.E. Duncanson and C.A.Coulson, Proc. Camb. Phil. Soc., 37, 406 (1941).

5. I.R. Epstein and W.N. Lipscomb, J. Chem. Phys., 53, 4418 (1970).

6. I.R. Epstein, J. Chem. Phys., 53, 4425 (1970).

7. M.H. Whangbo and V.H. Smith,Jr., Chem. Phys., 5, 234 (1974).

8. A.C. Tanner and I.R. Epstein, J. Chem. Phys., 61, 4251 (1974).

9. M.H. Whangbo, V.H. Smith, Jr., E. Clementi, G.H. Dierksen and W. Von Niessen, J. Phys., B7, 1427 (1974).

10. D.M. Hirst and S.P. Liebmann, Mol. Phys., 30, 597 (1975).

11. D.M. Hirst and S.P. Liebmann, Mol. Phys., 30, 1693 (1975).

12. D.M. Hirst and S.P. Liebmann, Chem. Phys. Letters, 42, 404 (1976).

13. B. Hicks, Phys. Rev., 57, 151 (1940).

14. P. Eisenberger, Phys. Rev., A2, 1678 (1970).

15. W.C. Phillips and R.J. Weiss, Phys. Rev., 182, 923 (1969).

16. Unpublished results of Paakkari et al. quoted by O. Aikala, K. Mansikka and T. Paakkari in "The Compton Effect", Ed. B.G. Williams, McGraw Hill (to be published).

17. J. Felsteiner, R. Fox and S. Kahane, Phys. Rev., B9, 4689 (1972).

18. P. Eisenberger and W.C. Marra, Phys. Rev. Letters, 27, 1413 (1971).

19. R.W. Klapthor and J.S. Lee, Chem. Phys. Letters, 45, 513 (1977).

20. R. Holt, P. Pattison and M. Cooper, Chem. Phys. Letters, 43, 606 (1976).

21. A. Lahmam-Bennani (private communication).

22. M. Cooper, R. Holt, P. Pattison and K.R. Lee, Commun. on Phys., 1, 159 (1976).

23. A.A. Frost, J. Chem. Phys., 47, 3707 (1967).

24. J.L. Nelson and A.A. Frost, Theoret. Chim. Acta (Berl.), 29, 75 (1973).

25. For review see R.E. Christoffersen in Adv. Quantum Chem., 6, 333 (1972), Ed. P.O. Lowdin (Academic Press).

26. R.A. Rouse and A.A. Frost, J. Chem. Phys., 50, 1705 (1969).

27. K.M. Karunakaran and R.E. Christoffersen, J. Chem. Phys., 62, 1992 (1975).

28. B. Ford, G.G. Hall and J.C. Packer, Int. J. Quantum Chem., 4, 533 (1970).

29. P. Eisenberger and P.M. Platzman , Phys. Rev., A2, 415 (1970).

30. A.A. Frost, J. Chem. Phys., 67, 3714 (1967).

31. R.E. Brown and V.H. Smith, Jr., Phys. Rev., A5, 140 (1972).

32. A.A. Frost, J. Phys. Chem., 72, 1289 (1968).

33. R.A. Rouse, private communication (1977).

34. A.A. Frost and R.A. Rouse, J. Amer. Chem. Soc., 90, 1965 (1968).

35. R. Benesch and V.H. Smith, Jr., Chem. Phys. Letters, 5, 801 (1970).

CHAPTER V

SEMI-EMPIRICAL WAVEFUNCTIONS AND COMPTON PROFILES

CHAPTER V

SEMI-EMPIRICAL WAVEFUNCTIONS AND COMPTON PROFILES

V.1 INTRODUCTION

Ahlenius and Lindner[1] have recently studied the valence Compton profiles (VCP) of some small and medium-sized molecules calculated from various semi-empirical MO methods. In this study, they have examined iterative extended Huckel (IEH), CNDO/2 and INDO wavefunctions in the momentum space and the corresponding VCP's. They have calculated various $\langle p^n \rangle$ values for small and medium sized systems and discussed briefly the question of transferability of bond profiles in the INDO-localized picture. They employed the iterative localization procedure of Edmiston and Ruedenberg.[2] This localization procedure produces localized molecular orbitals (LMO) which show

marked resemblance to the chemist's picture in terms of bond-pairs, lone-pairs etc. Ahlenius and Lindner applied this procedure to INDO wavefunctions and found that the total VCP's before and after localization agree through four decimals. More recently, Figeys, Geerlings and Alsenoy[3] have studied the problem of rotational invariance of the momentum density and radial momentum density obtained from NDO (Neglect of Differential Overlap) approximate wavefunctions. They found out that only following two approximations are physically significant after the above two requirements are imposed:

(i) NDO wavefunctions are used and $\rho_s(p)$ and I(p) are approximated to INDO or CNDO level.

(ii) Overlap integrals are explicitly taken into account while solving Roothaan SCF[4] equations, together with unapproximated expressions.

Due to explicit treatment of only valence electrons, using minimal basis-set and employing various approximations to molecular integrals, semi-empirical calculations are computationally easier and much less expensive than the ab-initio ones. Yet the one-particle density matrix obtained by semi-empirical procedures bears close similarity to Hartree-Fock-Roothaan density matrix in many cases. Due to these reasons, they are very suitable for handling relatively large and chemically interesting molecules and have gained popularity in such calculations.

In this chapter, we present our VCP results obtained for some small hydrocarbons from CNDO/2 wavefunctions and consider specifically the question of bond-transferability of CP's for some chemically interesting systems such as allene and butadiyne.

V.2 CNDO/2 WAVEFUNCTIONS

In the CNDO (Complete Neglect of Differential Overlap) method[5] only valence electrons are considered explicitly, all the inner shells being treated as part of an unpolarizable core. The MO ψ_i is then expressed as a linear combination of atomic orbitals (LCAO) ϕ_i

$$\psi_i = \sum_i c_i \phi_i \tag{5.1}$$

This leads to Roothaan's equations

$$\Sigma\, c_\nu (F_{\mu\nu} - E S_{\mu\nu}) = 0 \tag{5.2}$$

or, in matrix notation

$$\underline{\underline{F}}\underline{C} = \underline{\underline{E}}\underline{\underline{S}}\underline{C} \tag{5.3}$$

In (5.2) $F_{\mu\nu}$ is the matrix element of the Fock operator F, given by

$$F_{\mu\nu} = H_{\mu\nu} + G_{\mu\nu} \tag{5.4}$$

H being one-electron operator which includes kinetic energy operator and the nuclear-electron potential energy operator.

$$H_{\mu\nu} = \int \phi_\mu \{ -\frac{1}{2} \nabla^2 - \sum_A V_A(\underset{\sim}{r}) \} \phi_\nu \, d\underset{\sim}{r} \tag{5.5}$$

$V_A(\underset{\sim}{r})$ being the potential for the atom A due to its nucleus and inner shells. G contains the electron-electron repulsion terms and

$$G_{\mu\nu} = \Sigma \, P_{\sigma\lambda} \left[(\mu\nu|\sigma\lambda) - \frac{1}{2} (\mu\sigma|\nu\lambda) \right] \tag{5.6}$$

where $(\mu\nu|\lambda\sigma)$ is the two electron repulsion integral

$$(\mu\nu|\lambda\sigma) = \int \phi_\mu(1) \, \phi_\nu(2) \, \frac{1}{r_{12}} \, \phi_\lambda(1) \, \phi_\sigma(2) \, d\underset{\sim}{r}_1 \, d\underset{\sim}{r}_2 \tag{5.7}$$

and P is the density matrix where

$$P_{\lambda\sigma} = 2 \sum_{i=1}^{occ} c_{i\lambda} \; c_{i\sigma} \tag{5.8}$$

An iterative procedure is then followed to obtain self-consistent MO's.

In the CNDO method, the number of electron-electron repulsion integrals is drastically reduced by introducing the zero differential overlap (ZDO) approximation[6]

$$\phi_\mu(\underset{\sim}{r}) \cdot \phi_\nu(\underset{\sim}{r}) \; d\underset{\sim}{r} = 0 \tag{5.9}$$

for arbitrary values of $d\underset{\sim}{r}$ and ϕ_μ and ϕ_ν centred on different atoms. Some of the important approximations involved in the CNDO method are:

(i) The overlap integrals $S_{\mu\nu}$ are set to zero unless $\mu = \nu$.

(ii) $(\mu\nu|\lambda\sigma) = 0$ unless $\mu = \nu$ and $\sigma = \lambda$, in which case

$$(\mu\nu|\lambda\sigma) = (\mu\mu|\lambda\lambda) = \gamma_{\mu\lambda} \qquad (5.10)$$

(iii) $\gamma_{\mu\lambda}$ are assumed to depend only on the atoms A and B on which μ and λ are centred, and not the actual type of the orbitals. Thus we have $\gamma_{\mu\nu} = \gamma_{AB}$ for all μ and λ.

(iv) Integrals $(\mu | V_B | \nu)$ where ϕ_μ and ϕ_ν belong to the same atom, A, are put equal to zero unless $\mu = \nu$ in which case the integral is taken to be identical for all valence AO's on A

$$(\mu | V_B | \mu) = V_{AB} \qquad (5.11)$$

V_B is the potential for the atom B due to its nucleus and inner shell electrons.

(v) The off-diagonal core matrix elements between AO's ϕ_μ and ϕ_ν (which are centred on A and B respectively) are approximated by

$$H_{\mu\nu} = \beta_{\mu\nu} = \beta^{\circ}_{AB} S_{\mu\nu} \qquad (5.12)$$

$S_{\mu\nu}$ being the overlap integral and β°_{AB} is a parameter depending only on the nature of A and B.

The Fock-operator matrix elements for the CNDO/2 version are given by

$$F_{\mu\mu} = -\frac{1}{2}(I_\mu + A_\mu) + \{(P_{AA}-Z_A) - \frac{1}{2}(P_{\mu\mu} - 1)\}\gamma_{AA} + \sum (P_{BB} - Z_B)\gamma_{AB} \qquad (5.13a)$$

$$F_{\mu\nu} = \beta_{AB} - \frac{1}{2} P_{\mu\nu} \gamma_{AB} \qquad (5.13b)$$

where I_μ and A_μ are the ionization potential and the electron affinity respectively of the orbital μ, P_{AA} is the total charge density on atom A and Z_A is the 'core charge' of atom A. Using (5.13) calculation is carried out till self consistency is achieved in the Fock-operator matrix elements.

Pople and Beveridge[7] have published a standard CNDO/2 and INDO computer program. All the calculations reported in this chapter were carried out using this program to generate the CNDO/2 wavefunctions.

V.3 COMPTON PROFILES FROM CNDO WAVEFUNCTIONS

For the calculation of CP's the $\underset{\sim}{r}$-space wavefunction is Fourier transformed to the $\underset{\sim}{p}$-space

$$f_i(\underset{\sim}{p}) = (2\pi)^{-3/2} \int \psi_i(\underset{\sim}{r})\, e^{-i\underset{\sim}{p}\cdot\underset{\sim}{r}}\, d\underset{\sim}{r} \qquad (5.14)$$

The momentum density $|\chi(\underset{\sim}{p})|^2$ is given,[8] apart from constants, as

$$|\chi(\underset{\sim}{p})|^2 = \sum_i \sum_j \rho_{ij} f_i(p)\, f_j(p) \cdot Y_{l_i m_i}(\theta_p, \phi_p) \cdot Y_{l_j m_j}(\theta_p, \phi_p)\, e^{-i\underset{\sim}{p}.\underset{\sim}{r}_{ij}} \tag{5.15}$$

where $\underset{=}{\rho}$ is the density matrix with

$$\rho_{ij} = 2 \sum_{\mu=1}^{occ} c_{i\mu}\, c_{j\mu} \tag{5.16}$$

In the ZDO approximation, in momentum-space only diagonal matrix elements in Eq. (5.15) survive and the radial momentum density is given by

$$I(p) = \sum_i \int \rho_{ii} |f_i(p)|^2 |Y_{l_i m_i}(\theta_p, \phi_p)|^2 . p^2 \sin\theta_p \, d\phi_p \, d\theta_p \tag{5.17}$$

As pointed out earlier, Figeys et al.[2] have proved the rotational invariance of I(p) for CNDO wavefunctions. This also leads to rotationally invariant CP. The CP, J(q), within the impulse approximation[9] is given by

$$J(q) = \frac{1}{2} \int_{|q|}^{\infty} I(p)/p \, dp \tag{5.18}$$

which reduces to

$$J(q) = \sum_i \rho_{ii} J_i(q) \tag{5.19}$$

on substitution from (5.17). Here $J_i(q)$ is the CP due to i^{th} orbital. Hence, the CP can be calculated, from wavefunctions employing ZDO approximation, with the diagonal elements of the density matrix $\underline{\rho}$ and the individual orbital CP's.[1]

For the STO basis used in the CNDO/2 method, the momentum space wavefunctions for the individual orbitals are given analytically.[10] We present in Table 5.1 various expressions needed in the CP calculations using STO.

It may be noted here that the valence Compton profiles (VCP) have been extracted[11] from the experimentally measured total CP's by subtracting out the corresponding atomic inner shell contributions.[12] In the literature two different sets of values have so far been used for this inner-shell contribution to theoretically calculated CP's. Epstein[8] has subtracted out the atomic C_{1S} CP[12] whereas Whangbo et al.[13,14] have calculated the core contribution by using canonical molecular orbitals. These two sets differ considerably, e.g., they differ by $\sim$12% at the peak. As pointed out by Smith et al,[13] this discrepancy between CMO and LMO core profiles is not due to quality of the basis-set but to localization itself. Localization leads to more contracted core and hence to broader profile. Therefore a comparison among CNDO/2 and LMO theoretical as well as experimental VCP's which employ different levels of approximation for the core contribution, has to be done cautiously.

Table 5.1

Compton Profiles from STO's

Orbital	(r)	f(p)	J(q)
1s	$\left(\frac{\zeta^3}{\pi}\right)^{1/2} e^{-\zeta r}$	$\frac{(8\zeta^5)^{1/2}}{\pi(\zeta^2+p^2)^2}$	$\frac{8\zeta^5}{3\pi(\zeta^2+q^2)^3}$
2s	$\left(\frac{\zeta^5}{3\pi}\right)^{1/2} re^{-\zeta r}$	$\frac{(\frac{8\zeta^5}{3})^{1/2}(3\zeta^2-p^2)}{\pi(\zeta^2+p^2)^3}$	$\frac{2\zeta^5(92\zeta^4-80\zeta^2q^2+20q^4)}{45\pi(\zeta^2+q^2)^5}$
$2p_m$	$\left(\frac{\zeta^5}{3\pi}\right)^{1/2} re^{-\zeta r}.Y_{l,m}(\theta,\phi)$	$\frac{(\frac{128\zeta^7}{3})^{1/2}.p.Y_{l,m}(\theta_p,\phi_p)}{\pi i(\zeta^2+p^2)^3}$	$\frac{32\zeta^7(\zeta^2+5q^2)}{15\pi(\zeta^2+q^2)^5}$

V.4 RESULTS AND DISCUSSION

In Table 5.2 we present VCP's of methane and ethane calculated from CNDO/2 wavefunctions alongwith the profiles calculated from the data of Eisenberger and Marra[11] and experimental CP data of Klapthor and Lee.[15] The corresponding LMO profiles[14] are also given there. In Table 5.3 CNDO/2 VCP's of ethylene and acetylene alongwith those calculated using the data of Eisenberger and Marra[11] are presented. The corresponding LMO[14] VCP for ethylene is also given there. As noted earlier by Ahlenius and Lindner[1] the agreement between CNDO and LMO VCP's is fairly good except for higher values of q where CNDO/2 profiles are broader than the corresponding LMO ones. In the case of methane the agreement between the profile obtained from the data of Eisenberger and Marra,[11] the experimental CP[15] and the CNDO-theoretical profile is fairly good. However, as pointed out in Section V.3, different sets of values have been used in the literature[8,13] for the C_{1S} contribution to CP's in LMO approach. On the other hand, CNDO/2 method treats only valence electrons explicitly. Thus an ambiguity is introduced in the comparison between LMO and CNDO/2 theory as well as experiment.

Ahlenius and Lindner have pointed out that VCP's are not sensitive to localization and the VCP's before and after localization agree through four decimals. Hence in the present work we have considered it unnecessary to proceed with localization.

Table 5.3

Valence Compton Profiles of Ethylene and Acetylene

	ETHYLENE			ACETYLENE
q	CNDO/2	LMO+	E-M*	CNDO/2
0.0	6.962	6.996	6.744	5.563
0.1	6.868	6.920	6.664	5.497
0.2	6.594	6.716	6.456	5.304
0.3	6.171	6.368	6.100	5.002
0.4	5.609	5.896	5.648	4.615
0.5	5.043	5.312	5.104	4.172
0.6	4.424	4.672	4.512	3.700
0.7	3.815	4.004	3.904	3.226
0.8	3.241	3.352	3.304	2.768
0.9	2.719	2.752	2.740	2.343
1.0	2.255	2.216	2.052	1.960
1.2	1.513	1.376	1.172	1.331
1.4	0.992	0.820	0.860	0.880
1.6	0.641	0.484	0.708	0.572
1.8	0.413	0.292	0.412	0.370
2.0	0.267	0.180	0.296	0.239

+Constructed from LMO data of Smith and Whangbo.[13,14]

*Constructed from bond-contributions to experimental CP's following Eisenberger and Marra.[11]

From the VCP's of CH_4, C_2H_6, C_2H_4 and C_2H_2 and consideration of bond additivity of CP's we may write

$$\begin{aligned} J_{CH_4} &= 4J_{C-H} \\ J_{C_2H_6} &= J_{C-C} + 6J_{C-H} \\ J_{C_2H_4} &= J_{C=C} + 4J_{C-H} \\ J_{C_2H_2} &= J_{C\equiv C} + 2J_{C-H} \end{aligned} \tag{5.20}$$

We present CNDO/2 VCP's for these bonds derived from (5.20) in Table 5.4. By employing these bond VCP's, VCP's for some other hydrocarbons may be computed, e.g.,

$$\begin{aligned} J_{C_4H_6(\text{butadiene})} &= 2J_{C=C} + J_{C-C} + 6J_{C-H} \\ J_{C_4H_2(\text{butadiyne})} &= 2J_{C\equiv C} + J_{C-C} + 2J_{C-H} \\ J_{C_3H_4(\text{allene})} &= 2J_{C=C} + 4J_{C-H}. \end{aligned} \tag{5.21}$$

We have also computed the VCP's directly from CNDO/2 wavefunctions for these systems. The geometries of butadiene (trans) and allene were taken from ref. 16. The bond length data in the case of butadiyne was taken from ref. 17. We present VCP's calculated for these systems directly as well as from additivity procedure (5.21) in Table 5.5. We note that the difference between the directly calculated CP using CNDO/2 and CP obtained by addition of bond-profiles is approximately 0.07%, 0.03% and 0.18% respectively at the peak of the profile in the case of

Table 5.4

CNDO/2 Valence Compton Profile Contributions from Various Bonds*

q	C-H	C-C	C=C	C≡C
0.0	1.223	1.026	2.070	3.117
0.1	1.204	1.018	2.052	3.089
0.2	1.149	0.993	1.997	3.006
0.3	1.066	0.948	1.909	2.871
0.4	0.962	0.891	1.790	2.690
0.5	0.849	0.821	1.647	2.474
0.6	0.734	0.743	1.487	2.232
0.7	0.624	0.660	1.318	1.978
0.8	0.523	0.577	1.150	1.723
0.9	0.433	0.496	0.987	1.478
1.0	0.355	0.421	0.836	1.250
1.2	0.234	0.292	0.579	0.864
1.4	0.151	0.197	0.388	0.578
1.6	0.097	0.129	0.254	0.379
1.8	0.062	0.084	0.165	0.246
2.0	0.040	0.055	0.107	0.157

*Vide Eq. (5.20) of text. CP's normalized to 2, 2, 4 and 6 electrons respectively.

Table 5.5

Valence Compton Profiles of Butadiene (trans), Butadiyne and Allene

q	BUTADIENE		BUTADIYNE		ALLENE	
	Direct calculation (CNDO/2)	Addition of bond profiles	Direct calculation (CNDO/2)	Addition of bond profiles	Direct calculation (CNDO/2)	Addition of bond profiles
1	2	3	4	5	6	7
0.0	12.496	12.505	9.703	9.706	9.016	9.032
0.1	12.336	12.344	9.600	9.603	8.904	8.920
0.2	11.874	11.883	9.298	9.303	8.578	8.590
0.3	11.154	11.160	8.818	8.821	8.069	8.082
0.4	10.241	10.245	8.194	8.196	7.422	7.428
0.5	9.208	9.209	7.465	7.466	6.687	6.690
0.6	8.122	8.122	6.674	6.675	5.911	5.910
0.7	7.043	7.040	5.863	5.864	5.136	5.132
0.8	6.016	6.013	5.068	5.067	4.395	4.392
0.9	5.071	5.068	4.318	4.317	3.711	3.706
1.0	4.225	4.222	3.631	3.631	3.097	3.092
1.2	2.854	2.851	2.489	2.487	2.097	2.094
1.4	1.880	1.872	1.655	1.654	1.383	1.380

Table 4.5 (contd.)

1	2	3	4	5	6	7
1.6	1.220	1.219	1.081	1.080	0.899	0.896
1.8	0.787	0.786	0.700	0.699	0.580	0.578
2.0	0.509	0.509	0.453	0.452	0.375	0.374

butadiene, butadiyne and allene respectively. We also note that the directly calculated CP's predict somewhat higher $\langle p^n \rangle$ values than those obtained from bond profiles. This is in accordance with the observation that these molecules contain at least one C-C bond shorter than the corresponding average C-C bonds, giving the molecule extra stability and thus predicting lower energy than that obtained from the 'synthetic' profiles. On the whole one can see the remarkably good agreement between the CNDO/2 results and those obtained using bond-additivity. However, whether these profiles in turn will agree with experiment after taking proper care of the core contributions remains to be seen. Epstein[18] has recently pointed out that CP measurements using high-energy electron scattering techniques, when pushed to maximum accuracy, may be capable of giving J(0) with an error less than 0.1%. Very accurate CP measurements can also be undertaken by scattering of synchrotron radiation.[19] This method is capable of giving large scattered intensity with a much better signal to background ratio than the other methods. It is hoped that the validity of bond additivity for CP's as well as semi-empirical wavefunctions for calculation of CP's may be substantiated in a large number of molecules in the near future with the availability of more refined experimental techniques.

V.5 SUMMARY

VCP's of methane, ethane, ethylene and acetylene calculated from CNDO/2 wavefunctions have been compared with LMO-theoretical

and experimental CP's. The agreement among them is fairly good. However, as noted in Sections V.3 and V.4, the VCP's obtained by LMO approach are not unique due to use of different sets of values of "core contributions". These CNDO/2 VCP's were employed to obtain C-H, C-C, C=C and C≡C bond VCP's. The VCP's of trans butadiene, allene and butadiyne were "synthesized" from the VCP contributions. The results were then compared with directly calculated CNDO/2 VCP's for these molecules and found to agree to within 0.2%. It is pointed out that with the possibility of increased accuracy in the experimental measurements of CP's the bond additivity and semi-empirical approaches may be evaluated more thoroughly and assigned their rightful places.

REFERENCES

1. T. Ahlenius and P. Linder, J. Phys., B8, 778 (1975).

2. C. Edmiston and K. Ruedenberg, Rev. Mod. Phys., 35, 457 (1963).

3. H.P. Figeys, P. Geerlings, C. Alsenoy, Theoret. Chim. Acta, 41, 335 (1976).

4. C.C.J. Roothaan, Rev. Mod. Phys., 23, 69 (1951).

5. J.A. Pople and G.A. Segal, J. Chem. Phys., 44, 3289 (1966).

6. For a review refer to M.J.S. Dewar, "Molecular Orbital Theory of Organic Chemistry", McGraw Hill, New York (1969).

7. J.A. Pople and D.L. Beveridge, "Approximate Molecular Theory", McGraw Hill (1970).

8. I.R. Epstein and W.N. Lipscomb, J. Chem. Phys., 53, 4419 (1970).

9. P. Eisenberger and P.M. Platzman, Phys. Rev., A2, 415 (1970).

10. I.R. Epstein, Chem. Phys. Letters, 9, 9 (1971).

11. P. Eisenberger and W.C. Marra, Phys. Rev. Letters, 27, 1413 (1971).

12. R.J. Weiss, W.C. Phillips and A. Harvey, Phil. Mag., 17, 241 (1968).

13. V.H. Smith, Jr., and M.H. Whangbo, Chem. Phys., 5, 234 (1974).

14. M.H. Whangbo, V.H. Smith, Jr., and W. Von Niessen, Chem. Phys., 6, 282 (1974).

15. R.W. Klapthor and J.S. Lee, Chem. Phys. Letters, 45, 513 (1977).

16. L.C. Snyder and H. Basch, "Molecular Wave Functions and Properties", John Wiley and Sons (1972).

17. L.E. Sutton, "Interatomic Distances", Chem. Soc. (London) Spec. Publ., 11 (1958).

18. I.R. Epstein in "MTP International Review of Science", Phys. Chem., Series II, Theoretical Chem., Eds.A.D. Buckingham and C.A. Coulson, Butterworths, London (1975).

19. M. Cooper, R. Holt, P. Pattison and K.R. Lea, Commun. Phys., 1, 159 (1976).

CHAPTER VI

LOCALIZED MOLECULAR ORBITALS AND γ-RAY COMPTON PROFILES OF ACETONE AND ALLYL ALCOHOL

CHAPTER VI

LOCALIZED MOLECULAR ORBITALS AND γ-RAY COMPTON PROFILES OF ACETONE AND ALLYL ALCOHOL*

VI.1 INTRODUCTION

The localized molecular orbital (LMO) approach (discussed earlier in Section I.9) to Compton profiles (CP) makes it possible to break-up the theoretical CP of a molecule in terms of CP's of components such as inner shells, bond-pairs and lone-pairs. These localized component CP's are transferable and can be used to estimate theoretically CP's of several other molecules by involving additivity of such localized components. Epstein[1] and Smith and Whangbo[2] have obtained LMO contributions to CP's

*The experimental measurements presented in this chapter were made on γ-ray Compton profile set-up at the Nuclear Physics Division, Bhabha Atomic Research Centre (BARC), Bombay. The author is grateful to Dr. N.S. Satya Murthy, Head, Solid State Physics Section, BARC for making available to him the experimental facilities at BARC. Thanks are due to Mr. Praveen Chaddah for making the author conversant with their CP set-up at BARC and several helpful discussions. The author also wishes to thank Dr. V.C. Sahni for his kind interest in this work.

from inner shells, bond-pairs and lone-pairs of molecules containing first-row atoms from Hartree-Fock quality wavefunctions. On the experimental side, Epstein et al.[3] studied three isomers of molecular formula $C_4H_8O_2$, viz., dioxane, n-butyric acid and iso-butyric acid by X-ray scattering technique and compared the experimental CP's with LMO-theoretical profiles. Holt et al.[4] have measured the CP's of cyclopropane and propylene followed by a comparison with LMO-theory. Chaddah and Sahni[5] have carried out a similar study on methyl formate and formic acid. In this chapter we present results of our CP measurements on two isomers, viz., allyl alcohol and acetone. These are then compared with the CP's constructed from Epstein's[1] LMO contributions to CP's. In the following section, we give the experimental details. The present work was carried out using the γ-ray CP set-up at the nuclear Physics Division of the Bhabha Atomic Research Centre, Bombay.

VI.2 EXPERIMENT

The γ-ray Compton profile set-up used for the measurements was similar to that shown schematically in Fig. 1.4. The measurements were carried out at room temperature with 59.54 keV γ-radiation from a ^{241}Am source of strength 100 MCi. The scattering angle was $165\pm2.5^{\circ}$. The scattered γ-ray photons were detected by a Si(Li) solid-state detector. The overall instrumental resolution was 650 eV (full-width at half maximum) and can be

assumed to be quite satisfactory for studying the CP's of acetone and allyl alcohol which are expected to have a width $\sim$ 1.5 keV based on LMO approach. The output from the detector was fed to a preamplifier, followed by a gated biased amplifier and finally energy-analyzed by a multichannel analyzer (MCA) with 400 channels. The overall stability of this detecting system was not very good and readings which showed a drift of more than one channel per run were discarded. The MCA employed for accumulating counts was found to be non-linear in energy and had to be calibrated to obtain the energy corresponding to a given location of MCA. The calibration curve is given in Fig. 6.1. The energy scale was fixed by using the 26.3 keV and 59.54 keV γ-ray peaks from the ^{241}Am source. The region around 290$\pm$30 channels was found to be very nearly linear. The energy corresponding to 292nd channel was 48.45 keV (the CP was centred at $\sim$ 292nd channel) and the slope in this region was 0.112 keV/channel. Samples were kept in glass cups in an air-tight vessel covered with a thin mylar foil. Background runs were recorded with the sample removed. However, during the course of the measurements it was found that the background was quite high, typically $\sim$ 40% of the scattered intensity observed with the samples in position in the Compton peak region. The counts for acetone and allyl alcohol were accumulated for 4000 and 3600 min. respectively, giving $\sim$ 8000 and $\sim$ 7500 counts respectively in the Compton peak region. The background counts in this region were $\sim$5000 and $\sim$4500 respectively. Thus the statistical uncertainty

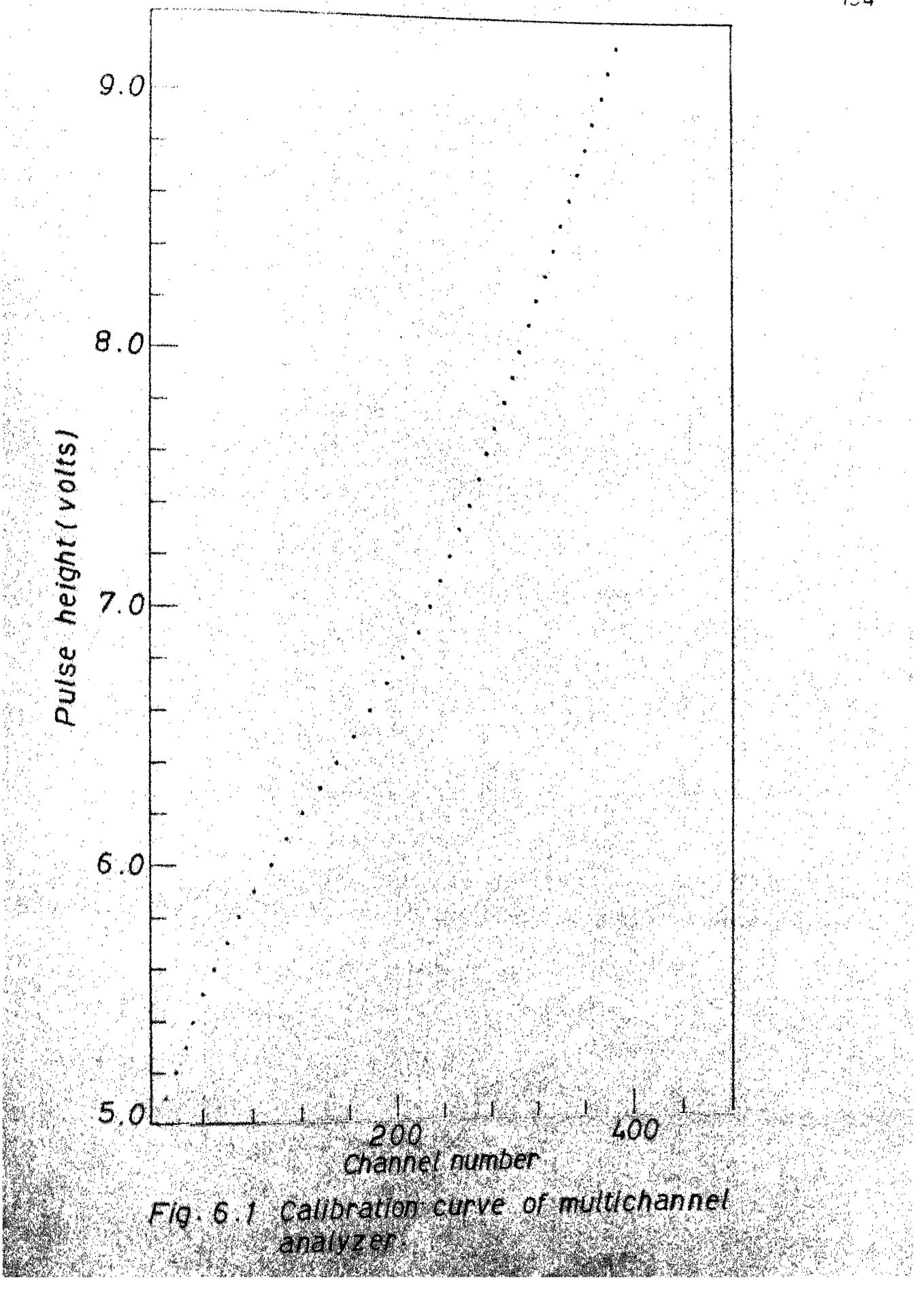

Fig. 6.1 Calibration curve of multichannel analyzer.

in the Compton peak region was of the order of 1.6%. The raw experimental data are presented in Table 6.1. The instrumental resolution function (IRF) was measured with a 1μCi ^{241}Am source in order to ensure approximately similar counting rate as in the actual experimental measurement. The IRF is shown in Fig. 6.2.

VI.3 DATA ANALYSIS AND RESULTS

As discussed earlier in Section I.5.A, two different approaches can be followed for data analysis:

(i) Deconvolution of the experimental CP with the instrumental resolution function (IRF) and comparing the results with theory.

(ii) Convolution of the theoretical CP with IRF followed by comparison with experiment.

Paatero et al.[6] have studied convolution in CP measurements in detail. The deconvolution approach poses numerical problems due to the algorithm used and yet one has to convolute the theoretical CP with the residual instrumental function[6] before comparison with the experiment. The residual instrumental function may be quite broad and may have oscillatory character. To avoid these difficulties, we have chosen the latter approach of convoluting the theoretical CP with IRF, which was used earlier by Chaddah and Sahni.[5] Theoretical CP's were obtained following the LMO approach of Epstein.[1] Thus

Table 6.1

Compton Scattering by Acetone and Allyl-Alcohol-Raw Experimental Data

Channel No.	Energy (keV)	ACETONE			ALLYL ALCOHOL		
		Total counts+ (A)	Back-ground (B)	(A-B)	Total Counts* (C)	Back-ground (D)	(C-D)
1	2	3	4	5	6	7	8
276	46.660	2548	847	1701	2167	762	1405
277	46.772	2698	894	1804	2459	805	1654
278	46.884	2862	878	1984	2650	790	1860
279	46.996	3103	927	2176	2907	834	1073
280	47.108	3477	954	2523	3249	859	2390
281	47.220	3858	971	2887	3657	874	2783
282	47.332	4374	1043	3331	4034	939	3095
283	47.444	4937	1107	3830	4778	996	3782
284	47.556	5649	1223	4426	5395	1101	4194
285	47.668	6532	1444	5088	6047	1300	4747
286	47.780	7254	1541	5713	6585	1387	5198
287	47.892	8530	2153	6377	7854	1938	5926
288	48.004	9741	2714	7027	8801	2443	6358
289	48.116	10892	3317	7575	9820	2985	6835
290	48.228	12091	4291	7800	11499	4375	7124
291	48.340	12899	4917	7982	11742	4425	7317
292	48452	13115	5068	8041	11980	4561	7419
293	48.564	12896	5164	7832	12015	4738	7277
294	48.676	12474	4963	7511	11459	4467	6992

Table 6.1 (contd.)

1	2	3	4	5	6	7	8
295	48.788	12016	4674	7342	10854	4207	6647
296	48.900	10809	3970	6839	9708	3573	6135
297	49.012	9118	2892	6236	8296	2603	5693
298	49.124	7695	2194	5501	6749	1975	4774
299	49.236	6833	1954	4879	5809	1757	4152
300	49.348	5898	1760	4138	5254	1584	3670
301	49.460	5027	1595	3468	4356	1382	2974
302	49.572	4158	1180	2978	3543	1062	2481
303	49.684	3547	962	2585	3142	866	2276
304	49.796	2992	636	2354	2756	572	2184
305	49.908	2551	450	2101	2316	405	1911
306	50.020	2202	321	1880	1974	289	1685
307	50.132	1804	258	1546	1705	232	1473
308	50.244	1657	205	1452	1455	185	1270

+ Data accumulated in 4000 minutes.

* Data accumulated in 3600 minutes.

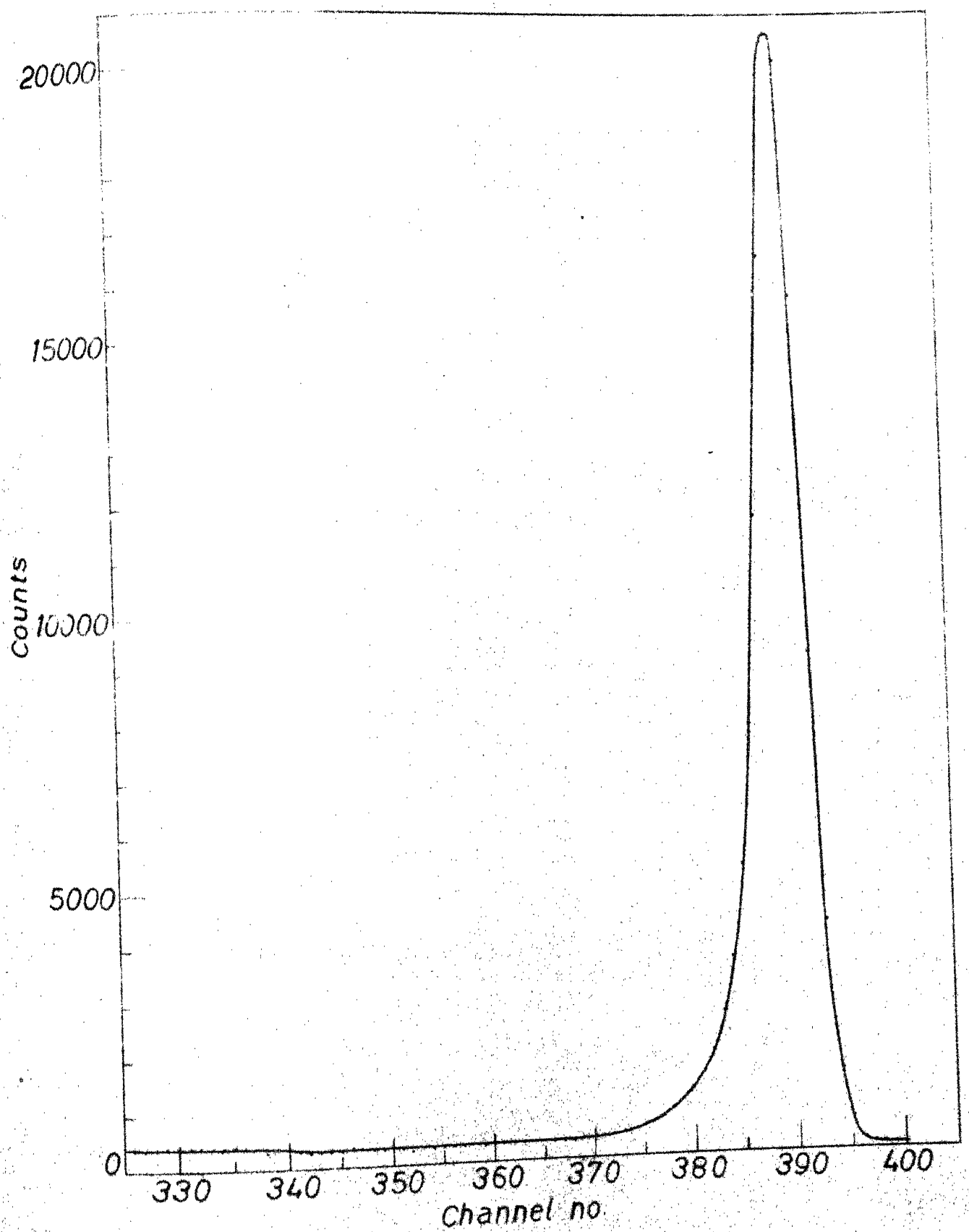

Fig. 6.2 Instrumental resolution function (IRF) measured with 1 μCi ^{241}Am source

for acetone we have

$$J_{Acetone} = 4J_{C_{1s}} + 2J_{O_{1s}} + 4J_{O_{lp}} + 12J_{C-H} + 4J_{C-O} \qquad (6.1)$$

while for allyl alcohol

$$J_{\substack{Allyl \\ alcohol}} = 4J_{C_{1s}} + 2J_{O_{1s}} + 4J_{O_{lp}} + 10J_{C-H} + 2J_{C-O} + 2J_{O-H} \qquad (6.2)$$

The LMO-CP's of acetone and allyl alcohol calculated from equations (6.1) and (6.2) employing Epstein's[1] data are given in Table 6.2.

Data analysis was carried out with the formulae given in references 7 and 8. The theoretical CP was converted to energy scale by the formula

$$p_z = mc \frac{\omega_2 - \omega_1 + \omega_1\omega_2 (1-\cos\theta)/mc^2}{(\omega_1^2 + \omega_2^2 - 2\omega_1\omega_2 \cos\theta)^{1/2}} \qquad (6.3)$$

where mc = 137 in atomic units, thus obtaining a function $J(\omega_2)$. Subsequently corrections for absorption in the sample, energy dependence of relativistic Compton cross section and energy dependence of detector efficiency were applied. $I(\omega_2)$ was obtained after applying all these corrections.

$$I(\omega_2) = A(\omega_2) \cdot C(\omega_2) \cdot D(\omega_2) \cdot J(\omega_2) \qquad (6.4)$$

Table 6.2

LMO- Theoretical* Compton Profiles of Acetone and Allyl Alcohol

q	Acetone	Allyl alcohol	q	Acetone	Allyl alcohol
0.0	13.504	13.440	1.7	2.068	2.064
0.1	13.392	13.332	1.8	1.812	1.804
0.2	13.036	13.013	1.9	1.617	1.611
0.3	12.482	12.474	2.0	1.465	1.459
0.4	11.752	11.750	2.1	1.325	1.319
0.5	10.888	10.902	2.2	1.208	1.202
0.6	9.929	9.952	2.3	1.132	1.128
0.7	8.901	8.957	2.4	1.027	1.023
0.8	7.871	7.911	2.5	0.962	0.958
0.9	6.888	6.926	2.6	0.904	0.900
1.0	5.952	5.984	2.7	0.845	0.843
1.1	5.112	5.138	2.8	0.795	0.791
1.2	4.376	4.396	2.9	0.753	0.751
1.3	3.732	3.742	3.0	0.717	0.715
1.4	3.188	3.198			
1.5	2.743	2.743			
1.6	2.370	2.366			

*Constructed from LMO CP data of Epstein.[1]

Here, A (ω_2) is the correction due to absorption in a flat sample

$$A(\omega_2) = \frac{1-e^{-d(\mu(\omega_1)\ \mathrm{cosec}\ \alpha + \mu(\omega_2)\ \mathrm{cosec}\ \beta)}}{\{\mu(\omega_1) + \mu(\omega_2) \cdot \frac{\sin\alpha}{\sin\beta}\}} \qquad (6.5)$$

$\mu(\omega_1)$ and $\mu(\omega_2)$ are linear absorption coefficients, d is the sample thickness (0.4 cm in the present case) and α and β are the angles between the sample surface and the incident and scattered beams respectively. The linear absorption coefficient data were taken from the tables given by Victoreen.[9]

The energy dependence of the relativistic Compton cross section is given by[8]

$$C(\omega_2) = \left(\frac{e^2}{4m_o^2\pi^2c^2}\right)^2 \cdot \left\{\frac{\omega_1(1+p_z/m_oc)}{\omega_2(1-p_z/m_oc)} + \frac{\omega_2(1-p_z/m_oc)}{\omega_1(1+p_z/m_oc)}\right\}$$

$$\times \frac{\omega_2 m_o c}{2\omega_1\ (\omega_1^2 + \omega_2^2 - 2\omega_1\omega_2\ \cos\theta)^{1/2} + (p_z/m_oc)(\omega_1-\omega_2)} \qquad (6.6)$$

The data on energy dependence of the detector efficiency was kindly provided to us by Chaddah. The detector efficiency at various energies was calculated by interpolation of this data.

$I(\omega_2)$ thus obtained by application of the above corrections via Eq. (6.4) was convoluted after detector efficiency corrections with the IRF given in Fig. 6.2. The IRF presented

in Fig. 6.2 was measured for the Compton line at 59.54 keV, but the same line shape was used to carry out convolution of the theoretical CP centred at $\sim$48.4 keV. The convolution in the present case is reduced to a matrix multiplication:

$$h(x_j) = \sum_i g(x_j - x_i) \cdot f(x_i) \Delta\omega \qquad (6.7)$$

where the subscripts refer to channel number, f is the theoretical spectrum, g is the IRF and h is the observed spectrum. The theoretical CP's corrected for the energy dependent terms and convoluted with IRF were thus obtained. The multiple scattering corrections to Compton scattering data were discussed earlier in Section I.4. However, we did not apply these multiple scattering corrections. Accordingly, the present CP data may be uncertain to 3-5% at the peak. Figs. 6.3 and 6.4 show the experimental CP's of acetone and allyl alcohol respectively alongwith the theoretical profiles with all corrections stated above followed by convolution with IRF. The agreement can be seen to be good in both the cases. However, with the accuracy available in the present measurements, comparison between the experimental CP's of acetone and allyl alcohol is not meaningful.

VI.4 SUMMARY AND CONCLUSIONS

Experimental CP's of acetone and allyl alcohol were measured by scattering of 59.54 keV γ-rays from a ^{241}Am source and the results compared with the LMO-theoretical profiles after

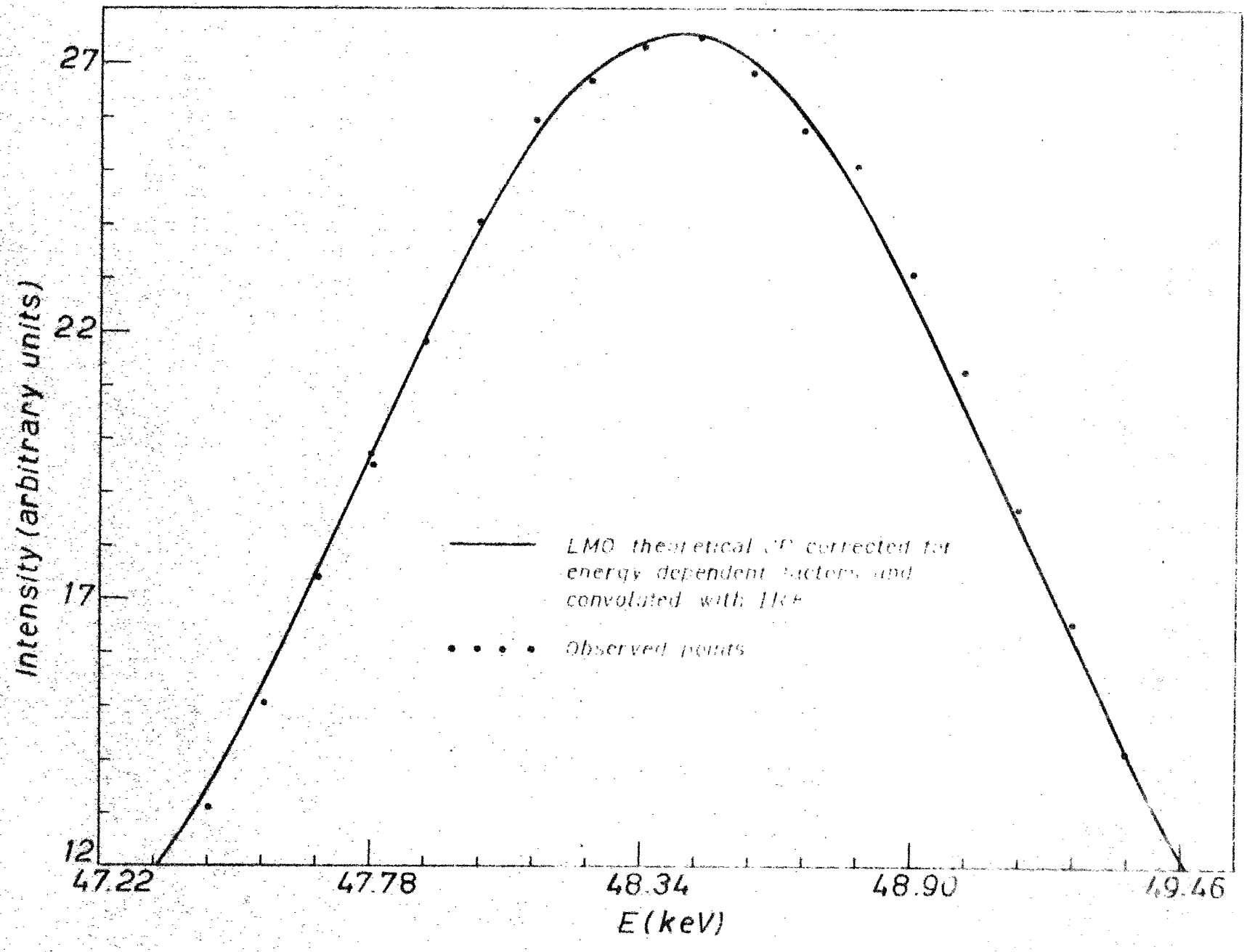

Fig. 6.3 Comparison of the measured and theoretical profiles for allyl alcohol.

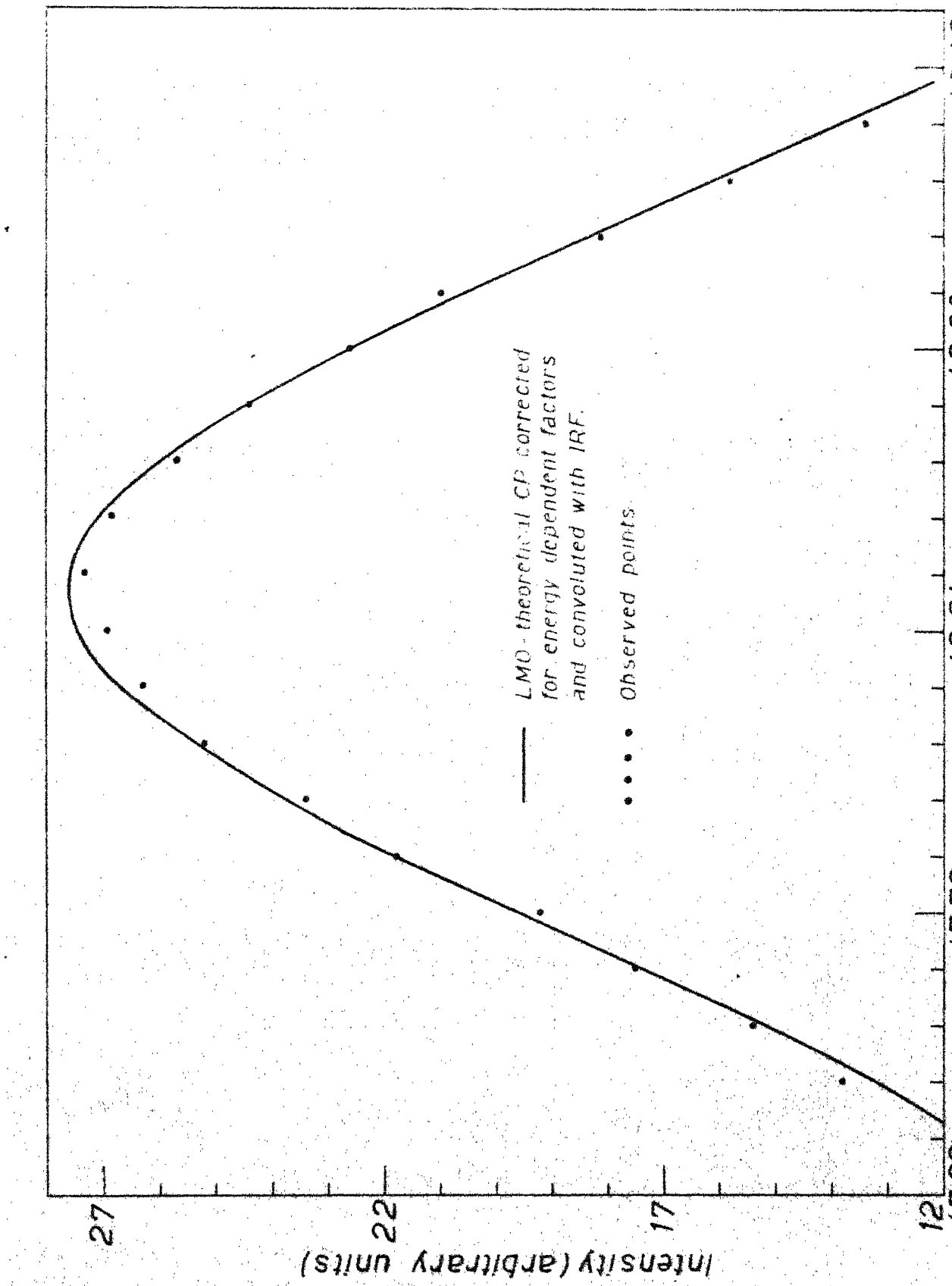

Fig. 6.4 Comparison of the measured and theoretical profiles for acetone.

the latter were corrected for energy dependent terms and convoluted with the instrumental resolution function. Multiple scattering corrections were not applied. The agreement between theory and experiment is good. However, due to several limitations of the experimental set-up and owing to accumulation of relatively smaller number of counts (implying larger statistical uncertainties) no meaningful comparison can be carried out between the present experimental CP's themselves. Very few attempts have so far been made to measure CP's of isomeric compounds and correlate these with some other molecular property. However, with recent revival of interest in this area and use of very strong annular γ-ray sources[10] it may be hoped that many more of such studies would be forthcoming.

REFERENCES

1. I.R. Epstein, J. Chem. Phys., 53, 4425 (1970).

2. V.H. Smith, Jr. and M.H. Whangbo, Chem. Phys., 5, 234 (1974).

3. I.R. Epstein, B.G. Williams and M.J. Cooper, J. Chem. Phys., 58, 4098 (1976).

4. R. Holt, P. Pattison and M. Cooper, Chem. Phys. Letters, 43, 606 (1976).

5. P. Chaddah and V.C. Sahni, Chem. Phys. Letters, 46, 311 (1977).

6. P. Paatero, S.Manninen and T.Paakkari, Phil. Mag., 30, 1281 (1974).

7. S.Manninen, T.Paakkari and K. Kajantie, Phil. Mag., 29, 167 (1974).

8. P. Eisenberger and W.A. Reed, Phys. Rev., B8, 3237 (1974).

9. J.A. Victoreen, J. Appl. Phys., 20, 1141 (1949).

10. W. Weyrich, private communication (1977).

CHAPTER VII

CALCULATION OF ATOMIC AND MOLECULAR ENERGIES FROM EXPERIMENTAL COMPTON PROFILES

CHAPTER VII

CALCULATION OF ATOMIC AND MOLECULAR ENERGIES FROM EXPERIMENTAL COMPTON PROFILES*

VII.1 INTRODUCTION

In this chapter we shall examine the theoretical relationship between Compton profile (CP) data and one of the most important quantities of interest to chemists, viz., energy. Relationships between the Compton profile, $J(q)$ and $\langle p^n \rangle$ where $n = 0, 1, \ldots$ are available in the literature. The test of the relationship between $J(q)$ and $\langle p^2 \rangle$ in particular has been made here by fitting the experimental CP data to a linear combination of Gaussians thereby facilitating the evaluation of total energy.

---

*The material presented in this chapter has been published in the form of a Research Note: S.R. Gadre and P.T. Narasimhan, Mol. Phys., 31, 1613 (1976).

VII.1.A Relationship Between Energy and Compton Profile

Coulson,[1] Benesch and Smith[2] and Epstein[3] have independently derived the relationship between the electronic momentum expectation values $\langle p^n \rangle$ and J(q), the Compton profile (CP), of an atomic or molecular system. Coulson's[1] derivation is as follows: Let p be the momentum of the electron. The expectation value of kinetic energy in the N-electron system is then $\langle T \rangle = \frac{1}{2} N \langle p^2 \rangle$. Applying virial theorem, viz., $E_{Total} = -\langle T \rangle$ where E_{Total} is the total energy of the system. Thus

$$E_{Total} = -\frac{1}{2} N \langle p^2 \rangle = -\frac{1}{2} \int p^2 . \rho (\underset{\sim}{p}) \; p^2 \sin\theta_p \, d\theta_p \, d\phi_p \, dp \qquad (7.1)$$

Using the definition

$$I(p) = \int \rho(\underset{\sim}{p}) . p^2 \sin\theta_p \, d\theta_p \, d\phi_p \qquad (7.2)$$

expression (7.1) is reduced to

$$E_{Total} = -\frac{1}{2} \int_0^\infty p^2 . I(p) . dp \qquad (7.3)$$

Since the CP, J(q), within the impulse approximation,[4] is given by

$$J(q) = \frac{1}{2} \int_{|q|}^\infty \frac{I(p)}{p} \, dp \qquad (7.4)$$

the radial momentum density I(p) is

$$I(p) = -2p \left. \frac{dJ(q)}{dq} \right|_{q=p} \qquad (7.5)$$

Hence (7.3) is reduced to

$$E_{Total} = \int_0^\infty p^3 \left.\frac{dJ(q)}{dq}\right|_{q=p} dp \qquad (7.6)$$

Carrying out the integration in (7.6) by parts

$$E_{Total} = p^3.J(p)\Big|_0^\infty - 3\int_0^\infty p^2.J(p)\,dp \qquad (7.7)$$

If the CP dies out faster than q^{-3} as $q \to \infty$, the first term in (7.7) vanishes and the expression for E_{Total} is reduced to

$$E_{Total} = -3\int_0^\infty q^2\,J(q)\,dq \qquad (7.8)$$

Coulson[1] also pointed out that if J(q) is found empirically as a sum of the individual component J(q)'s (e.g., according to the localized molecular orbital (LMO) approach[5]), E_{Total} is also additive. Thus the additivity of CP's implies the additivity of bond energies.

VII.1.B Relationship Between $\langle p^n \rangle$ and Compton Profile

A more general expression (7.9) for $\langle p^n \rangle$ was derived independently by Epstein[3] using an approach similar to that of Coulson's[1]:

$$\langle p^n \rangle = 2(n+1)\int_0^\infty q^n.J(q)\,dq \qquad , n \geq 0 \qquad (7.9)$$

Benesch and Smith[2] also arrived at this equation (Eq. (7.9)) by an identical approach. They also pointed out that this equation is valid for $0 \leq n \leq 4$ by considering the asymptotic behaviour of the natural orbitals (NO's). For s-type NO's

$$\chi_s(p) = \sqrt{\frac{2}{\pi}} \int_0^\infty \chi_s(r) . j_o(pr) . r^2 dr \qquad (7.10)$$

where $\chi_s(r)$ and $\chi_s(p)$ are the NO's in $\underset{\sim}{r}$ and $\underset{\sim}{p}$ space respectively and $j_o(pr)$ is the Bessel function

$$j_o(pr) = \sin(pr)/pr \qquad (7.11)$$

For large values of p, (7.10) yields

$$\chi_s(p) = -\left(\frac{8}{\pi}\right)^{1/2} \left(\frac{\partial \chi_s}{\partial r}\right)_{r=0} . p^{-4} + O(p^{-6}) \qquad (7.12)$$

where $O(p^{-6})$ denotes terms of the order of p^{-6}. Since the orbitals of higher angular momentum give leading contributions $O(p^{-5})$, $O(p^{-6})$ etc. which die out faster, the asymptotic behaviour of I(p) (and hence of J(q)) is governed by the s-type NO's. Using the cusp condition for s-type NO's, viz.

$$\left(\frac{\partial \chi_s}{\partial r}\right)_{r=0} = -Z \chi_s(0) \qquad (7.13)$$

Eq. (7.12) is simplified to

$$\chi_s(p) = \left(\frac{8}{\pi}\right)^{1/2} Z\, \chi_s(0).p^{-4} + O(p^{-6}) \qquad (7.14)$$

yielding for large q values,

$$J(q) = \frac{8Z^2}{3}\, \rho_o(0).q^{-6} + O(q^{-8}) \qquad (7.15)$$

where $\rho_o(0) = \Sigma\, \lambda_s\, \chi_s^{\,2}(0)$ (7.16)

λ_s being the occupation numbers of s-type NO's. Since the contribution to J(q) from s-type NO's is the slowest-varying term of the contributions from various NO's (viz., s, p, d...types), J(q) dies out $\sim q^{-6}$ as $q \longrightarrow \infty$. Thus the sum rule (7.9) is valid only for $0 \leq n \leq 4$.

VII.1.C Physical Significance of $\langle p^n \rangle$

Physical significance of various $\langle p^n \rangle$ values was explicitly pointed out by Epstein[3]. $\langle p^o \rangle$ is simply the normalization constant. Epstein has made a speculation that it may be possible to correlate $\langle p \rangle$, the average magnitude of the current density, to the shielding in nuclear magnetic resonance. $\langle p^2 \rangle$ is related to the electronic energy (vide Eq. (7.8)). Relativistic corrections are proportional to $\langle p^4 \rangle$. Another observable

directly available from the CP is $\langle p^{-1} \rangle = \frac{1}{2} J(0)$. Thus Eq. (7.8) and the more general Eq. (7.9) have potential applications in chemistry. Energies are conventionally derived from spectroscopic and thermodynamic data. However, Eq. (7.8) gives a new and novel method of obtaining E_{Total} directly from the experimental CP.

VII.1.D Errors in the Evaluation of $\langle p^n \rangle$ from Compton Profiles

Epstein[3] has examined this problem of evaluating various $\langle p^n \rangle$ values from the CP's in more detail. He has considered the effects of truncation of momentum-range and experimental errors. The former was studied by him by introducing partial expectation values

$$p^n(p_h) = 2(n+1) \int_0^{p_h} p^n J(p)\, dp \qquad (7.17)$$

where p_h is the highest momentum at which the CP is measured. $p^n(p_h)$ increases monotonically with p_h and

$$\mathrm{Lim}_{p_h \to \infty}\, p^n(p_h) = \langle p^n \rangle \qquad (7.18)$$

Epstein analyzed the behaviour of $p^n(p_h)$ for 1s and 2p type STO's for which analytic expressions for $J(q)$ are available. Denoting the difference $\{\langle p^n \rangle - p^n(s)\} / p^n(s)$ by Δ^n (where $s = p_h/a$, a being the orbital exponent), he studied the

systematic truncation error Δ^n. From this analysis, he obtained the highest momentum values(upto which the CP measurements should be carried out) for ensuring an arbitrary accuracy in various $p^n(p_h)$ expectation values. He also noted that a similar analysis using a linear combination of atomic orbitals should provide reasonable limits of the relative truncation errors and the momentum range required for obtaining a given accuracy in $p^n(p_h)$.

Epstein[3] also analyzed the effects of random experimental error associated with each point of the CP. He concluded that the problem of truncation error can only be resolved by increasing the range of momentum in CP measurements. With γ-ray scattering techniques the present limit is 30 a.u. However, given a fixed number of analyzing channels, increasing p_h will increase the energy spacing between two successive channels and lead to greater statistical errors. The statistical errors can be reduced by either increasing the counts taken at each point or by decreasing the spacing between two successive points. Another approach would be to record more accurate data at higher momentum than at low values of momentum. These points should be borne in mind when one makes use of experimental CP data available in the literature for evaluating $\langle p^n \rangle$.

VII.2 FITTING OF EXPERIMENTAL DATA TO A LINEAR COMBINATION OF GAUSSIANS

In the light of the above discussion, it was felt that one way to overcome the truncation problem in calculating $\langle p^n \rangle$ values from the experimental CP's would be to fit the available experimental CP data to a prescribed analytical form. Another approach[6] is to append the theoretically calculated high-momentum atomic "tails" to the experimental data.

We have studied the former approach and fitted the experimental CP's to a linear combination of Gaussians:

$$J(q) = \sum_i C_i \exp(-\alpha_i q^2) \tag{7.19}$$

Optimized C_i and α_i can be obtained by a least-squares fitting which minimizes the error in fitting given by

$$\text{Error} = \Sigma(J_{\text{expt.}}(q) - J(q))^2 \tag{7.20}$$

for all the q-values for which J(q) is available experimentally. The advantage of such a Gaussian-fit is that all $\langle p^n \rangle$ values (vide Eq. (7.9)) can be evaluated analytically. The energy, E_{Total}, is now given by

$$E_{\text{Total}} = -\frac{3\sqrt{\pi}}{4} \sum_i \frac{C_i}{\alpha_i^{3/2}} \tag{7.21}$$

and

$$\int_0^\infty J(q)\,dq = \frac{\sqrt{\pi}}{2} \sum_i \frac{C_i}{\alpha_i^{1/2}} \tag{7.22}$$

We have examined the CP's obtained by X-ray, γ-ray as well as electron scattering for some atomic and molecular systems. With 6-8 Gaussians (i.e., 12-16 parameters), reasonably good fits were obtained in all the cases examined. The error in fitting expressed by equation (7.20) was typically $\sim 10^{-4}$. Our Gaussian fits obeyed the normalization condition

$$\int_0^\infty J(q)\,dq = N/2\ , \tag{7.23}$$

N being the number of electrons in the system, to within 0.8%. Subroutine STEPIT[7] was employed to obtain these least-squares fits. We have also checked our fitting procedure by employing the theoretical CP[8] for Be 2s orbital. Our $< p^2 >$ value thus obtained agrees with the theoretical value to within 0.2%.

In the next section we give some relevant details about Subroutine STEPIT used for optimization.

VII.3 SUBROUTINE STEPIT

STEPIT is a general optimization subroutine. It can be used to find local minima of a real function of several variables. STEPIT uses only function values - no derivatives. It

can be employed for optimizing functions which are completely non-linear in the parameters. Only restriction is that the function to be minimized must be smooth, i.e., it must be a continuous function defined on a continuous domain and all the first partial derivatives must be continuous. A direct search procedure is employed in this routine, which is as follows: The direction of the valley is determined by a cyclic relaxation - first parameter is varied till the function value is minimized with respect to it. The same procedure is then applied successively to all the other parameters. When an improvement in the function value is obtained, step sizes are increased or decreased accordingly. When a minimum is bracketed,parabolic interpolation is used. After two such cycles of variation of parameters, a comparison is made between the direction of resultants. This variation of the direct search procedure has an advantage that the function value always decreases and the search never diverges except in the cases where there is a minimum at ∞ . To find a global minimum of functions of more than one variable, there is no known method. A judicious guess of the starting values of parameters followed by direct search appears to be the only solution to this problem.

The call statement is CALL STEPIT (FUNK). FUNK, to be declared EXTERNAL, is the name of the function-computing subroutine. The variables used in the COMMON statement are as

In the next section, we present our results of Gaussian fits to experimental CP data.

VII.4 RESULTS AND DISCUSSION

The Gaussian-fit parameters and the corresponding errors in fitting are given in Table 7.1. Table 7.2 presents our energy results calculated from the experimental CP's, the corresponding Hartree-Fock (HF) and experimental or the best theoretical energies along with the value of the normalization integral. As mentioned above, our Gaussian fits obey Eq.(7.23) to within 0.8%. The experimental profiles are generally normalized by extrapolation to large q-values. However, J(q), in most of the small atomic or molecular systems dies out at q values from 5 to 15 a.u.

The energy values presented in Table 7.2 are given only upto two decimals in view of the limited accuracy of the experimental CP data. We note here that the calculated energies are close to but generally greater than the corresponding HF energies. The deviation from HF energies is upto 6 per cent and can be attributed to large experimental errors (of the order of 10-20 per cent) as well as to the lack of data in the higher q-regions.

Klapthor and Lee[10] have recently fitted their methane CP to a form

Table 7.1

Gaussian-Fit Parameters (vide Eq. (7.19) of text) to Experimental Compton Profiles≠

System		Parameters					Error in fitting‡ x 10^4
He (X-ray)	C_i	-0.02064	0.37980	0.42539	0.17924	0.02455	
	α_i	1.63710	1.05000	1.92300	0.44444	0.38016	
	C_i	0.07101	0.01200				
	α_i	0.19777	20.00000				1.22
He (electron)	C_i	-0.23984	0.31340	0.85605	0.04080	-0.05285	
	α_i	2.09000	0.43000	1.72000	8.00000	0.20000	
	C_i	0.11269	0.03793				
	α_i	0.50000	0.12000				0.91
Ne (X-ray)	C_i	0.97174	0.80807	0.61127	0.15129	0.21545	
	α_i	0.82665	0.61200	0.25389	0.15761	0.10526	
	C_i	-0.05596	0.06835	-0.20383			
	α_i	0.56382	0.04089	3.75640			3.70
N_2 (γ-ray)*	C_i	1.07230	0.80091	0.24686	0.06224	0.05435	
	α_i	0.61382	1.58850	1.08010	0.38280	0.12983	
	C_i	0.10335	0.07966	-0.01815			
	α_i	0.14336	0.77843	10.00000			1.78
H_2 (X-ray)	C_i	0.52056	0.61567	0.35799	0.02095	0.00002	
	α_i	3.29720	1.11340	2.90770	0.24759	0.10000	
	C_i	-0.00022					
	α_i	2.00000					2.12
O_2 (X-ray)	C_i	0.98892	0.25790	0.89640	0.91695	-0.67547	
	α_i	0.49281	0.11049	0.85299	2.18040	3.15920	
	C_i	0.02099	0.02781				
	α_i	2.93450	3.95550				3.87

≠ Compton profile data were taken from the following: P. Eisenberger, Phys. Rev., A2, 1678 (1970)(He(liquid):X-ray, H_2:X-ray); P.Eisenberger, Phys.Rev.A5, 628(1972)(Ne: Ag X-ray, O_2: average of Mo and Ag X-rays); P. Eisenberger and W.A. Reed, Phys. Rev., B9, 3237 (1975)(N_2: γ-ray); H.F. Wellenstein and R.A. Bonham, Phys. Rev., A 7, 1568 (1973)(He: electron).

‡ Vide equation (7.20) of text.

Table 7.2

Energies (in atomic units) from Experimental Compton Profiles along with the Normalization Integral

System	$-E$(calculated from experimental Compton profiles)$^{\neq}$ (in a.u.)	$-E_{H-F}$ (in a.u.)	$-E_{T-E}$ the best theoretical or experimental (in a.u.)	$\int_0^\infty J(q)\,dq$ (total)*
He	2.69 (X-ray)	2.87‡	2.90‡	1.003
	2.73 (electron)			1.001
Ne	125.16 (X-ray)	128.55‡	129.94‡	5.009
H_2	1.13 (X-ray)	1.13[a]	1.17[b]	0.995
N_2	105.23 (γ-ray)	109.00[a]	109.56[b]	7.052
O_2	146.07 (X-ray)	149.67[a]	150.41[b]	7.973

$\neq$ For the sake of uniformity, 1s contributions were subtracted out wherever necessary from the literature experimental Compton profiles. $-\frac{1}{2}\langle p^2\rangle$ for core electrons from ref. 8 were added up as inner shell energies to those obtained from the fits.

* Normalization of the valence profile plus 0.5 per core electron.

‡ E. Clementi, IBM J. Res. Dev., 9, 2 (1965).

a A.C. Hurley in "Advances in Quantum Chemistry", 7, 322, Ed. P.-O. Löwdin, Academic Press (1973).

b R. Daudel "Electronic Structure of Molecules", pp. 15, 21, 42, Pergamon Press (1966).

$$\sum_{n=1}^{M} \frac{a_n}{\{1+\left(\frac{q}{\zeta_n}\right)^2\}^{n+2}} \qquad (7.24)$$

A similar form was also suggested by Epstein[11] as it yields correct asymptotic behaviour expressed by Eq. (7.15). This form has a distinct advantage over the presently used linear combination of Gaussians and should be studied further.

VII.5 SUMMARY AND CONCLUSIONS

Experimental CP's have been fitted to a linear combination of Gaussians. This procedure has the advantage that all $< p^n >$ values can be evaluated analytically from the Gaussian-fit parameters. The energies for He, Ne, N_2, H_2 and O_2 have been evaluated from X-ray, γ-ray as well as electron scattering CP data. These energies are generally larger than the corresponding Hartree-Fock energies and this deviation is upto 6 per cent. This can be attributed to truncation of CP data as well as other experimental errors. It, therefore, seems to us that the energies extracted by the use of Eq. (7.8) from the corresponding experimental CP's to assess the role of correlation[12] in momentum distributions must await further refinement in the quality of experimental data (see also Epstein[3,13]). With the recent revival of interest in CP's and advent of new techniques such as γ-ray

scattering, high energy electron impact spectroscopy[10] and use of synchrotron radiation[14] it appears likely that highly accurate experimental CP data would be forthcoming. With highly accurate CP data and with a better form of fit such as expression (7.24) one may have a novel method of obtaining molecular energies which are otherwise usually extracted from thermodynamic and spectroscopic data.

REFERENCES

1. C.A. Coulson, Mol. Phys., 26, 507 (1973).

2. R. Benesch and V.H. Smith, Jr. in "Wave Mechanics - The First Fifty Years", Ed. W.C. Price, S.S. Chissick and T. Ravensdale, Butterworths (1973), pp. 357-377.

3. I.R. Epstein, Phys. Rev., A8, 160 (1973).

4. P. Eisenberger and P.M. Platzman, Phys. Rev., A2, 415 (1970).

5. I.R. Epstein, J. Chem. Phys., 53, 4425 (1970).

6. B.G. Williams quoted by I.R. Epstein and A.C. Tanner in "The Compton Effect", Ed. B.G. Williams, McGraw Hill (to be published).

7. Subroutine STEPIT-QCPE program no. 66, written by J.P. Chandler, Phys. Dept., Indiana University and distributed by the Quantum Chemistry Program Exchange (QCPE), Department of Chemistry, Indiana University, U.S.A.

8. R.J. Weiss, A. Harvey and W.C. Phillips, Phil. Mag., 17, 241 (1967).

9. R. Hook and T.A. Jeeves, J. Asso. Computing Machinery, 8, 212 (1965).

10. R.W. Klapthor and J.S. Lee, Chem. Phys. Letters, 45, 513 (1977).

11. I.R. Epstein, private communication (1976).

12. R. Benesch and V.H. Smith, Jr., Chem. Phys. Letters, 5, 601 (1970).

13. I.R. Epstein, Accts. Chem. Res., 6, 145 (1973).

14. M. Cooper, R. Holt, P. Pattison and K.R. Lee, Commun. Phys., 1, 159 (1976).

CHAPTER VIII

ENERGY AND COMPTON PROFILE: EMPIRICAL CORRELATION IN ISO-ELECTRONIC SERIES

CHAPTER VIII

ENERGY AND COMPTON PROFILE: EMPIRICAL CORRELATION IN ISO-ELECTRONIC SERIES

VIII.1 INTRODUCTION

There have been very few attempts to correlate molecular Compton profile (CP) parameters, such as width of the CP, $J_{0.5}$ and the peak value J(0) and various $\langle p^n \rangle$ expectation values with other molecular properties. Epstein[1] has recently speculated that it may be possible to correlate $\langle p \rangle$, the average magnitude of current density, available from the CP data to some other molecular property such as shielding in nuclear magnetic resonance. However, no such correlation has as yet been established. Whangbo et al.[2] have attempted to correlate qualitatively the "molecular size" to the J(0) value in the ten-electron isoelectronic series Ne, HF, H_2O, NH_3 and CH_4. They

employed the definition, introduced by Robb et al.[3] of the size, Ω_a of a localized molecular orbital (LMO) electron ϕ_a as the second moment measured at the centre of the charge distribution, $\underset{\sim}{Ra}$,

$$\Omega_a = \langle \phi_a | r^2 | \phi_a \rangle_{\underset{\sim}{Ra}} \qquad (8.1)$$

where $$\underset{\sim}{Ra} = \langle \phi_a | r | \phi_a \rangle_o \ . \qquad (8.2)$$

Whangbo et al. calculated the sizes of the above molecules belonging to the ten-electron series. They argued that as the number of atoms increases in this series, the charge distribution becomes more expanded and leads to sharpening of the CP. However, they did not attempt to correlate quantitatively the J(O) value with the molecular size in this iso-electronic series. We may note here that this parameter, viz., molecular size is purely theoretical, defined within an LMO approach and not experimentally measurable. Whangbo et al.[2] have carried out the calculation of molecular sizes with a basis-set of double-zeta quality. However, the effects of correlation are not included as these calculations are within the Hartree-Fock framework. These correlation effects are, however, reflected directly in experimental measurements. Their importance in the CP calculations has been emphasized.[4]

Chaddah and Sahni[5] have recently measured the CP's of two isomeric compounds of molecular formula $C_2H_4O_2$, viz., acetic

acid and methyl formate. Their experimental CP of acetic acid was broader (as measured by $J_{0.5}$) than that of methyl formate outside the experimental error. They attempted to explain this observation heuristically in two ways:

(a) Diamagnetic molecular susceptibility of methyl formate is higher than that of acetic acid, implying a larger $\langle r^2 \rangle$ value for the former compound and hence larger $\langle p^2 \rangle$ and broader CP for the acid.

(b) The sum of bond energies is larger for acetic acid than that for methyl formate, explaining the broader CP for the acid.

However, regarding their arguments, three points should be borne in mind:

(i) These criteria (a) and (b) are only qualitative.

(ii) They have not been studied for a more general case of iso-electronic series of molecules.

(iii) Many cases of pairs of isomers are encountered where the above criteria (a) and (b) are not mutually consistent, ie., if (a) predicts a broader profile for an isomer A than that of B, the cirterion (b) suggests just the opposite. For example, in the case of diethyl ether and n-butanol, criterion (a) above suggests a broader profile for the former molecule whereas exactly opposite trend is predicted by criterion (b). Similarly in the case of hexene and cyclohexane, a broader profile is predicted for the former compound by criterion (a)

above, whereas criterion (b) predicts a broader profile for the latter compound. It is therefore not possible to decide upon which of the criteria (a) or (b) is applicable *a priori*.

Robb et al.[3] have pointed out that the size and directional property of electronic charge distribution must be correlated with the total energy of the molecular system. In the light of the results of Whangbo et al.[2] discussed above, it may thus be possible to correlate energy of a molecule in an iso-electronic series to its J(0) value. In the following sections, we present our attempt to correlate CP in iso-electronic series with molecular energy.

VIII.2 COMPTON PROFILE PARAMETERS J(0) AND $J_{0.5}$ AND ENERGY IN ISO-ELECTRONIC SERIES

We have recently attempted the correlation[6] between energy E and J(0) using theoretical CP's calculated for CH_4, NH_3, H_2O and HF. Floating spherical Gaussian orbital (FSGO) wavefunctions with two Gaussians to represent an electron pair (double Gaussian FSGO model[7] were employed. In Fig. 8.1 we present the graph of J(0) *vs* $|E|$ within the double-Gaussian FSGO model. The curve is a smooth one and it will be noticed that J(0) decreases monotonically with increasing $|E|$. In Fig. 8.2, our graph of $J_{0.5}$, the width of the CP, *vs* $|E|$ for these molecules within the double-Gaussian FSGO model is presented. The plot turns out to be a straight line in this case and $J_{0.5}$ increases monotonically with $|E|$.

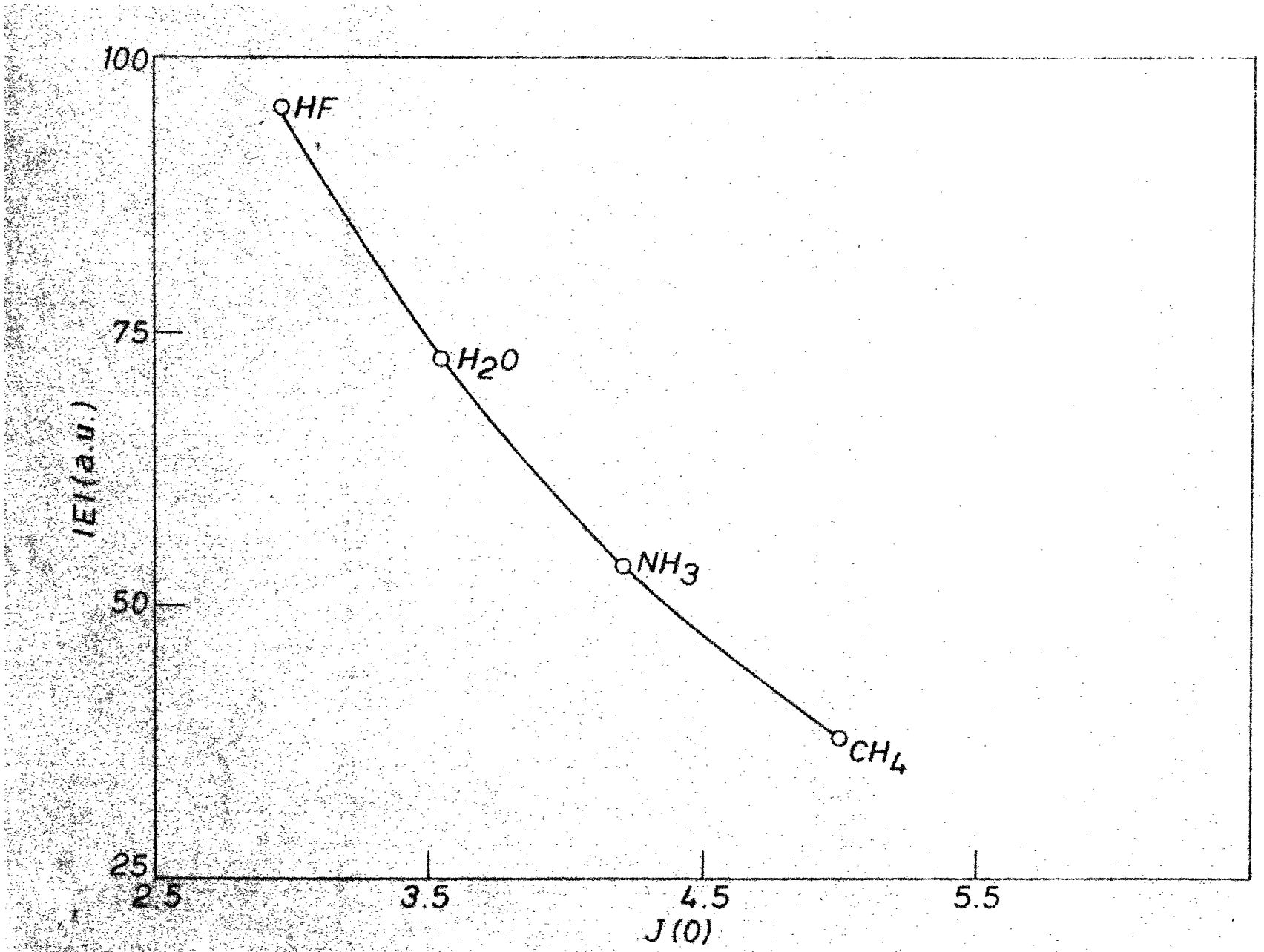

Fig. 8.1 Ten electron isoelectronic series :|E| vs J(0) (in a.u.) calculated in the framework of double Gaussian FSGO model.

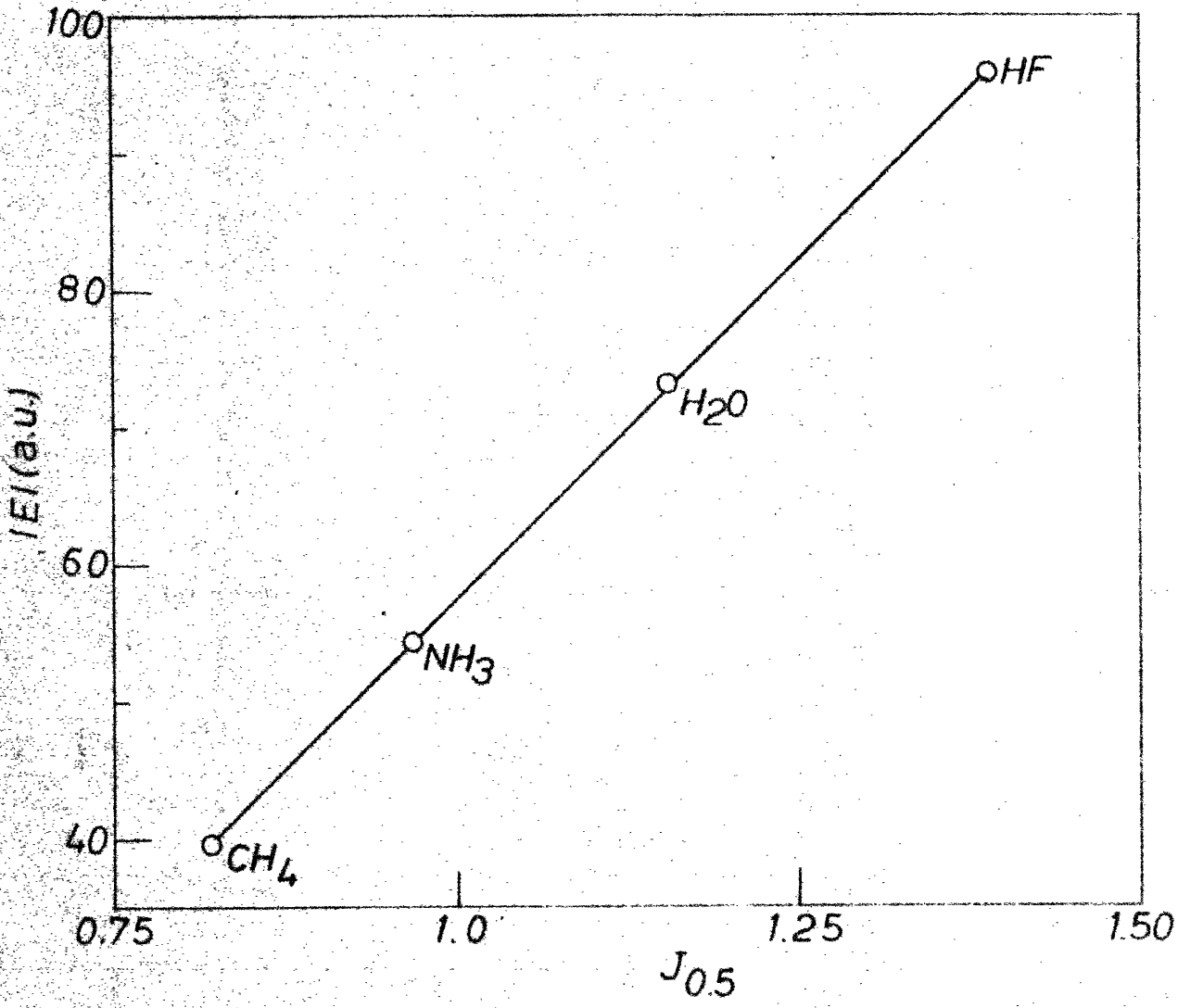

Fig. 8.2 *Ten electron isoelectronic series: $|E|$ vs $J_{0.5}$ (in a.u.) calculated in the framework of double Gaussian FSGO model.*

We may attempt to understand the reason for the monotonic nature of the curves in the following way. It is known that $\langle p^{-1} \rangle$ is related to the peak height of the profile viz., J(0), through the relation

$$\langle p^{-1} \rangle = \frac{1}{2} J(0) \tag{8.3}$$

If the wavefunctions satisfy the virial theorem

$$-\frac{1}{2} \langle p^2 \rangle = E \tag{8.4}$$

then we see that in an iso-electronic series, numerically higher energy values correspond to higher $\langle p^2 \rangle$. However, with higher $\langle p^2 \rangle$ values, one may qualitatively expect lower $\langle p^{-1} \rangle$ values and consequently lower J(0). This trend of higher $|E|$ values corresponding to lower J(0) values is clearly seen in Fig. 8.1. In the ten-electron iso-electronic series considered here, $J_{0.5}$ corresponds to q values around 1 a.u. This region of q is significant from the energy point of view. It may be recalled (see chapter VII) that the molecular energy E is related to J(q) by the relation[8]

$$E = -3 \int_0^\infty q^2 J(q)\, dq \tag{8.5}$$

From the above relation we see that the smaller q-value region

is not significant for energy. Further at very large q values[9] we have J(q) dying out as q^{-6} and hence this region is also not siginificant for energy. Hence, it is the intermediate q-region which is relevant for energy and the values of q corresponding to $J_{0.5}$ belong to this region. The monotonic increase of $|E|$ with $J_{0.5}$ is to be understood in this context.

We have also tested the smooth correlations between $|E|$ and J(0) as well as $|E|$ and $J_{0.5}$ on the ten-electron series of atoms and ions, viz., Mg^{2+}, Na^{+}, Ne, F^{-} and O^{2-}. The free ion CP's were computed from Hartree-Fock wavefunctions obtained by Paschalis and Weiss.[10] For Ne, CP calculated from Hartree-Fock wavefunctions[11] was employed. Figures 8.3 and 8.4 show the graphs of Hartree-Fock $|E|$ vs J(0) and Hartree-Fock $|E|$ vs $J_{0.5}$ respectively for this iso-electronic series. The general trends in these graphs are very similar to those observed above in the case of double-Gaussian FSGO-CP's.

We have attempted to examine the more general empirical correlation of J(q) at a given value of q with $|E|$ for a few iso-electronic series employing a wide variety of wavefunctions. We present the results of this attempted correlation in the following section.

VIII.3 CORRELATION OF J(q) WITH MOLECULAR ENERGY IN ISO-ELECTRONIC SERIES

In Fig. 8.5 we present the graph of theoretical $|E|$ vs J(q) at different values of q for CH_4, NH_3, H_2O and HF calculated within

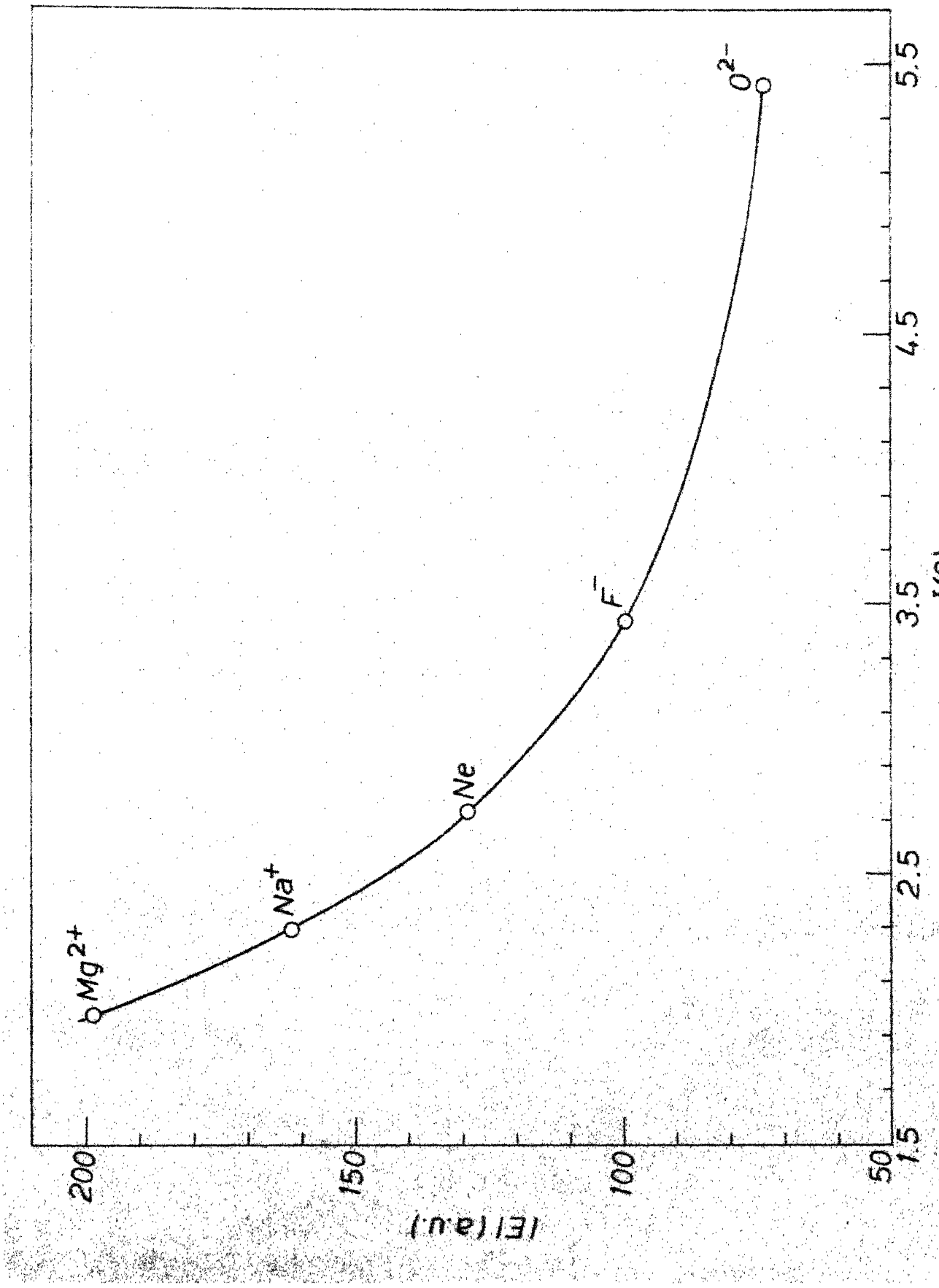

Fig. 8.3 Graph of HF-theoretical IEI vs J(0) (in a.u.) for 10-electron series of atoms and ions.

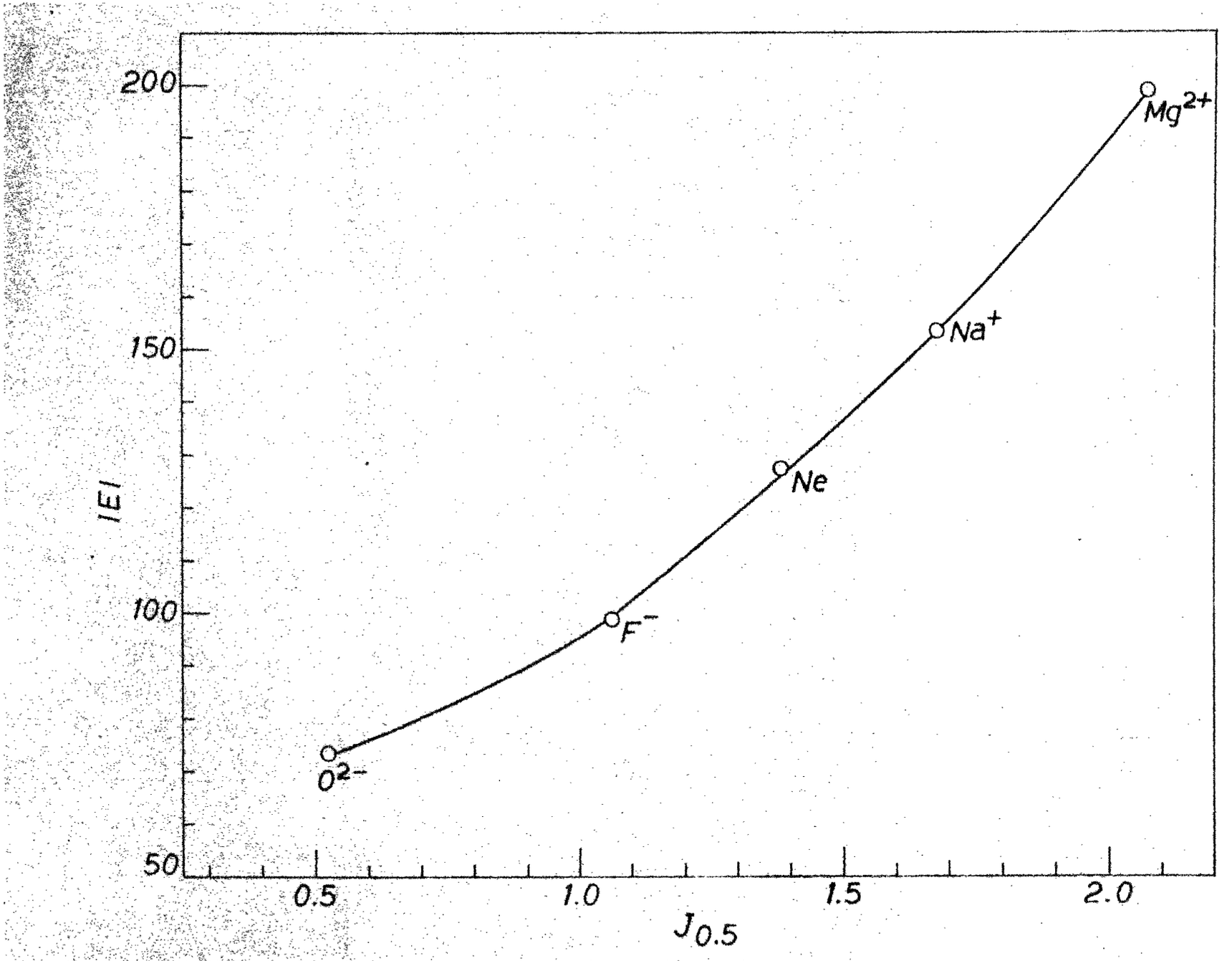

Fig. 8.4 Graph of HF-theoretical IEI vs $J_{0.5}$ (in a.u.) for 10-electron series of atoms and ions.

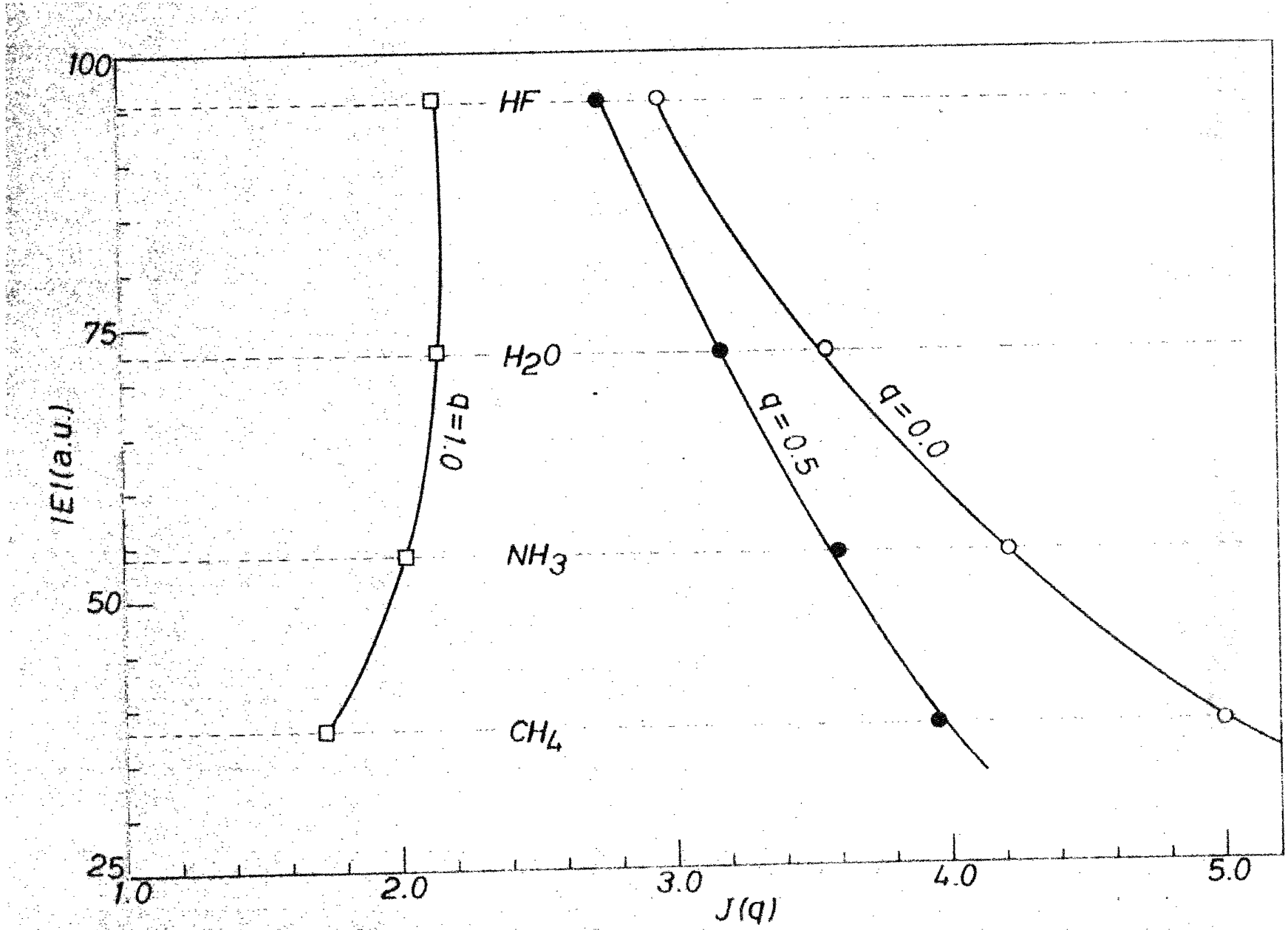

Fig. 8.5 Graph of |E| vs J(q) (in a.u.) at various q-values for 10-electron series within double-gaussian FSGO model

the double Gaussian FSGO model. We again observe that all the points fall on a smooth curve for a given value of q. However, as q increases, the monotonic nature of the curves changes. For lower values of q, the J(q) decreases monotonically with increasing $|E|$. For intermediate q-values, a family of curves is obtained in which the monotonic nature changes gradually, (to monotonically increasing behaviour). For higher values of q, J(q) exhibits monotonically increasing behaviour when $|E|$ increases.

In going down the series $HF \rightarrow H_2O \rightarrow NH_3 \rightarrow CH_4$, we find that the nuclear charge of the heavier atom decreases and lone pairs on the heavier atom are successively replaced by bond pairs. Since the dominant contribution to J(q) comes from more diffuse valence electrons, it is expected that J(q) at small q-values should increase in the series $HF \rightarrow H_2O \rightarrow NH_3 \rightarrow CH_4$. This is clearly seen from Fig. 8.5. Since these CP's are normalized to ten electrons each, it may then be expected that (in order to satisfy the normalization condition) J(q) should decrease in the series $HF \rightarrow H_2O \rightarrow NH_3 \rightarrow CH_4$ for higher values of q.

The behaviour of CP at higher q-values is governed by the core electrons. These electrons contribute most significantly to the energy. The core energies for these molecules can be measured directly by Electron Spectroscopy for Chemical Analysis (ESCA).[12] Since the long-range behaviour of the CP is governed

by the more tightly bound inner shells, it may also be possible to correlate the ESCA core binding energies, E_B with J(q) for higher values of q. In Fig. 8.6 we present a graph of ESCA core binding energies, E_B vs experimental J(q) at q = 5.0 for CH_4, NH_3, H_2O and Ne. These points also fall on a smooth curve which increases monotonically with E_B. Coming now to the total molecular energies in this series, one would expect the core energy contribution to dominate. In that event the molecular |E| vs J(q) curve should increase monotonically for higher values of q. This is also clearly borne out by graphs presented in Fig. 8.5. Thus it may be expected from the above qualitative arguments that in an isoelectronic series J(q) should increase monotonically with |E| for higher values of q, whereas it should decrease monotonically for lower q-values. For intermediate q-region, a gradual transition between these two limiting behaviours is expected.

In Fig. 8.7 we present a family of curves of |E| vs J(q) for various q-values for the 10 electron series of atoms and ions, viz., Mg^{2+}, Na^{+}, Ne, F^{-} and O^{2-}. Hartree-Fock wavefunctions and energies were used to obtain the CP and |E| data. In Fig. 8.8 a similar family of curves for the 18-electron series consisting of C_2H_6, CH_3NH_2, CH_3OH and CH_3F is presented. Here we have employed theoretical CP's and energies calculated by Hirst and Liebmann[13] with wavefunctions which use polarization.[14] Another set of curves is shown for molecules belonging to the 24-electron

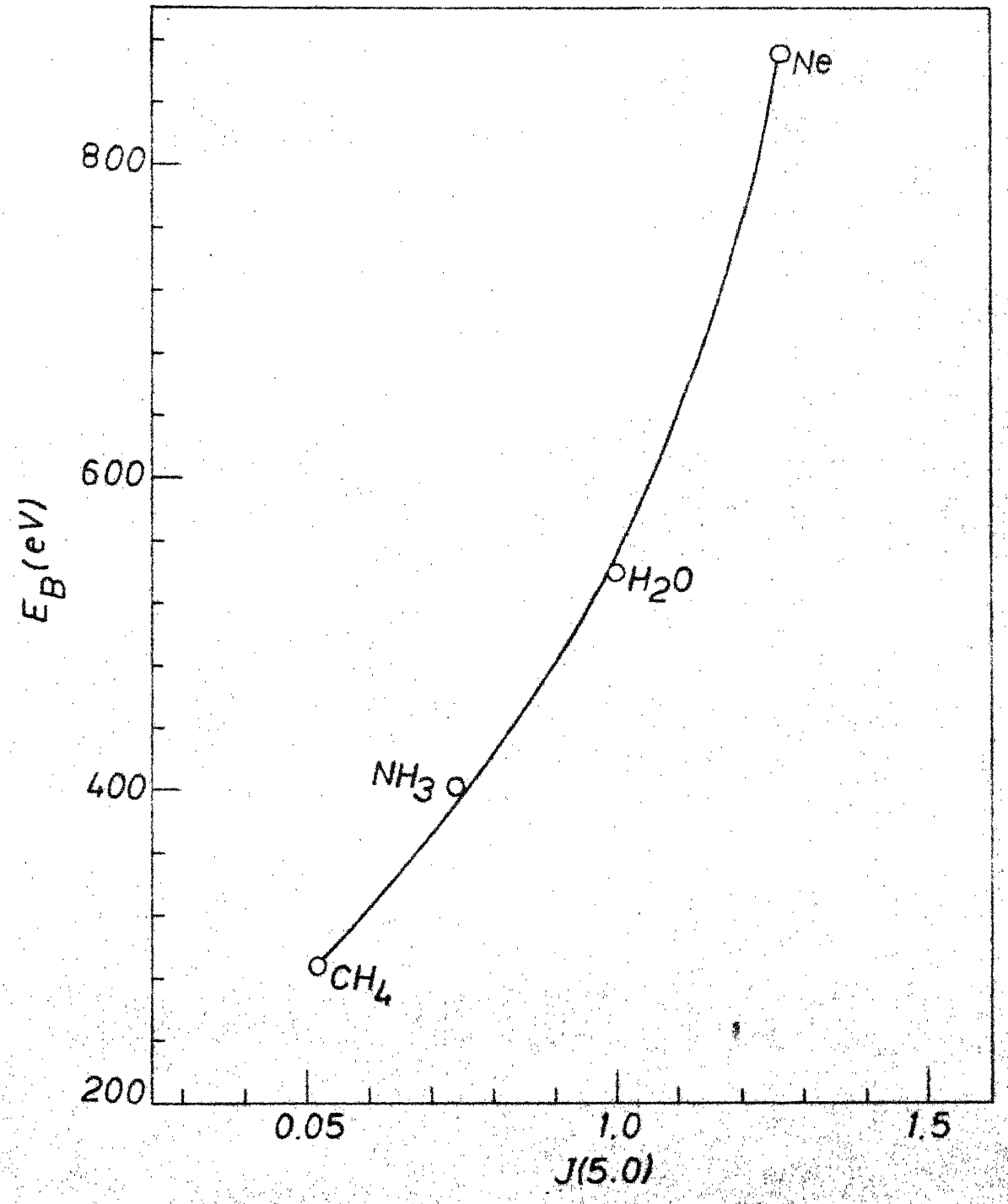

Fig. 8.6 Graph of ESCA binding energies E_B(eV) vs experimental J(5.0) for 10-electron atoms and molecules.

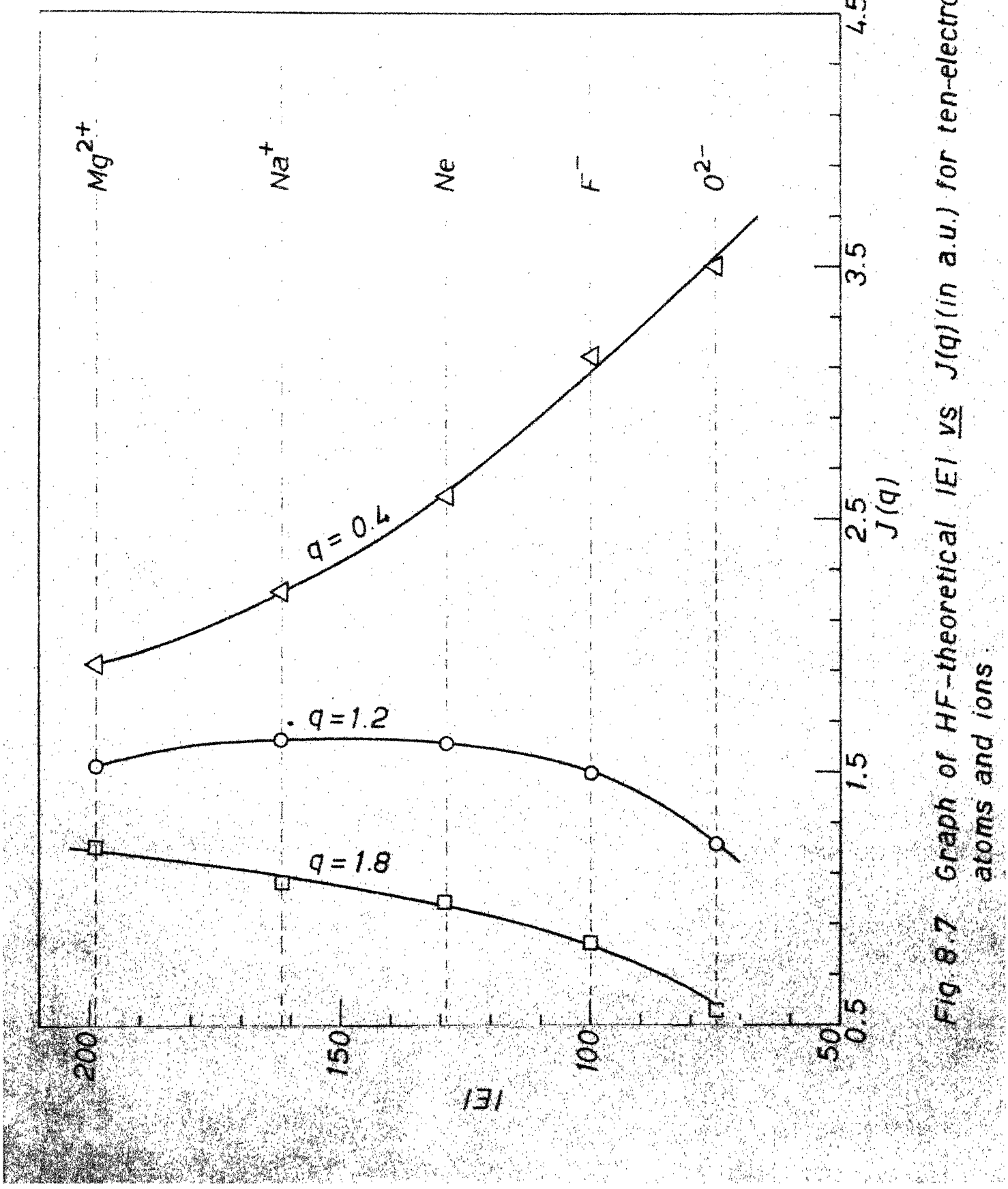

Fig. 8.7 Graph of HF-theoretical IEI vs J(q) (in a.u.) for ten-electron atoms and ions.

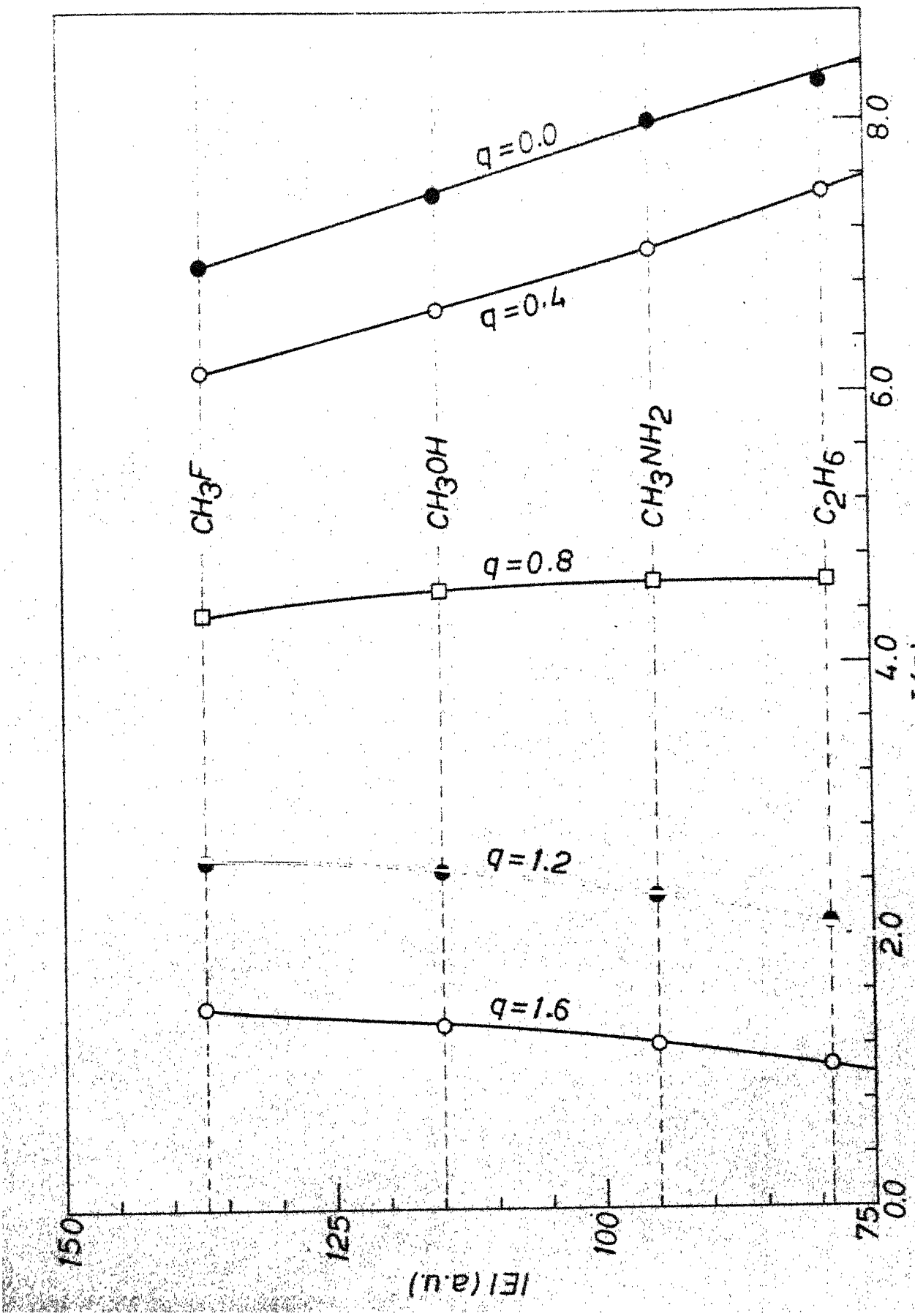

Fig. 8.8 Graph of theoretical IEI vs J(q) (in a.u.) at various q-values for 18-electron series of molecules.

series using the CP data and energies of Hirst and Liebmann[15] in Fig. 8.9. It may be pointed out here that the energy values of some of the molecules for which CP data are available in reference 15 lie very close to each other. Hence we have selected four molecules, viz., $CH_2=CH-CH_3$, $CH_3-CH=NH$, $CH_3-CH=O$ and $H-\overset{O}{\overset{\|}{C}}-NH_2$, which do not have too close energy values, to facilitate the clarity in plotting the graph. The graphs in Fig. 8.7 through 8.9 have the same general features as those observed in Fig. 8.5 in that $|E|$ vs $J(q)$ points lie on a smooth curve for any given value of q. For lower values of q, $J(q)$ decreases monotonically with increasing $|E|$ while for higher values of q, $J(q)$ increases monotonically with $|E|$.

Encouraged by the above observations with theoretical energy and CP data employing a wide variety of wavefunctions, we have attempted to use the smooth nature of $|E|$ vs $J(q)$ curves to predict empirically the CP of molecules belonging to an iso-electronic series. Experimental energy and CP data of a few other molecules in the iso-electronic series are used first to establish the nature of the smooth curve. Then using the experimental energy for the molecule of interest, we can interpolate and obtain the $J(q)$ values. Since a family of curves $|E|$ vs $J(q)$ is available, the entire CP for the molecule of interest can be constructed.

In the literature, unfortunately, experimental CP data for molecules belonging to an iso-electronic series are scanty. In

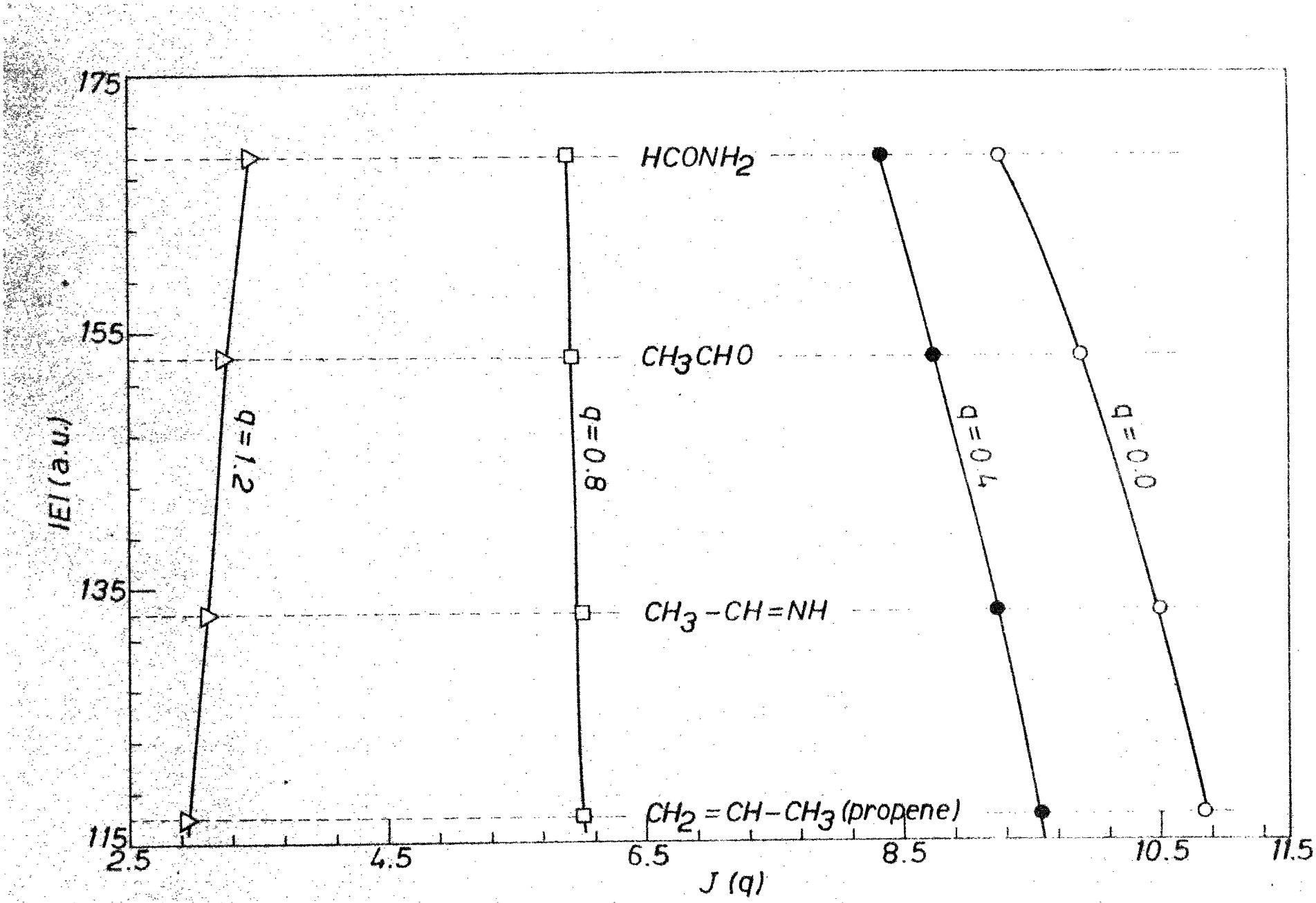

Fig. 8.9 Graph of theoretical |E| vs J(q) (in a.u.) at various q-values for 24-electron series of molecules.

fact we were able to locate in the literature, the experimental CP data for only one iso-electronic series. This series is the 10-electron series CH_4, NH_3, H_2O, HF and Ne. Even here experimental CP data on HF are not available. The CP data on CH_4,[16] H_2O[17] and Ne[18] were taken from the literature. We have employed in the present work the experimental CP data of only three molecules (CH_4, H_2O and Ne) to establish the nature of $|E|$ vs $J(q)$ curves. From these curves we were able to empirically predict CP's of NH_3 and HF. In Fig. 8.10 we present the graph of the absolute value of experimental energy, $|E|$ vs $J(q)$ for various values of q for this iso-electronic series. For each value of q, three points corresponding to CH_4, H_2O and Ne were connected by a smooth curve and experimental energies for NH_3 and HF were then employed to empirically predict their CP's. In Table 8.1 we present the results of the empirical prediction of CP's of NH_3 and HF along with experimental and/or CI-theoretical data for these molecules. We note here that in the case of NH_3, the results are in excellent agreement with the CI-theoretical CP of Ahlenius and Lindner.[19] They also agree, within the limits of experimental error, with the experimental CP of NH_3 measured by scattering of 35 keV electrons.[20] It has been pointed out to us that more precise CP measurements are being carried out on NH_3.[20] It is hoped that the empirically predicted CP curve for NH_3 would be confirmed with higher accuracy. As mentioned earlier, no theoretical CP data are available in the case of HF. Our

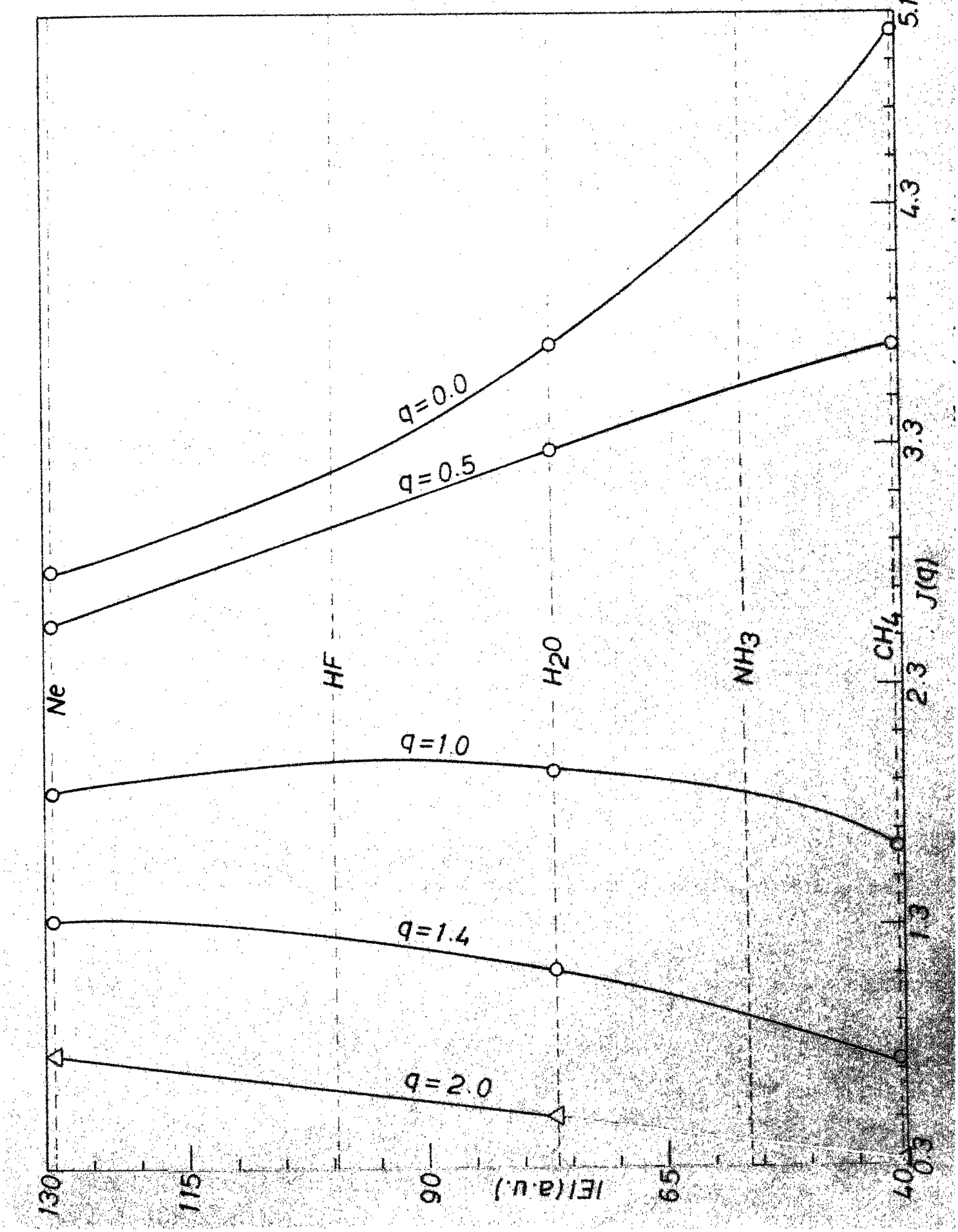
q=0.0
q=0.5
q=1.0
q=1.4
q=2.0
Ne
HF
H2O
NH3
CH4
J(q)
5.1
4.3
3.3
2.3
1.3
0.3
130
115
100
85
70
IEI (a.u.)

Table 8.1

Comparison of Compton Profiles Predicted from Fig. 8.10 with Other Experimental and/or Theoretical Data

q	HF predicted	LMO[a]	NH_3 predicted	CI-Theory[b]	Expt.[c]
0.0	3.20	3.24	4.35	4.38	4.35 ± 0.26
0.5	2.96	2.90	3.56	3.59	3.44 ± 0.24
1.0	1.98	1.97	1.85	1.83	1.72 ± 0.14
1.4	1.24	1.27	0.93	0.93	0.90 ± 0.10
2.0	0.64	0.64	0.41	0.41	0.42 ± 0.06

a Vide reference 2.

b Vide reference 19.

c Vide reference 20.

predicted CP agrees well with the CP constructed from the LMO-theoretical data of Whangbo et al.[2]

If the presently observed smooth correlation between the CP and energy in an iso-electronic series of molecules turns out to be a general one, it has yet another potential application. The smoothness of J(q) vs |E| can be used to establish the nature of these curves from data on three or four molecules belonging to an iso-electronic series. The CP of any other molecule of interest belonging to the same iso-electronic series can then be measured and the family of J(q) vs |E| curves for the iso-electronic series can be used to empirically predict the energy of this molecule. As the % error in J(q) is minimum around $q = 0$, it would be better to obtain energy empirically from the J(0) vs |E| curve. Thus, the energy of a molecule may be predicted empirically, apart from the conventional spectroscopic and thermochemical methods.

VIII.4 SUMMARY AND CONCLUSIONS

A remarkable empirical correlation that the variation of J(q) with |E| is a smooth one for any given value of q in an iso-electronic series has been established. For lower values of q, J(q) decreases monotonically with increasing |E|, whereas for higher q-values J(q) increases monotonically with increasing |E|. This correlation has been verified to exist for

theoretically computed CP's and the corresponding theoretical energies of a host of wavefunctions as well as experimental J(q) and experimental $|E|$. This result has been used to empirically predict the CP's of NH_3 and HF from their known experimental energy data. The CP's thus obtained agree well with the available CI-theoretical data on these two molecules. The predicted CP results of NH_3 also agree with the experimental data within the limits of experimental error. Confirmation of our predictions with regard to molecules in other iso-electronic series must await further experimental work. It may thus be worthwhile to measure CP's of a number of molecules belonging to an iso-electronic series with the same experimental set-up. If the empirical correlation illustrated here is verified to be a general one, as we suspect, it will have a useful predictive value.

REFERENCES

1. I.R. Epstein, Phys. Rev., A8, 160 (1973).
2. M.H. Whangbo, V.H. Smith, Jr. and W. Von Niessen, Chem. Phys., 6, 288 (1974).
3. M.A. Robb, H.J. Haines and I.G. Csizmadia, J. Amer. Chem. Soc., 95, 42 (1973).
4. R. Benesch and V.H. Smith, Jr., Chem. Phys. Letters, 5, 801 (1970).
5. P. Chaddah and V.C. Sahni, Chem. Phys. Letters, 46, 311 (1977).
6. S.R. Gadre and P.T. Narasimhan, Chem. Phys. Letters (to be published).
7. R.A. Rouse and A.A. Frost, J. Chem. Phys., 50, 1705 (1969).
8. C.A. Coulson, Mol. Phys., 26, 507 (1973).
9. R. Benesch and V.H. Smith, Jr., in "Wave Mechanics- The First Fifty Years", Eds. W.C. Price, S.S. Chissick and T. Ravensdale, Butterworths, London (1973).
10. E. Paschalis and A. Weiss, Theoret. Chim. Acta (Berl.), 13, 381 (1969).
11. R.J. Weiss, W.C. Phillips and A. Harvey, Phil. Mag., 17, 241 (1968).
12. J.A. Carlson, "Photoelectron and Auger Spectroscopy", Plenum Press, New York and London (1975).
13. D.M. Hirst and S.P. Liebmann, Mol. Phys., 30, 597 (1975).
14. T.H. Dunning, J. Chem. Phys., 52, 43 (1970).
15. D.M. Hirst and S.P. Liebmann, Mol. Phys., 30, 1693 (1975).
16. R.W. Klapthor and J.S. Lee, Chem. Phys. Letters, 45, 513 (1977).
17. Experimental Y-ray CP data quoted by A.C. Tanner and I.R. Epstein, J. Chem. Phys., 61, 4251 (1974).
18. P. Eisenberger, Phys. Rev., A5, 628 (1972).
19. T. Ahlenius and P. Lindner, Chem. Phys. Letters, 34, 123 (1975).
20. A. Lahman-Bennani, private communication (1977).

VITAE

Born on May 20, 1950 at Akola, Maharashtra, the author had his earlier education at M.E.S. Boys' School, Pune. He took his B.Sc. degree in 1970 at M.E.S. College, Pune and M.Sc. degree at the Department of Chemistry, University of Poona in 1972. He joined the Ph.D. programme of the Department of Chemistry, Indian Institute of Technology, Kanpur in July 1972. He was appointed Research Assistant in this department in November 1974 and is presently continuing in the same post.